Palaeoclimatology potential of the Australian floodplain mussel, *Velesunio ambiguus*

Thesis submitted in accordance with the requirements of the University of Adelaide for an Honours Degree in Environmental Geoscience

Kiana Day

November 2014

THE UNIVERSITY of ADELAIDE

PALAEOCLIMATOLOGY POTENTIAL OF *VELESUNIO AMBIGUUS*

ABSTRACT

A study of the Australian floodplain mussel, *Velesunio ambiguus*, from Lake Alexandrina, South Australia, was conducted to assess its suitability as a palaeo-climate and -environment indicator. Using 57 shell samples from two sites, the study was based upon the analysis of the macro-structure, micro-morphology and elemental geochemistry of growth increments of the aragonitic shells. Light microscopy and scanning electron microscopy (SEM) analysis of resin-impregnated cross-sections revealed the nature of shell growth increments. Measurements of growth increment frequency and width, with comparison to instrumental temperature and water chemistry data, were used to decipher the environmental controls over mussel growth rate. These comparisons also provide a validation of annual growth periodicity, and ages of shells were estimated to between four and 15 years. Micro-morphology measurements from SEM analysis of three samples revealed 67 to 374 micro-increments (tabular aragonitic crystallites) per growth increment that may imply a daily periodicity. Micro-increment widths commonly exhibit a bimodal pattern, with overall increase, across growth increments. Laser-ablation inductively-coupled-plasma mass-spectrometry (LA-ICP-MS) analysis of a suite of elements revealed a variety of signals. Although strong patterns were not observed for established palaeo-climate and -environmental indices such as Mg/Ca (temperature) and Sr/Ca (salinity), Ba/Ca and Mn/Ca ratios often exhibited bimodal oscillations, similar to micro-increment widths, with concentrations increasing over the course of the growing year. Ba/Ca and Mn/Ca ratios were suggested to reflect intra-annual fluctuations in primary productivity in the lake, which is an indirect function of regional hydrology and climate. This interpretation is supported by the similarity of micro-increment widths, as growth rate of the primary consumer (the mussel) varies with food availability. This study highlights the potential of *Velesunio ambiguus* as a recorder of intra-annual lake productivity and hydrology, however further studies are necessary to improve the interpretation of data before application to the fossil record.

KEYWORDS

Sclerochronology, bivalves, environment, *Velesunio ambiguus*, micromorphology, geochemistry, growth increments, aragonite

TABLE OF CONTENTS

LIST OF FIGURES AND TABLES

INTRODUCTION

As the anthropogenic pressures of modern society cause imbalances in large-scale climatic and environmental systems across the globe, so we see the responses manifested on regional and local scales. Radiative forcing facilitated by emission increases in carbon dioxide and an enhanced greenhouse effect has resulted in changes in global climates and a general trend in global warming (Meehl et al. 2000, IPCC 2013). Mainland Australian climate is co-dependently governed by three large-scale climate modes – the Indian Ocean Dipole (IOD), the Southern Annular Mode (SAM), and the El Nino-Southern Oscillation (ENSO) (Ummenhofer et al. 2009, Neukom and Gergis 2012) - which drive seasonal abnormality and weather extremes in a climate already characterised by wide seasonal fluctuations (BOM 2014). As the most arid inhabited continent on the planet with 80% of land receiving rainfall less than 600 millimeters per year, low rainfall coupled with very high evaporation results in low surface water flows and seasonal river systems (BOM 2014). This trend means that constraining hydroclimate variability in Australia is a matter of major economic, social and environmental significance.

The Murray Darling Basin (MDB) supports a significant proportion of Australia's economic, social and environmental interests, accounting for 41% of the nation's gross value of agricultural production and 70% of all irrigational water used in Australia (Nicholls 2004). In addition to the dominant economic activity prevalent the region, the MDB has significant ecological importance as it sustains many diverse terrestrial and aquatic ecosystems (EPA 2014). The effects of contemporary climate change have had considerable influences on the river system and agricultural land e.g. the 2007-2010

drought and the subsequent episodes of flooding (Gallant et al. 2012). Contests regarding water availability and its allocation to agricultural, domestic and environmental means have come to a fore, in the wake of such extreme climatic events and the forecasted increases in south-eastern Australian aridity (Meyer & Tyerman 2011). The effects of the compounding stresses of climate change and anthropogenic forces is driving the demand for improved knowledge and understanding of climate change trends, in an effort to better direct long-term sustainable development and management (Mills et al. 2013a).

Establishing an understanding of modern climate, environmental and hydrological change and isolating the effects of natural variability from anthropogenic forcing is unfeasible without first discerning the processes and responses of the past. There is a need for generation of pre-instrumental, precisely dated, high resolution climatic data in order to gain insight into past trends and variability, to contextualise the contemporary conditions within long-term climate history, and to validate predictive models. High resolution palaeo-climate records can be invaluable in such circumstances, however despite numerous records in the Northern Hemisphere, there remains a pressing need for annually resolved palaeo-climate records relating to the Southern counterpart (Neukom and Gergis 2012). This is certainly the case in south-eastern Australia, where considerable uncertainties exist due to a sparse collection of short duration palaeo-climate records (Neukom and Gergis 2012). Particularly, current understanding of Australian drought and rainfall variations is largely limited to the instrumental data acquired post-1900 (Fenby and Gergis 2013).

Regional studies within the MDB using a variety of palaeo-climate environmental records in recent years has attempted to contribute to this lack of long-term climate data, however limitations and restrictions in regional suitability have impeded their broad application. Hydroclimate variability has been reconstructed from pollen (Mooney 1997), ostracods (Radke 2000) and diatoms (Gell et al. 2005) found in lake sediments, however uncertainties lie in the origin of these indicators where intermittent connection to the Murray can introduce allochtronous climate signals (Mills et al. 2013b). Palaeo-hydrological reconstructions have been limited by poor resolution from coarse sampling of speleothems (Ayliffe et al. 1998, Desmarchelier et al. 2000, McDonald 2000), and dendrochronological studies in the MDB have been restricted by the preponderance of tree species that often lack discernible growth rings (Mills et al. 2013a).

Reconstructions of Murray River stream flow have been derived from a collection of regional climate records that are poorly calibrated to the subject of the study, i.e. river flow (Gallant and Gergis 2011). With the limitations in established proxies evident, other avenues must be explored in order to bridge the data gap.

Bivalve sclerochronology may provide a solution to this problem. Sclerochronology is the study of the physical and chemical properties of the accretionary hard tissues of organisms (Buddemeier et al. 1974). Bivalve shells are formed through biomineralisation of a biomaterial composite composed of calcium carbonate and an organic matrix. Accretion is characterised by periods of fast growth (growth increments), delimited by dark growth bands which represent periods of growth interruption or retardation, and can reflect annual, seasonal, fortnightly (tidal), circadian (24-hr), circalunidian (lunar day – 24-hr 50-min) and ultradian (less than a day) cycles (Schöne and Surge 2014). Such discrete accretionary patterns can be influenced by the

organism's growth rate response to changes in environmental parameters, and can therefore provide an indication of ambient conditions at the time of growth, such as temperature, salinity and food availability (Schöne and Surge 2014). Accreted carbonate geochemistry is similarly dependent on the ambient environment, with established indices such as Mg, Sr, Ba and Mn providing the potential to supply information on past temperature, salinity and primary productivity, respectively (Lazareth et al. 2003, Klünder et al. 2008). Both the microstructure and geochemistry of bivalves can therefore be used in the reconstruction of high resolution, precisely dated chronological records of past climate and environment variability (Schöne and Surge 2014).

There have been a number of successful studies that have utilised annual growth increments in bivalves to reconstruct climate and environment change. Founding studies determined that bivalves faithfully record a chronology of physico-chemical changes from the surrounding environment, such as temperature (Kennish and Olsson 1975), salinity (Davis and Calabrese 1964) and water quality (Frantsevich et al. 1996). Such environmental changes are captured in shell carbonate as variable growth rates (Kennish and Olsson 1975) and geochemical signals (Wefer and Berger 1991). With application of such findings and further advances in more recent years, Butler et al. (2013) resolved a 1357 year archive of marine climate variability on the North Icelandic shelf, based on analysis of carbonate growth increments of the bivalve *Arctica islandica*. Schöne et al. (2004b) developed a reconstruction of sea surface temperature from 1884 – 1983 using oxygen isotope ratios from *A. islandica*. Schöne et al. (2011) also found that Sr/Ca and Mg/Ca ratios in the hinge plate of *A. islandica* were inversely proportional to calcification temperature, once physiological effects were calculated and removed,

which supports findings from studies of abiogenic aragonite (Kinsman and Holland 1969). Although the majority of studies to date have targeted long-lived molluscs, such as the ocean quahog (*Arctica islandica*), Carré et al. (2013) demonstrated the potential of using more abundant, short-lived taxa. Carré et al. (2013) used oxygen isotope ratios within samples of the surf clam, *Mesodesma donacium,* collected off the coast of Peru whereby inter-annual variability in sea surface temperature (SST) is reflective of the El Nino – Southern Oscillation. Versteegh et al. (2009) studied the oxygen isotope ratios in freshwater mussels to investigate the variance in spring-summer river discharge conditions of the River Rhine in Germany and the Netherlands, and Vonhof et al. (2013) studied modern and ancient river oysters in the Turkana Basin, Kenya, to determine how oxygen and carbon isotope ratios reflect the wet-dry seasonal changes driven by monsoonal rainfall. Ferguson et al. (2013) used carbon isotope ratios and radiocarbon content of marine mussels to examine the extent of past coastal upwelling along the west coast of North America, and Schöne et al. (2004a) used long-lived freshwater pearl mussels from six different rivers to reconstruct summer air temperatures in Sweden over the period 1777-1993.

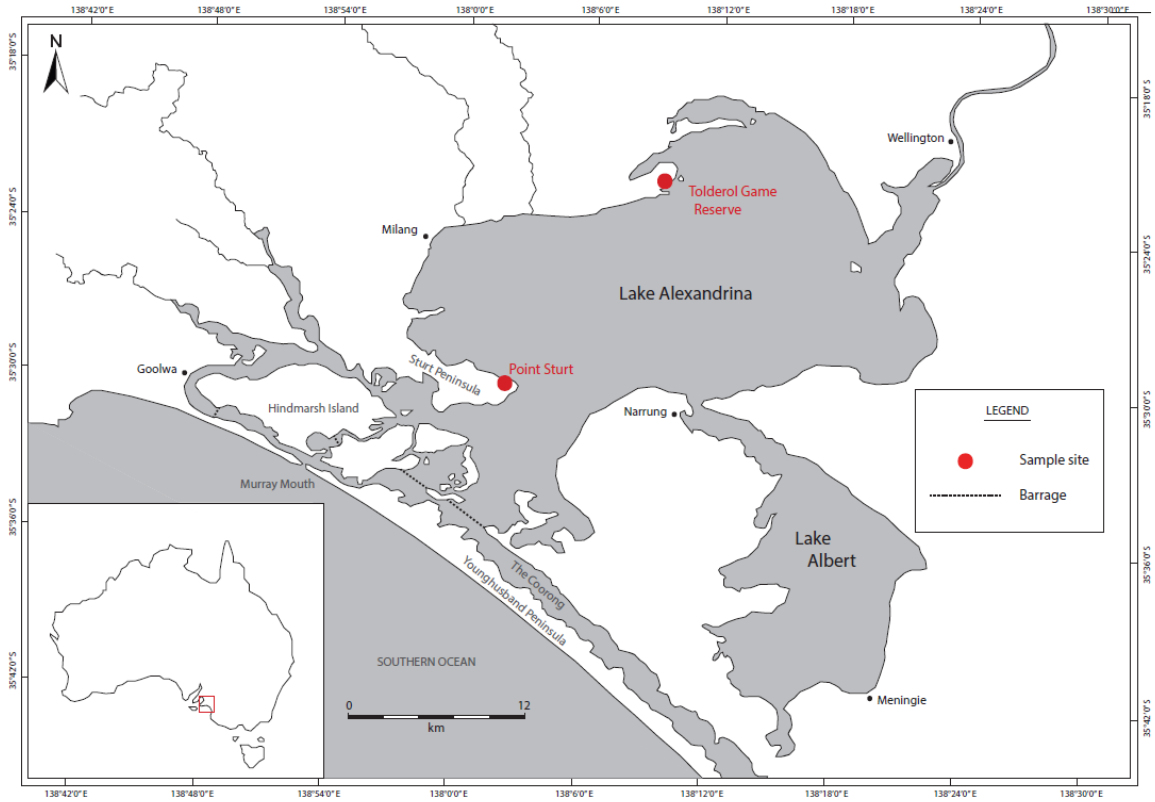

Figure 1: Location map of Lake Alexandrina, depicting study sample sites.

This project aims to explore the suitability of the Australian floodplain mussel, *Velesunio ambiguus*, as a high resolution archive of climate and environmental variability in south-eastern Australia, through samples obtained from Lake Alexandrina, South Australia (Figure 1). *V. ambiguus* is a suitable species of bivalve for this kind of study as it is distributed throughout the Murray-Darling system and eastern Australia (Walker, 1981). Although *V. ambiguus* is relatively short-lived (< 20 years), it is abundantly found in sedimentary deposits and archaeological middens (Wilson et al. 2012). Therefore, if an environmental signal can be demonstrated within the shells of modern *V. ambiguus*, this would hold considerable potential for future, high resolution studies of past climate and environmental change. Lake Alexandrina is an ideal location for a study of this nature as the lake experiences marked seasonal and inter-annual variability in river in-wash and lake water geochemistry, by which patterns may be

reflected in the geochemistry of carbonate shells. Scanning electron microscopy (SEM) and laser ablation inductively coupled plasma mass spectrometry (LA-ICP-MS) will be used to analyse shell cross-sections to determine whether seasonality and climatic conditions are evident in the micromorphology and geochemistry of this species of bivalve through comparisons to instrumental data, and whether these approaches work as indicators of past physico-chemical or biological conditions.

METHODS

Refer to Appendix A for extended methodology.

Sample collection

Mussel shells were collected from two locations in Lake Alexandrina in April 2014. Dead single and articulated shells were acquired from ~1 m water depths using hands and feet to locate. Thirty-nine dead articulated samples and 47 single valves were collected from Point Sturt (S35° 30’ 03.6, E139° 02’ 47.2), and 11 dead articulated samples and one live sample were collected from Tolderol Game Reserve (S35° 22’ 32.3, E139° 08’ 36.6). Water samples for each location were taken. Both shell and water samples were placed in cold storage.

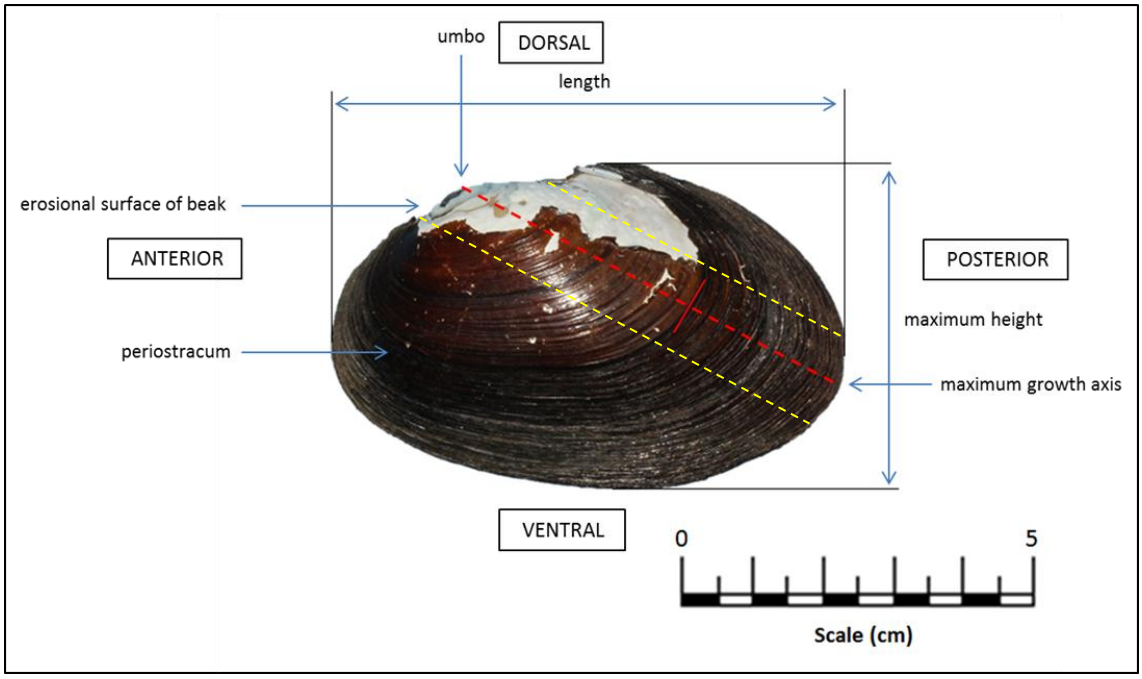

Figure 2: Morphology of left valve of *Velesunio ambiguus* dead-sample collected from Point Sturt, Lake Alexandrina. Maximum growth axis is perpendicular to outer concentric growth lines. Dashed yellow lines indicate where cuts are made during sectioning to incorporate maximum growth axis. Measurements to specify maximum height and length of a freshwater mussel shell after McMichael and Hiscock (1958, in Walker 1981).

Sample preparation

Samples were cleaned to remove organic material with a bristle brush and reverse osmosis (RO) water and air-dried. Articulated samples were separated and all samples were catalogued based on an abbreviation of the site name (PS = Point Sturt, TGR = Tolderol Game Reserve), numerical ordering and valve side (L = left valve, R = right side), e.g. TGR1L. Samples were measured according to McMichael and Hiscock (1958) and photographed.

Figure 3: Full growth axis section (top - SEM analysis) and mounted umbo sections on glass microscope slide (bottom - LA-ICP-MS analysis).

Using a diamond saw, eight left valve samples were sectioned to approximately 2 cm in width to incorporate the maximum growth axis from umbo to ventral margin, (Figure 2). Fifty-five additional left valve samples that were well preserved were cut to a 1 x 1 cm square that incorporated the umbo along the maximum growth axis (Widarto 2007, Schöne et al. 2011). All samples were impregnated in clear-set epoxy resin (Epofix, Stuers) spiked with indium (40 ppm, resin indicator for laser analysis) in 8 x 3 cm (8 full growth axis sections) and 1.5 x 3 cm (47 umbos) moulds and set overnight at 40°C. Sections approximately 1.5 mm thick were cut from the resin blocks along the maximum growth axis of the shell using low-speed Buehler IsoMet 1000 precision sectioning saw at a speed of 150 rpm. All sections were wet-polished using three varying grades of lapping film (30 µm, 9 µm and 3 µm) on a Buelher Metaserv 250 grinder/polisher at 250 rpm, and a further two hand polishes with a 3 µm diamond paste and a 0.04 µm colloidal silica solution. Three of the best preserved full growth axis

sections were carbon-coated at Adelaide Microscopy, in preparation for scanning electron microscopy (Figure 3, top slide). Lots of eight umbo sections were mounted onto individual glass microscope slides using indium-spiked thermoplastic glue (Crystalbond™ 509, Figure 3). The slides were stored in zip-lock bags and cleaned with ethanol prior to elemental analysis.

Light & Scanning Electron Microscopy

Growth bands observed in all slide cross-sections were photographed using a Leica light microscope and Leica DFC 320 D-SLR camera at 16x magnification.

A QUANTA 500 Scanning Electron Microscope was used to examine the three full growth axis samples (TGR1L, TGR4L and TGR87L) whereby detailed analysis and transect imaging of shell structure and microstructure was conducted through the umbo at 43,000x (10kV) magnification.

For these three shells, SEM images were used to measure and count micro-increments (tabular aragonite crystal layers). When counting micro-increments within growth increments of *V. ambiguus* shell cross-sections, occasionally minor cracks persisting parallel to the orientation of the aragonite crystallites were encountered, believed to have been caused either prior to shell collection (general exposure to environment) or during shell preparation (pressures to structure from resin impregnation and sectioning). The assumption was made that cracks were a clean break and that no micro-increment crystallites were missing from the space, and therefore counting could continue across a crack without loss of micro-increments. Image analysis, incremental counts and measurements were conducted using the image analysis program, ImageJ, with ObjectJ plug-in (Vischer and Nastase 2014).

LA-ICP-MS

After removal of the carbon coating on full growth axis sections using ethanol and tissue wipes, both full growth axis sections and mounted umbo slides (Figure 3) were inserted into the New Wave UP-213 Nd:YAG laser-ablation system chamber for geochemical analysis. Transects through the umbo, perpendicular to growth increments, were ablated using a beam spot size of 16 μm, with a laser repetition rate of 5 Hz and energy set to produce a fluence of 3.5-4.0 Jcm^{-2}. Dwell times for each element were set as shown in Table 1. Geochemical data acquired from laser ablation was corrected against a NIST-612 standard to account for drift using GLITTER data reduction software program. Raw element data were converted to Me:Ca ratios.

Table 1: Elemental variables and dwell times for LA-ICP-MS

Element	Dwell time (ms)
7Li	0.2
23Na	0.01
24Mg	0.05
39K	0.05
43Ca	0.01
55Mn	0.05
57Fe	0.05
63Cu	0.1
88Sr	0.1
115In	0.1
138Ba	0.05
208Pb	0.1

RESULTS

Table 2: Analytical method undertaken in study and number of samples used.

Analytical method	No. of samples analysed
Macro growth increment structure and counts (Light microscopy & SEM)	58
Micro-increment counts (SEM)	3
Geochemistry (LA-ICP-MS)	58

Macro-increment frequency and morphology

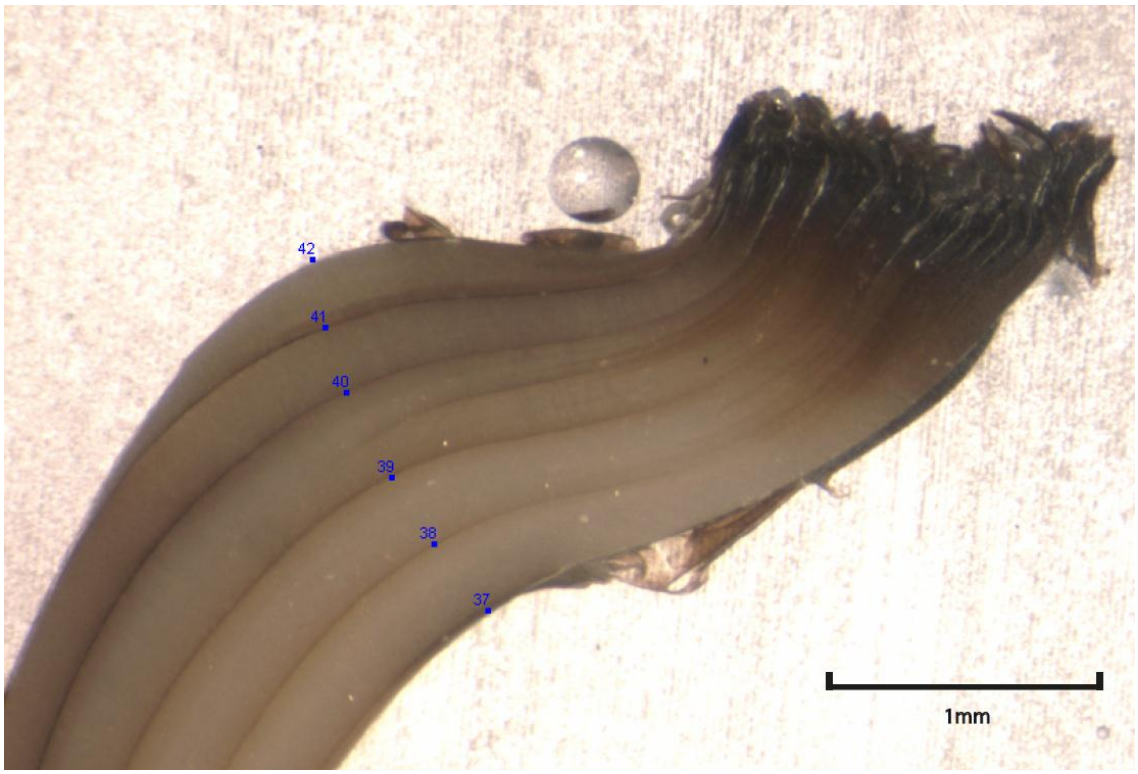

Figure 4: Five macro growth increment counts of PS5L using ObjectJ plug-in in ImageJ image processing program. Increments were counted closest to the umbo where growth lines were most discrete and LA-ICP-MS transects were run where minimal interruption of 'false' line geochemistry was likely to occur.

Growth increments, comprising aragonite layers (~0.05 – 0.45 mm thickness) bounded by organic growth interruption layers are hereby termed macro-increments (Figure 4). Macro-increments within shells collected from Point Sturt (no. of shells = 50) vary in number from four (PS77) to 15 (PS69). Shells from Tolderol Game Reserve (no. of shells = 8) have increment numbers ranging from six (TGR9L) to 11 (TGR10L). The

mean number of increments across samples from Point Sturt is 9.05, with a standard deviation of 2.64 and standard error of 0.40. The mean number of increments across samples from Tolderol Game Reserve is 8.20, with a standard deviation of 1.92 and standard error of 0.86. The mean number of increments across all samples is 8.96, with a standard deviation of 2.57 and standard error of 0.37.

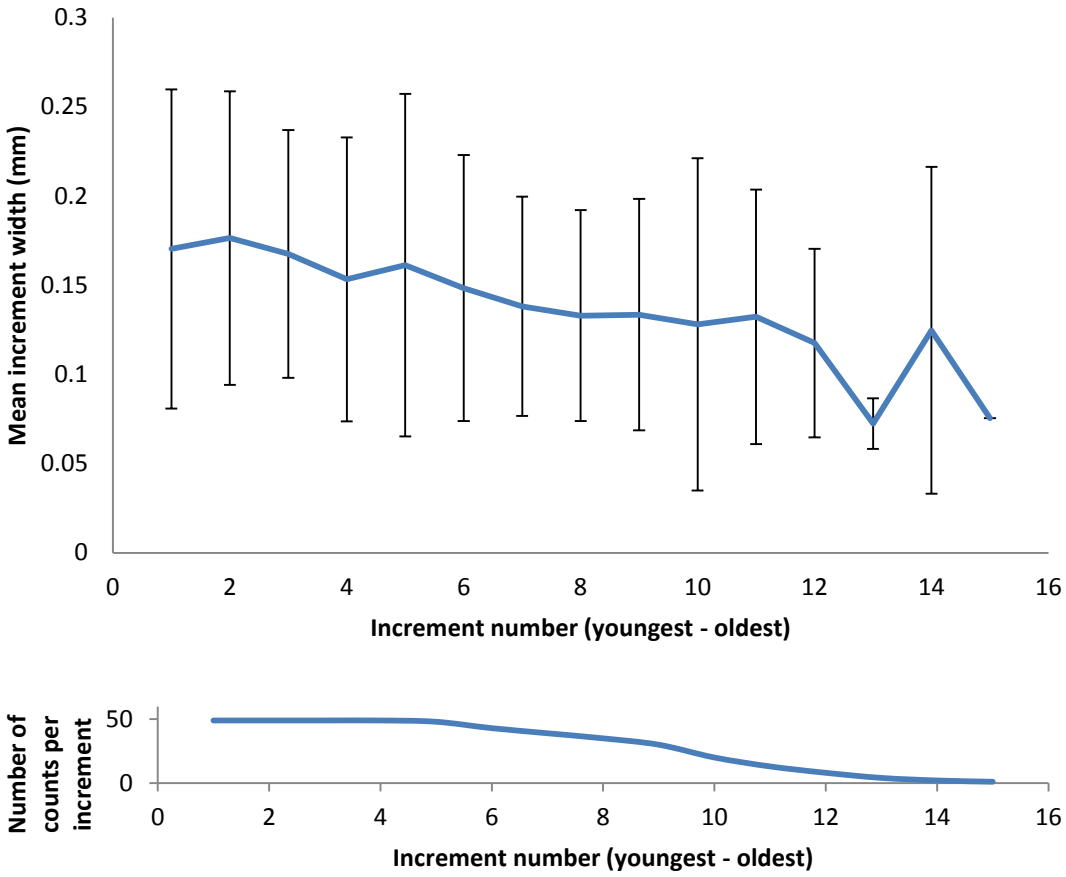

Figure 5: Mean widths and standard deviation of growth increments from youngest to oldest across all *V. ambiguus* samples from Point Sturt and Tolderol Game Reserve, Lake Alexandrina. Bottom plot indicates decreasing number of representative growth increment widths from samples for increasing growth increment number (1-15, youngest to oldest).

In the majority of cases, the youngest macro-increments measured in a particular shell are shown to be generally wider than older, narrower increments (Figure 5). There is, however, a high standard deviation for the mean of individual increment numbers, indicating that widths were variable among samples.

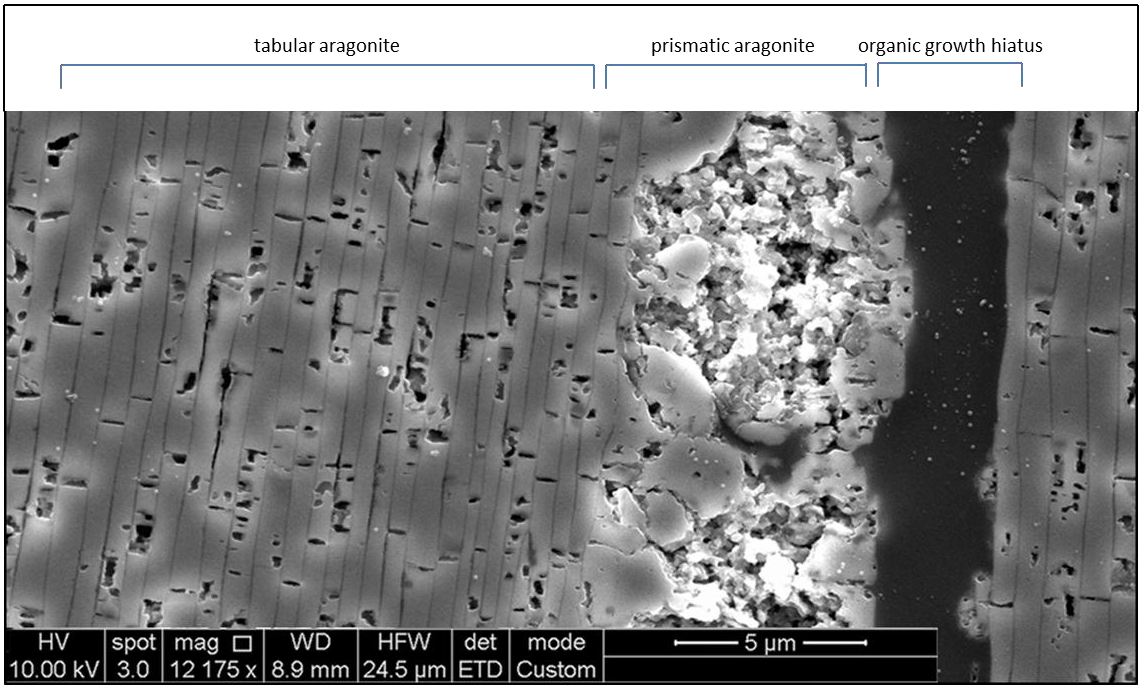

Figure 6: Scanning electron microscope secondary electron photomicrograph depicting crystallography of *Velesunio ambiguus* valve cross-section from sample TGR1L. Shell crystallography is typified by an outer protective organic layer called the periostracum. Prismatic aragonite is then formed to the base of this layer. This is followed by tabular aragonite crystal growth which dominates the shell composition. Hiatuses in shell growth are defined by the same sequence of crystal growth, as shown above.

Scanning electron microscopy (SEM) of cross-sections of shell carbonate indicate three main constituents – dark organic bands which are generally 1 – 4 µm in width and constrain the macro-increments; subjacent prismatic aragonite which varies in width from 2 – 6 µm; and tabular aragonite crystallites which are layered and grow parallel to the dark organic bands (Figure 6). This pattern of shell microstructure, which defines the macro-increments, is consistent throughout the shell, as observed from transect imaging perpendicular to dark organic bands. An example of the micromorphology of an entire macro-increment is shown in Figure 7.

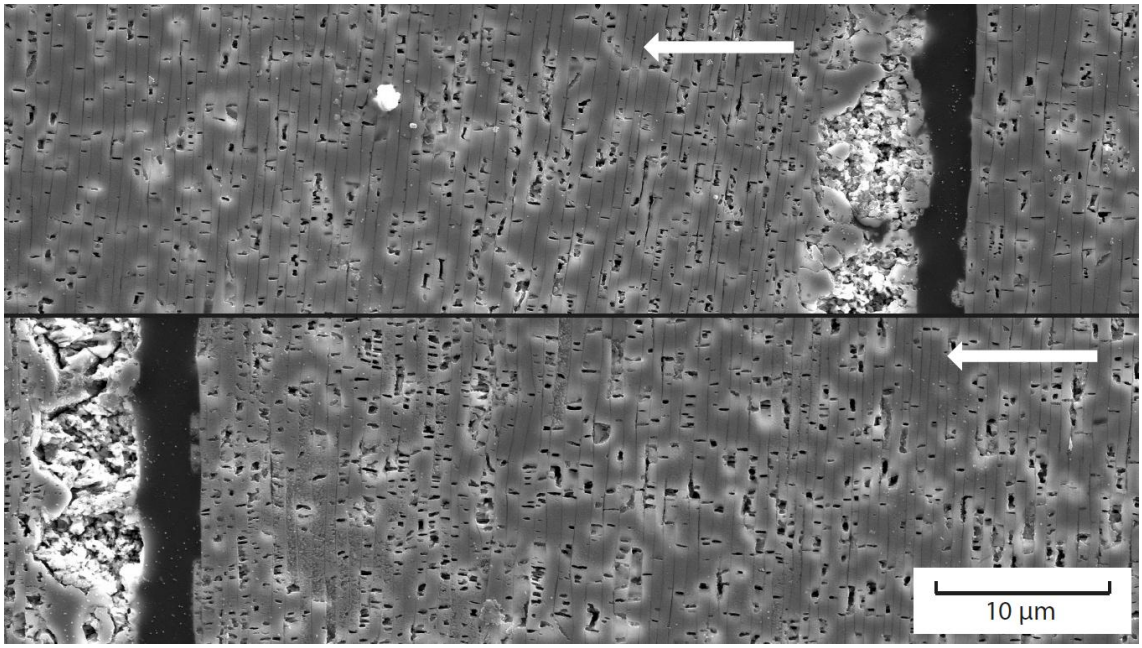

Figure 7: Scanning electron microscope secondary electron photomicrograph depicting entire macro growth increment from TGR1L. Bottom image is a continuation of the top image. Arrows indicate direction of growth. This macro growth increment is composed of 159 micro-increments.

Micro-increment counts

Layers of tabular aragonite which comprise the carbonate component of macro-increments are hereby termed micro-increments. Three shell samples, TGR1L, TGR4L and TGR87L, were observed under SEM to obtain images for micro-increment counts. These three samples were used as they were the best preserved of eight samples that were impregnated in resin. Many of the samples developed pervasive cracks through this process, and these could not be sectioned without further damaging the sample. The process of counting the many micro-increments across nine transects is time-consuming, and with time-constraints on this study, only three shells were analysed by this process.

Figure 6 shows an SEM image of the nacreous tablets that form the majority of the shell composition. These tablets vary in width from ~0.5 – 2.0 µm. The numbers of layered

aragonite crystallites vary between macro-increments, and micro-increments occasionally lack consistency in width and continuity along the length of the micro-increment.

Micro-increments within growth increments vary in number from 67 to 374, based upon 13,494 increments in total from nine transects. Three sample increments with counts of 405, 414 and 502, were identified as outliers using the Thompson Tau method (Dieck 2007).

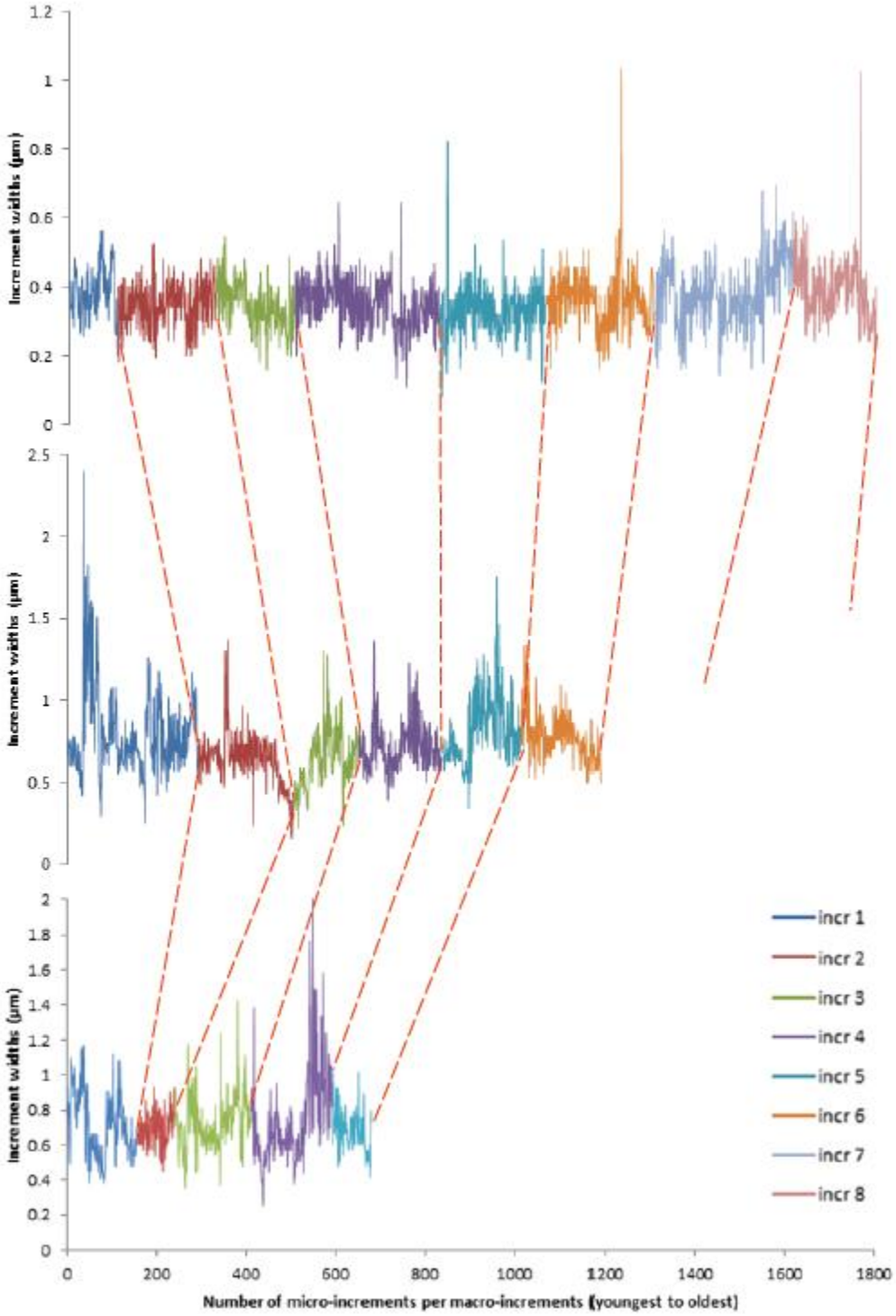

Figure 8: TGR1L transect correlation based on macro-increments. Trendlines of Transects 1, 2 and 3 (top - bottom) show widths of micro-increments and number of micro-increments per macro-increment (defined by colour). X-axis runs back in time, left to right.

From three image transects across sample TGR1L, macro-increments can be correlated.

(Figure 8). There is continuity exhibited for all macro-increments, indicated by red

dashed correlation lines. Although it is challenging to perform a rigorous correlation test between the three transects, it is possible to observe a visual correspondence between the patterns in the widths of some of the micro-increments. This indicates that micro-increment thicknesses can be maintained, to a degree, along the length of the increment.

The same continuity can be observed for sample TGR4L, with the exception of the discontinuity evident in increment 5 which it is not observed in Transect 3 (Figure 9). The dotted red line, as opposed to the dashed, indicates a growth line that gradually disappears between image transects. Similarly to sample TGR1L, patterns are observed across transects that indicate a persistence in the widths of micro-increments along the length of macro-increments.

In sample TGR87L, which was the only live sample collected, it was difficult to correlate the dark growth bands across all three transects as a number of the macro-increments were discontinuous and did not continue through the length of the shell (e.g. increment 3/4) or developed outside of the hinge area (e.g. increment 1a), however most were able to be correlated across two transects (Figure 10).

In samples TGR1L, TGR4L and TGR87L, a consistent bimodal oscillation is observed, with variability in this pattern evident in all samples. The widths of micro-increments across macro-increments begin narrow, with an overall increase in width to an initial peak. Following these thicker micro-increments, widths reduce again, before increasing again to form a second peak. There is some variability in the maximum width values between the two peaks of each macro-increment, however the most common trend is a slightly higher second peak compared to the first (e.g. Figure 11, Transect 1, incr. 1).

There appears to be consistency in the distribution of micro-increment widths along each macro-increment, as traced across the three image transects for each sample (e.g. Figure 10, incr. 3).

Long-term trends in micro-increment widths appear to vary between all three samples. TGR1L appears to show a consistent, unchanging trend in minimum and maximum values, on average, across the three transects. TGR4L appears to exhibit an overall increasing trend in micro-increment widths through time. TGR87L lacks consistency in the long-term trend across the three transects, with Transect 1 (closest to the umbo) showing a slight increase in micro-increment width over time, and Transects 2 and 3 showing an overall decrease in micro-increment width over time.

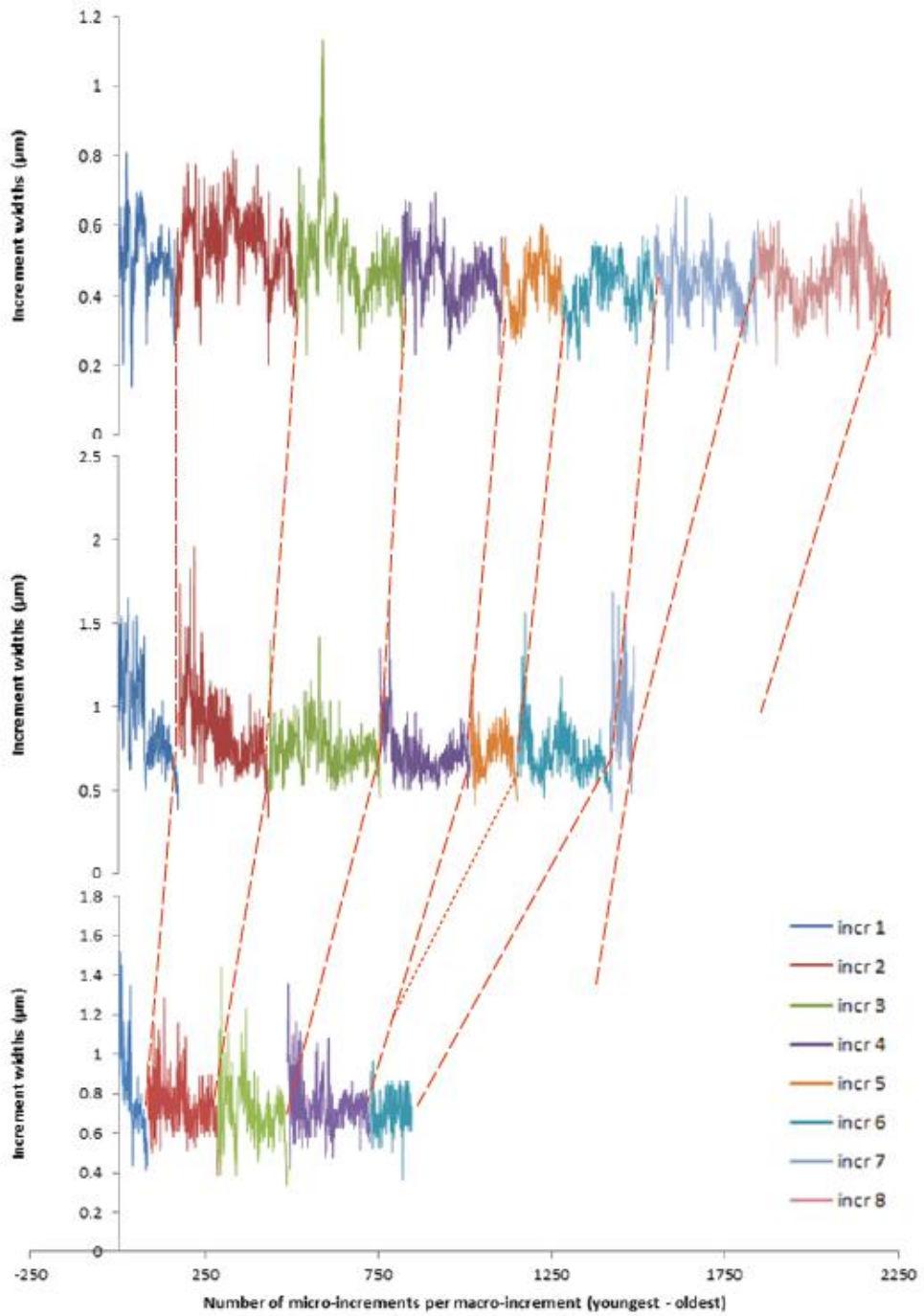

Figure 9: TGR4L transect correlation based on macro-increments. Trendlines of Transects 1, 2 and 3 (top - bottom) show widths of micro-increments and number of micro-increments per macro-increment (defined by colour). X-axis runs back in time, left to right.

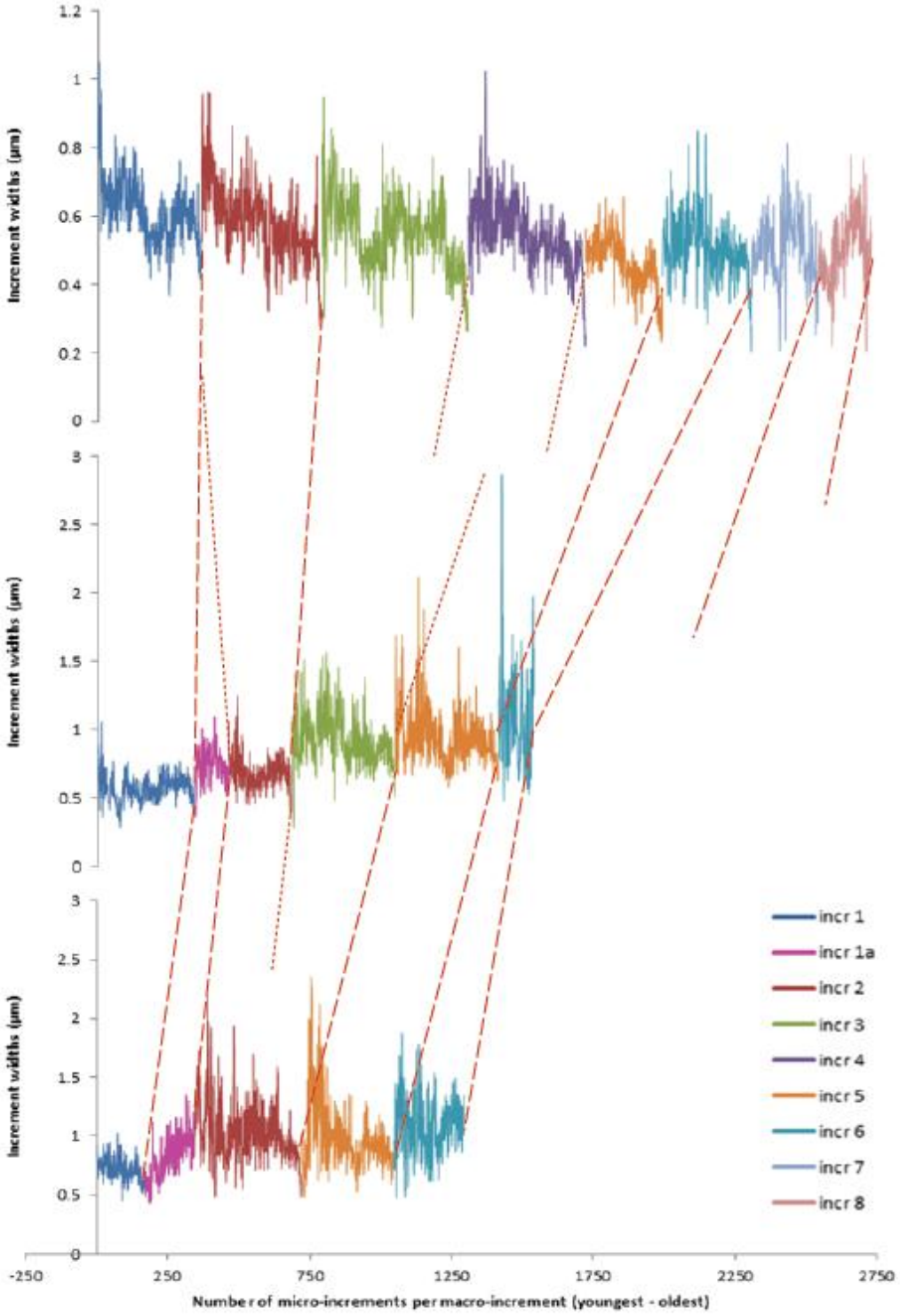

Figure 10: TGR87L transect correlation based on macro-increments. Trendlines of Transects 1, 2 and 3 (top - bottom) show widths of micro-increments and number of micro-increments per macro-increment (defined by colour). X-axis runs back in time, left to right.

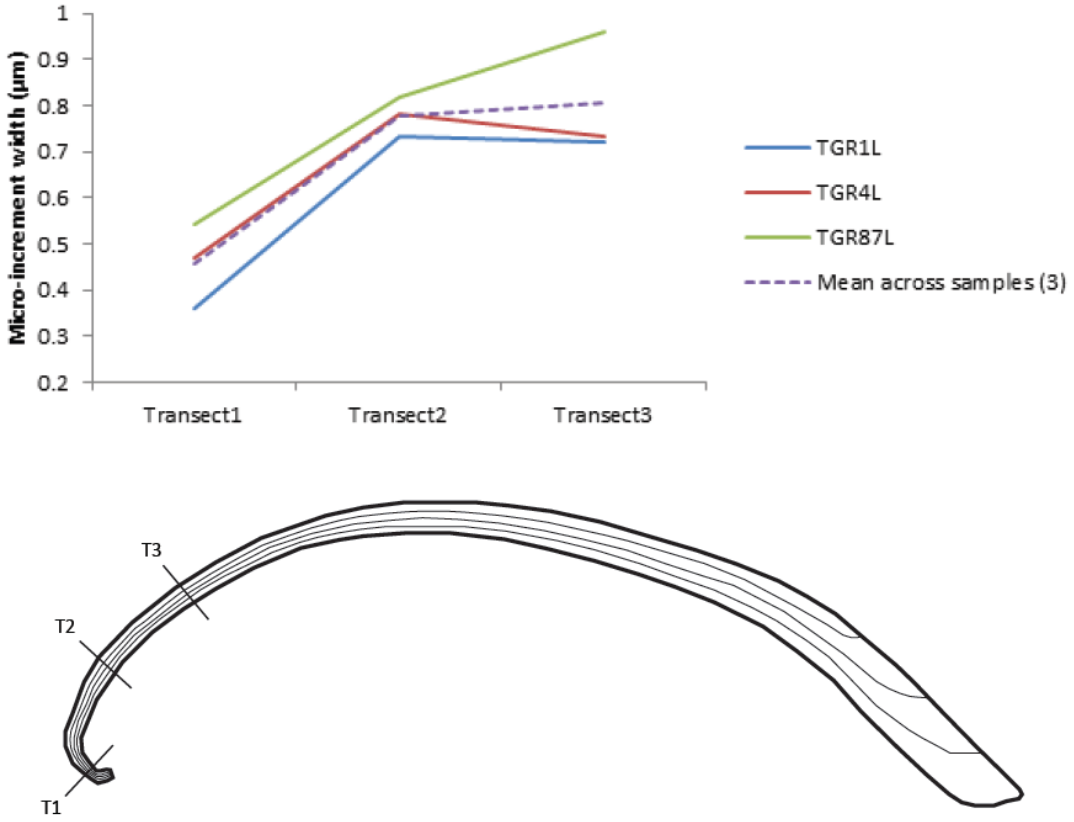

Figure 11: Mean sample micro-increment widths across transects. Micro-increments are on average most narrow within the umbo region, and increase in size across Transect 2 and again in Transect 3.

Comparison across three transects of the same shell show a relative increase in the widths of micro-increments from the more condensed umbo region (Transect 1) through to Transect 3 (Figure 11).

Elemental chemistry of shells

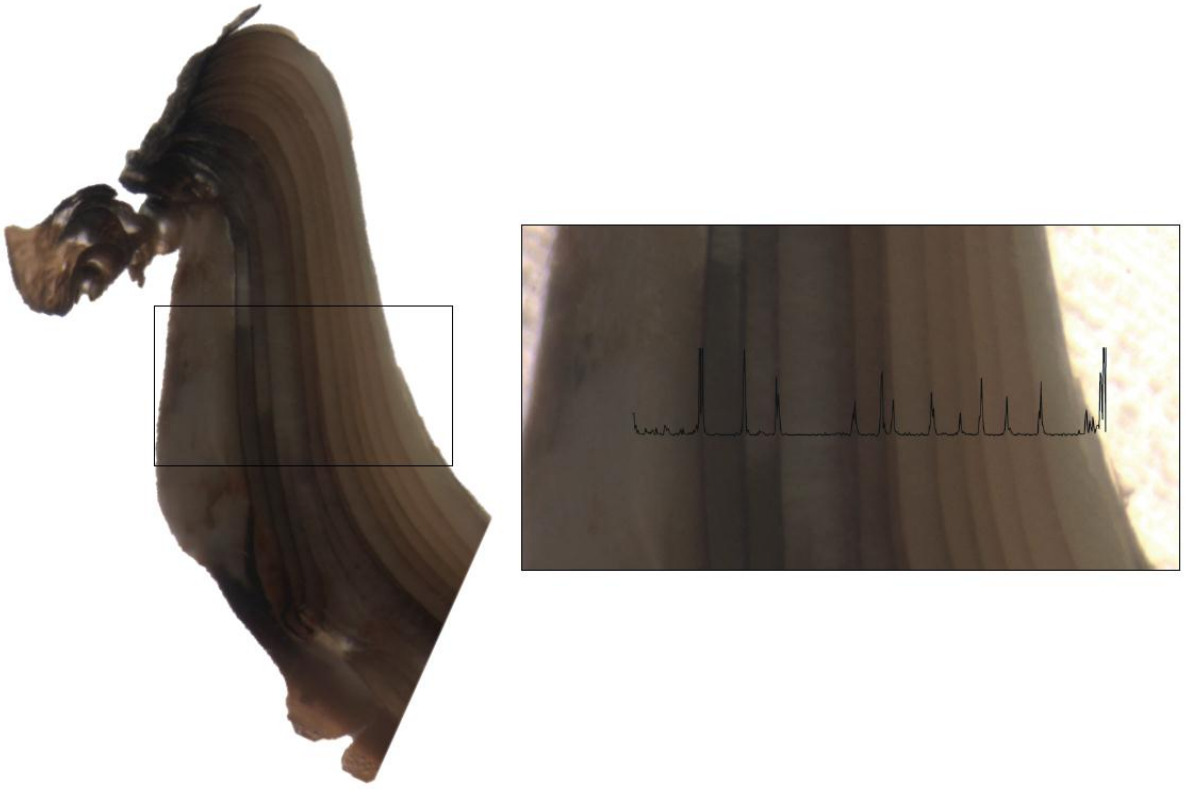

Figure 12: Cross-sectional image of umbo region (PS23L) showing how Cu/Ca transect elemental profile correlates to dark organic growth lines. In the left hand side figure, the shell exterior is the angled surface to the right to the cross-section. The affinity of Cu to organic matter provides a means to constrain the position of macro-increments using geochemical data.

LA-ICP-MS transects were performed on all samples across the umbo region (i.e. T1 in Figure 11 and example transect in Figure 12). All data are presented in Appendix B, with representative examples given in Figures 14, 15, 16 and 17.

Variability in the Cu content of the mussel shells, as indicated by the Cu/Ca ratio, exhibit a marked correspondence with the dark organic bands (Figure 10). Cu was the only element that was clearly concentrated in the dark organic bands lines, with comparatively minimal signal across the carbonate (Figure 12). The Cu/Ca peaks vary across transects, from subtle fluxes in the background signal of the carbonate to large pronounced peaks (Figure 13). In all samples, the peaks were discrete enough to

confidently identify. The Cu/Ca ratio was therefore used to constrain the position of macro-increments in the context of the other geochemical data.

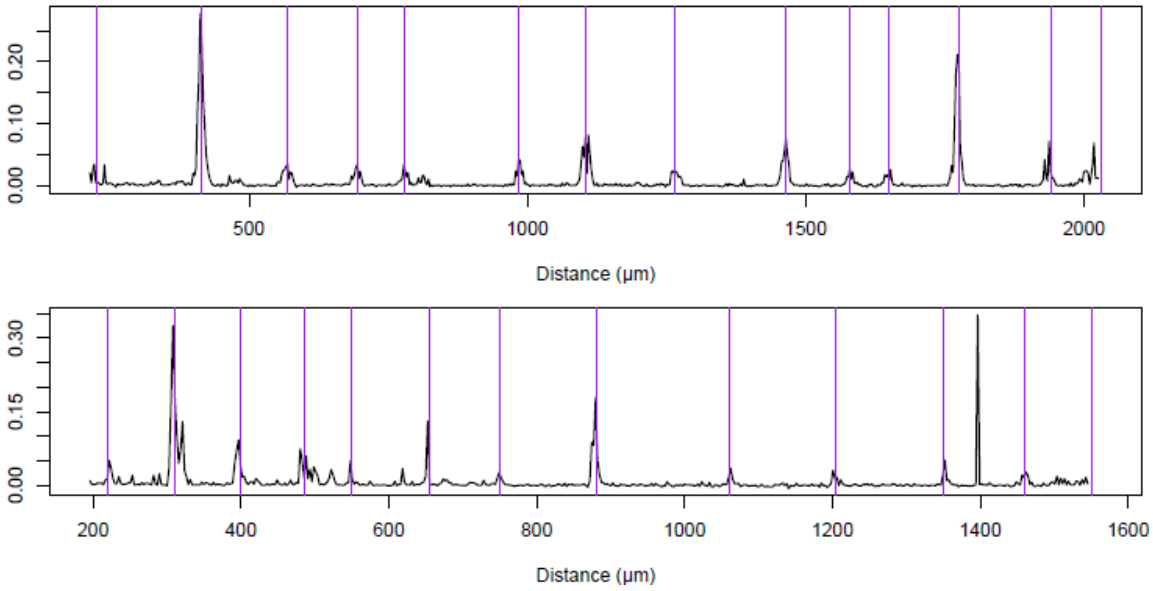

Figure 13: Cu/Ca rations from PS65L and PS66L indicating the subtle and pronounced peaks that are generated from laser ablation.

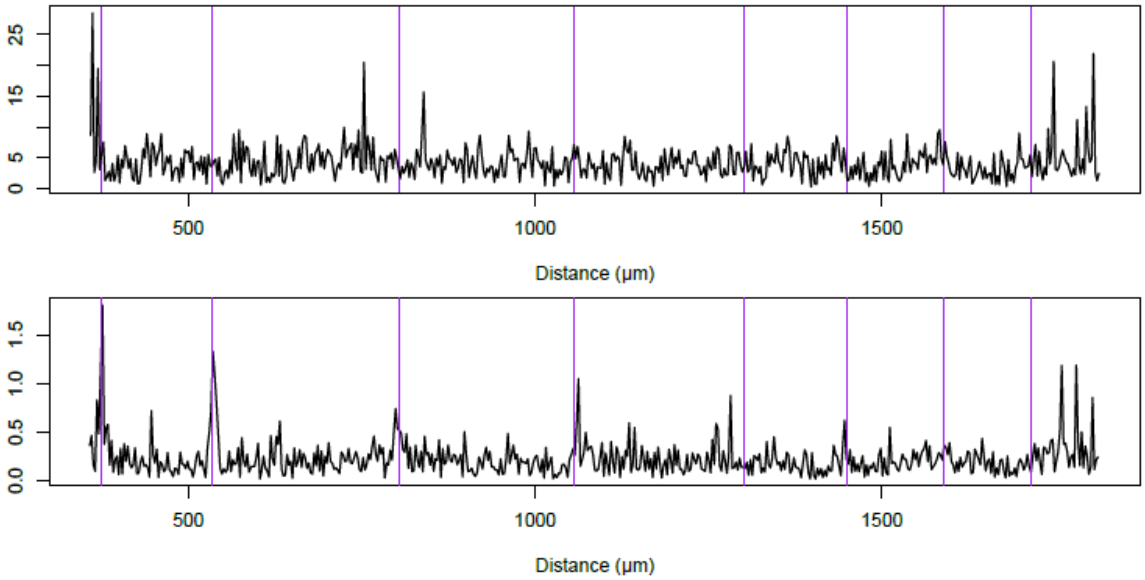

Figure 14: Geochemical profiles of Mg/Ca and Sr/Ca for PD24L. There are no clear patterns evident that appear to reflect physico-chemical parameters of seasonality.

There were a variety of signals observed in elemental ratio profiles from the LA-ICP-MS data. Well-known palaeo-climate and environment geochemical indices, such as Mg/Ca and Sr/Ca, exhibited only indiscrete patterns or signals (Figure 14).

By contrast, changes in the Ba/Ca and Mn/Ca exhibited defined patterns which were largely consistent between shells. It was therefore decided to focus attention on these two elemental ratios.

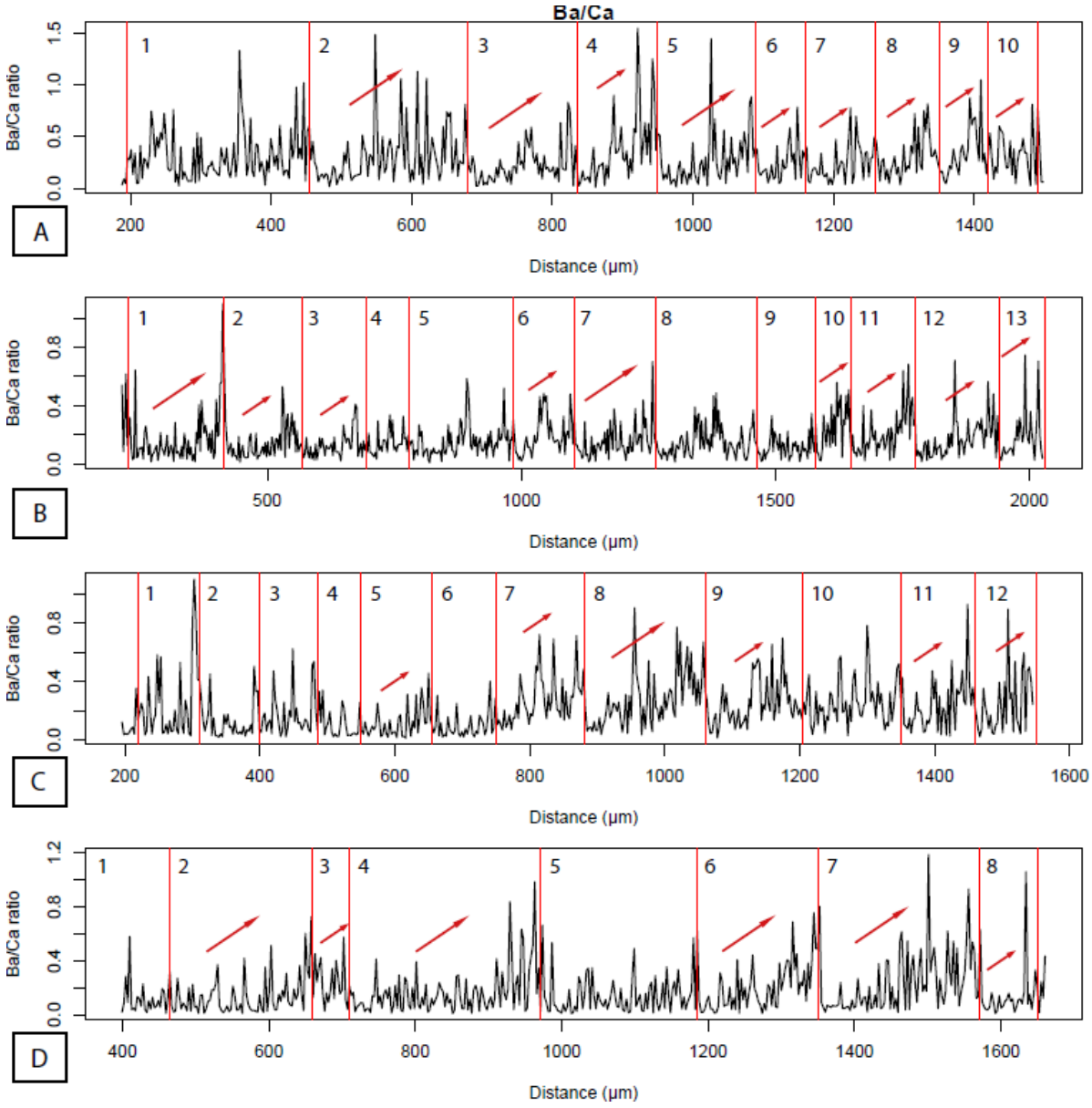

Figure 15: Ba/Ca transect elemental profiles for samples PS33L (A), PS34L (B), TGR11L (C) and PS15L (D) from LA-ICP-MS. Red lines show where growth lines occur, as indicated by Cu peaks in the same transect, and arrows highlight the general increasing trend in Ba/Ca ratios across each growth increment. Examples of weakly bimodal distributions are observed in increments 3, 4 and 5 in profile A, and increments 5, 6, 7, 8 and 12 in profile B. Distance (µm) begins at oldest shell carbonate through to most recently accreted shell.

Figure 12 shows a generally repeating pattern of increasing Ba/Ca across macro-increments. The trend of Ba/Ca is typified by erratic peaks that result in an overall increase. Ba/Ca concentration is generally lowest at the start of a macro-increment and at its maximum towards the dark organic band. An abrupt reduction in Ba/Ca occurs

across the dark organic bands, and a repeat of the aforementioned trend occurs, from low Ba/Ca concentration to high Ba/Ca concentration. Apparently superimposed on this trend is a weakly bimodal pattern. This is particularly evident in samples PS33L, PS34L, TGR11L and PS15L (Figure 15), but is apparent in the many of the 58 shells analysed.

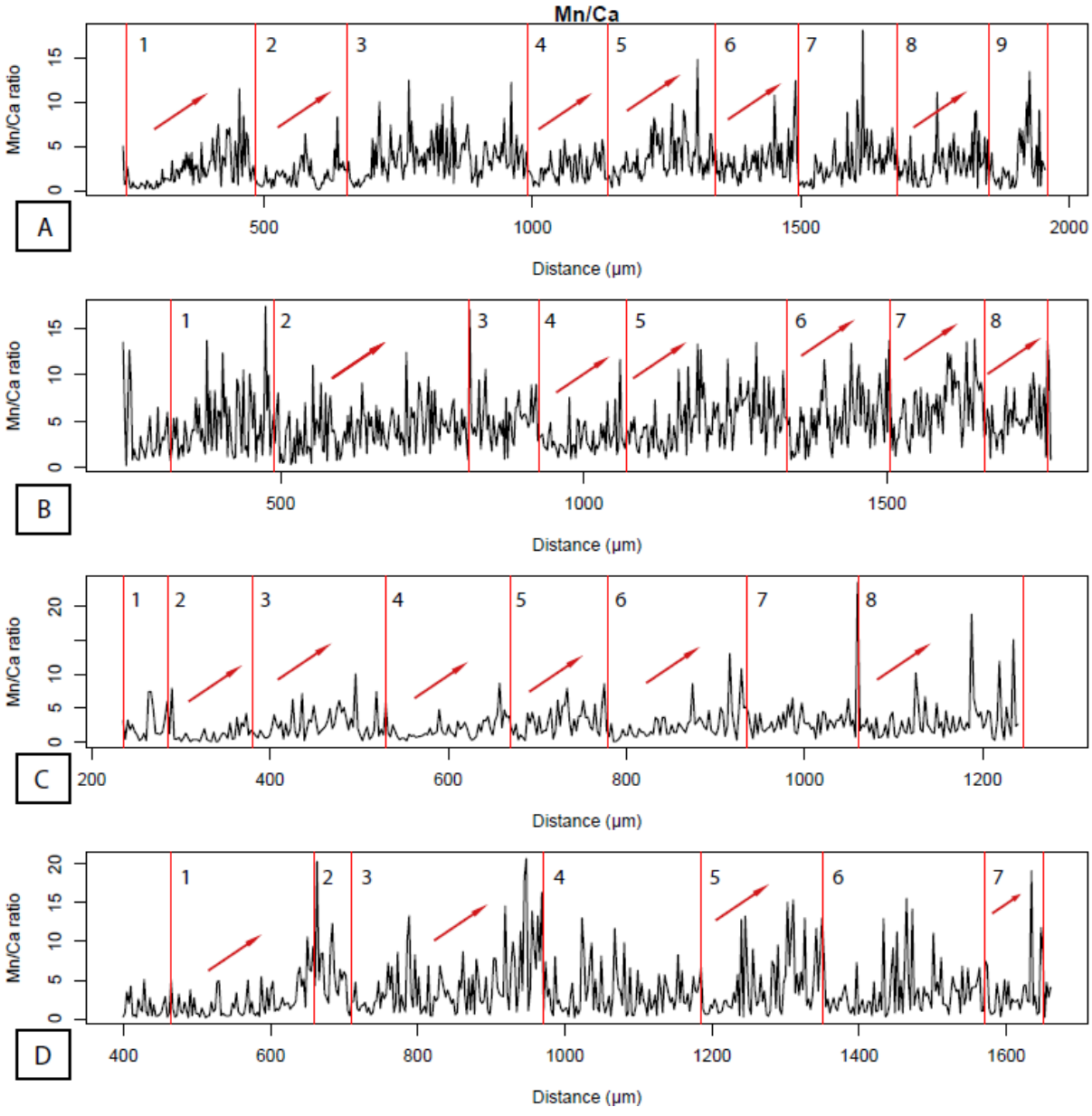

Figure 16: Mn/Ca transect elemental profiles for samples PS38L, PS65, PS66 and PS15L from LA-ICP-MS. Red lines show where growth lines occur, as indicated by Cu peaks in the same transect, and arrows highlight the general increasing trend in Mn/Ca ratios across each growth increment. Examples of what appear to be weakly bimodal distributions are observed in increments 2 and 3 of

profile A, and increments 3 and 5 of profile D. Distance (µm) begins at oldest shell carbonate through to most recently accreted shell.

Figure 16 shows an increasing trend in Mn/Ca, which generally repeats across each carbonate macro-increment and is similar to parts of the signal exhibited by Ba/Ca. A weakly bimodal distribution in Mn/Ca concentration is also observed for a number of the macro-increments, such as increment 3 in profile A, increment 5 in profile B, and increment 5 in profile D. The majority of patterns exhibited in the Mn/Ca transects appear to be in phase with the Ba/Ca patterns, although in some cases there appears to be a decrease after the second peak prior to the dark organic growth line.

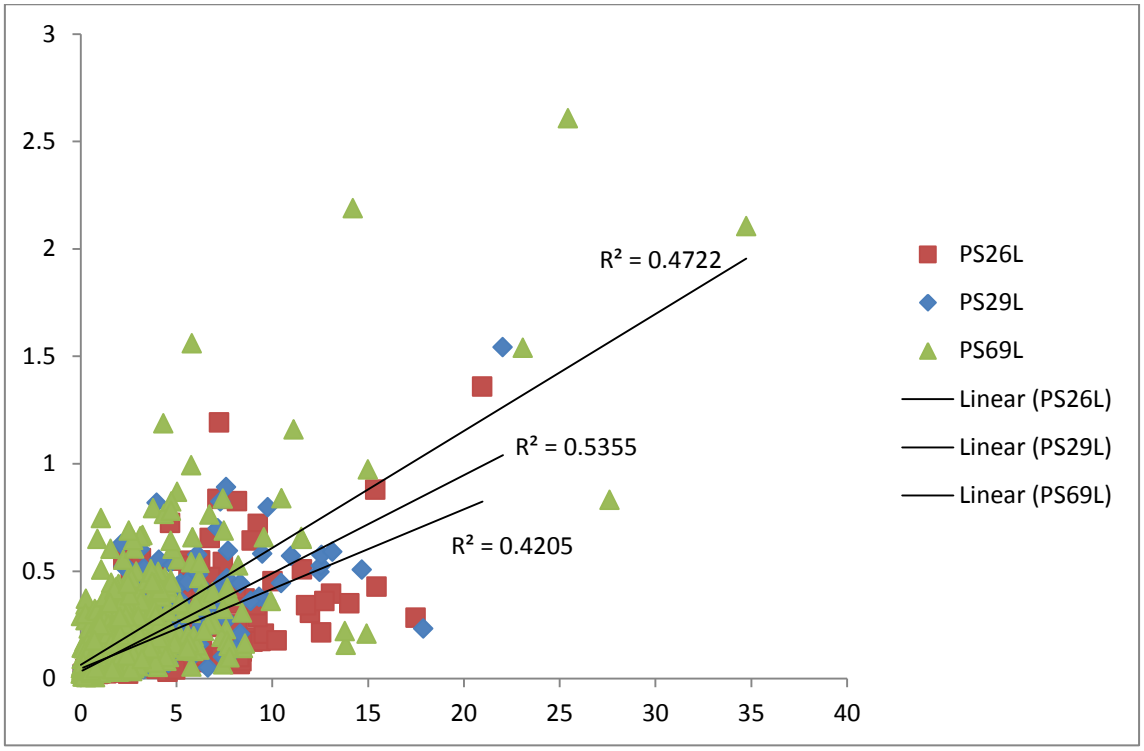

Figure 17: Correlation between Ba/Ca and Mn/Ca with trendline and R^2 values from three shells (PS26L, PS29L and PS69L) picked at random

The correlation between Ba/Ca and Mn/Ca for three random shells is determined in Figure 17. These correlations indicate that changes in Ba and Mn might be responding to something similar. These correlations are not strong (R2 = 0.5355, 0.4722, 0.4205), however considering the degree of noise apparent in the data and the inherent variability

in nature, this is not unexpected and the relationship between the two variables is not insignificant.

DISCUSSION

Lake Alexandrina

Lake Alexandrina is an unusual site in that the modern-day hydrology is heavily regulated to maintain a regular lake water level, both by locks upstream of the lake and by the Goolwa barrages, which control the degree of sea water incursion. A typically seasonal dilution of lake water salinity during winter rains and high river flow, and increases in salinity during summer due to lower river flows and evaporation are therefore not characteristic of contemporary Lake Alexandrina. Instead, lake water salinity reaches a maximum in winter, exhibiting an inverse relationship with lake water temperature (Figure 18). This is because, in general, the marine barrages are closed in summer and autumn due to low river flow, high evaporation and high irrigation extraction, and are re-opened again in late winter and spring (K. Walker pers. comm. 2014). High salinities in winter are caused by the influx of more salt from local catchments transported with flows from increased rainfall (K. Walker pers. comm. 2014).

Shell carbonate morphology and its relation to mussel growth

In order to understand the controls on shell micromorphology, the incorporation of metals into the shell matrix, and their respective use as proxies for palaeo-climate and -environmental studies, it is important to first understand the nature of shell growth and the occurrence and control behind annual periodicity in growth increments, and to then attempt to validate the occurrence of annuli within the subject species (Jones 1983).

Velesunio ambiguus growth increments observed under light microscopy and SEM appear to support the mechanism of shell growth and development proposed by Checa (2000). In the direction of growth that dictates the thickness of the shell, prismatic aragonite is deposited in a narrow layer to the inner periostracum, upon which tabular nacre crystallites nucleate (Checa 2000). Shell composition is then dominated by this tabular aragonite and defines the micro-increment structure in *V. ambiguus* (Figures 6 and 7).

The shell samples from the Point Sturt and Tolderol Game Reserve populations exhibit and overall increase in micro-increment width from youngest to oldest, which implies an increase in growth rate with age (Figure 5).This observation contrasts with previous reports that fastest growth occurs in the earliest years of shell development as an ontogenetic effect, due to primary energy expenditure spent on shell growth prior to reaching sexual maturity (Walker 1981, Kennedy et al. 2001). One reason for this disparity might be that changes in environmental conditions during the lifespan of the mussels studied here may have had a stronger influence on growth rate than the inherent biological control.

ANNUAL GROWTH INCREMENTS

Very few studies have been made that discuss the periodicity of growth increments in the genus, *Velesunio*. Previously, Humphrey (1984) provided age estimates for *V. angasi* using growth lines that very likely were formed with an annual periodicity, and Durand (1992) used oxygen isotope ratios to confirm that growth lines in *V. wilsonii* were annuli. Walker (1981, 2001) noted that *V. ambiguus* appeared to show annual growth-interruption lines, and estimates of age have been made from these. It is also suggested, however, that disturbances in growth due to flood and drought could also be

manifested as a dark interruption line, and that validation of growth annuli should be made for each population studied.

Bivalve shell development is dictated by the extrinsic factors associated with seasonality, with accretion of carbonate during periods of fast growth and organic material during slow growth (dormancy). This changing growth rate, which is governed by the ambient environment, gives rise to annual growth increments. The majority of bivalve shells exhibit growth increments that develop with an annual periodicity (Lutz and Rhoads 1980). In terms of growth parameters, Walker et al. (2001) describes temperature as largely influencing growth and activity in *V. ambiguus*. The species is also particularly adept in surviving salinity extremes up to 3g/L, due to a tight valve seal (Walker et al. 2001). Extended closure of the shell valves has been shown to induce a disturbance line in many other species of bivalve (Thompson et al. 1980, Day 1984, Vakily 1992). These are known as false lines, as they do not occur with an annual periodicity and are representative of abnormal environmental disturbances. In previous studies, false line development has been attributed to several factors including dredging and change of temperature (Haskin 1954), scarcity of food (Comfort 1957), and pollution (Negus 1966). As an implication, error may exist in the counting of increments and aging of shells, due to the potential occurrence of false lines.

With 12ºC described as the lower limit for growth in *V. ambiguus* and an effective growing season of 11 months in the Lower Murray, in addition to the co-incidence of highest salinity levels in Lake Alexandrina during the coldest months of the year, it is suggested that growth lines form in winter. As the winter mean instrumental conductivity readings in Lake Alexandrina remain below 1000 µm (Figure 18), and salinities that cause disturbance lines (< 5558 µS/cm) are often associated with

abnormal climate events such as drought, there is reason to infer that the macro-increments observed in the samples of this study are driven by low winter temperatures and are true annuli.

LIMITATIONS OF GROWTH INCREMENT ANALYSIS

Following on from the assumption that macro-increments in *V. ambiguus* are annuli, the age of shells from Point Sturt varied from approximately > four years to >15 years, and from Tolderol Game Reserve, approximately > six years to > 11 years. However, one limitation of the use of *V. ambiguus* in Lake Alexandrina is that, irrespective of whether growth increments are annual or not, macro-increment counts of samples are not a true representation of the number of increments formed over the life of the organism, due to removal of outer shell layers via erosion (Figure 2). This is a limitation previously identified in a study of aging and validating annual growth increments in freshwater mussel shells (Rypel et al. 2008). This is a trait endemic across both the Point Sturt and Tolderol Game Reserve populations, probably due to the inability to maintain anchorage when live (Walker et al. 2001), and weathering of dead samples. It may be possible to find live populations in more protected aquatic environments that exhibit lower degrees of damage to the shell for use in similar studies.

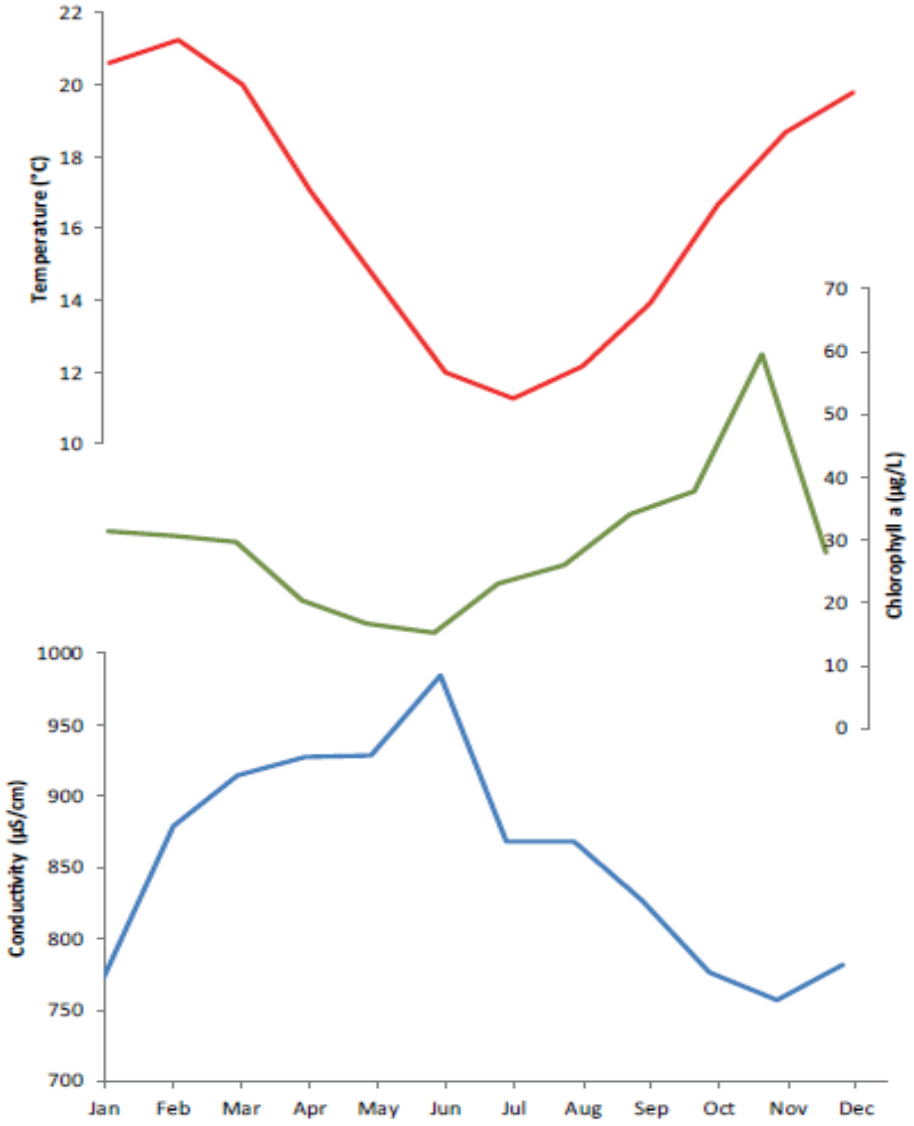

Figure 18: Temperature, chlorophyll a biomass and conductivity mean values for Lake Alexandrina from 1970 - 2014.

Shell micromorphology

Shell micromorphology can offer valuable information into the ontogenetic controls and biological mechanisms of bivalves, and the influence of their surrounding environment at intra-annual resolutions.

DAILY INCREMENTS

In the Lower Murray and Lake Alexandrina, the effective growing season for *Velesunio ambiguus* is 11 months of the year, i.e. ~335 days, however this period is likely to vary considerably (Walker 1981). The number of micro-increments per macro-increment varies between 67 and 373, with a mean of 221. Assuming that micro-increments arise from a periodic phenomenon, the periodicity of their deposition is most comparable to a daily cycle. Of other potential cycles, a semi-diurnal tidal cycle (~12.4 hr) would result in > 670 layers (Beentjes and Williams 1986, Kim et al. 1999), and a fortnightly cycle would form inverted patterns of either ~13 or ~15 thinner lunar-daily (24.8 hr) micro-increments associated with spring-tides, and thicker lunar-daily micro-increments associated neap-tides (Schöne and Surge 2012). As micro-increment width occurs with a bimodal pattern over the growing year, it is tentatively concluded that micro-increments develop with a daily periodicity. If this is true, variability in the number of micro-increments per macro-increment may be a useful marker of the duration of growing season through time, constrained by the extent of the warm/fresh conditions conducive to growth. The formation of discrete daily growth increments, or growth driven by circadian periodicity, was simultaneously shown to occur in bivalves by Pannella and MacClintock (1968), Clark (1968) and House and Farrow (1968), and has since been supported in a number of studies (Chauvaud et al. 1998, Schwartzmann et al. 2001). Daily micro-banding appears to be a widespread occurrence across this class of mollusca. Driving this pattern in shell markings is an endogenous time-keeping mechanism that controls the changing rates of shell formation, which is constantly re-set by environmental pacemakers, such as light, tides and food availability (Schöne and Surge 2014). It is these pacemakers that drive the formation of daily and sub-daily

increments. Considering diurnal (24.84 hr) tidal influence (and associated food availability) is usually observed in bivalves that populate the inter-tidal and sub-tidal zones in coastal regions (Richardson 1987, Richardson 1988), and Lake Alexandrina is now a eustatic, freshwater lake generally disconnected from the sea by barrage use (Geddes 1988), it is suggested that discrete daily growth is likely induced by the presence of a light/dark cycle (Kim et al. 2003).

On average, 221 micro-increments were observed per 'annual' growth increment, excluding three potential outliers whose micro-increment number of 405, 414 and 502 days may reflect possible miscounts or missing growth bands. It is suggested that the remaining days of the year (144 on average) were spent in dormancy due to environmental conditions outside the growth parameters for *V. ambiguus.* Such conditions are most likely temperature falling < 12°C during winter months in Lake Alexandrina, and possibly significant rises in salinity (< 3g/L).

High-resolution shell geochemistry

Changes in elemental geochemistry can also offer valuable information into the biology of mussels and their surrounding environment at sub-annual (perhaps daily) timescales. The majority of bivalves used for sclerochronology consist of both inner and outer carbonate layers (Schöne and Surge 2012).

Due to the morphology of *V. ambiguus* shells, which does not appear to include an outer layer, it was necessary to analyse the inner shell layer for geochemistry. Previous studies that focus on obtaining geochemical and isotopic proxies from the shells of bivalves generally avoid sampling the inner shell layer of bivalves due to shell dissolution, and therefore potential geochemical archival loss, during anaerobic metabolism (Schöne and Surge 2012). Carroll and Romanek (2008), however, suggest

that the similarity in elemental profiles from the inner shell and outer shell layers of freshwater bivalve, *E. complanata*, indicates that, despite the suggestion for potential historic episodes of shell dissolution, both layers accurately document the same geochemical information, but in relative proportions.

CU/CA PROFILES

Copper levels within the organic growth lines far exceed concentrations within the shell aragonite, probably due to the higher affinity of the metal with organic material (Tynan et al. 2005). This trend of copper relating closely to the organic content of the shell was similarly observed in the elemental composition of the freshwater bivalve, *Elliptio complanata* (Carroll and Romanek 2008). Reasons for the variability in Cu concentration both within and between shells are not clear. It is possible that the amount of Cu within the dark organic growth lines is merely reflective of the amount of organic matter. Alternatively, changes in Cu concentration may reflect the state of organic degradation (i.e. loss of Cu-bearing compounds to varying degrees) or changes in the uptake of Cu during the life of the mussel. Further research is required to evaluate these possibilities. For the purpose of this study, copper peaks were found to be a useful geochemical marker of the position of the dark organic growth lines within a LA-ICP-MS geochemical transect and were therefore used to constrain, in addition to cross-sectional photographs, the geochemical composition of individual growth increments.

MG/CA & SR/CA PROFILES

Elemental ratios of Mg/Ca and Sr/Ca are commonly used to infer past climate and hydrological change (Klünder et al. 2008). A variation of patterns are observed in the elemental profiles from laser transects. LA-ICP-MS transects across the umbo region of

V. ambiguus suggest that for this species, or in this setting, this interpretation is unlikely to be robust. This is likely due to the crystal polymorph of $CaCO_3$ in *V. ambiguus*, aragonite, of which the entirety of the shell is composed. Owing to the smaller lattice structure of aragonite, magnesium concentrations in aragonitic shells are consistently lower than for calcitic shells, whereby Mg^{2+} ions can more readily substitute into the crystal lattice. Substitution of Sr^{2+} over Mg^{2+} for Ca^{2+} is common in an aragonitic lattice, as ions with radii greater than Ca^{2+} are favoured, as opposed to calcite where preferentiality for magnesium and strontium ions is reversed (Mann 1982). This may explain the greater variance in Sr/Ca concentrations than Mg/Ca across transects. Indiscrete patterns exhibited by Mg/Ca and Sr/Ca could be attributed to strong ontogenetic controls on the uptake of these metals by this species, as shown in the fan mussel, *Pinna nobilis*, and the southern quahog, *Mercenaria campechiensis* (Freitas et al. 2005, Surge and Walker 2006).

BA/CA AND MN/CA PROFILES

In contrast to Mg/Ca and Sr/Ca, changes in Ba/Ca and Mn/Ca exhibited marked patterns which appear to be consistent across numerous samples. A pronounced oscillation, as shown in Figures 12 and 13, is characterised by low concentrations of the elemental ratios in the beginning of the growing season, with an overall increase (albeit erratic) through to the end of the growing season (marked by a dark growth band). There appears to be two modes of this oscillation. First and most commonly, a bimodal distribution occurs across growth increments, with a minimum concentration of the elemental variables at the beginning of the growing season increasing to a first peak, followed by a sharp decrease in concentration and a second peak that marks the end of the growing season. A second mode is also observed, characterised by overall

increasing concentrations across the growing season to a single peak. In both cases, the signal is extremely noisy. These modes are inferred to represent, in part, the nature of the seasonal biological and hydrological cycles.

Barium and manganese have previously been reported in a number of bivalves to reflect periods of high primary productivity (Stecher et al. 1996, Vander Putten et al. 2000, Lazareth et al. 2003). Barium has been shown to be incorporated into/onto phytoplankton, and barite is a common precipitate in organic-rich micro-environments (Bishop 1988, Dehairs et al. 1990, Stroobants et al. 1991). As filter-feeders, both phytoplankton and particulate barite is ingested by mussels, whereupon barium is incorporated during the calcification of new shell matrix. In the hard clam (*Mercenaria mercenaria*) and the surf clam (*Spisula solidissima*) barium peaks were associated with episodic increases in phytoplankton (Stecher et al. 1996). Barium associations in the blue mussel (*Mytilus edulis*) and the mangrove pearl oyster (*Isognomon ephippium*) were also reported to coincide with seasonal changes in primary production and phytoplankton blooms associated with increased river discharge (Vander Putten et al. 2000, Lazareth et al. 2003). The correlation between barium and manganese in the last two instances has been reason to suggest that manganese concentrations are also governed by changes in primary productivity (Lazareth et al. 2003). In support of this, there have been studies that illustrate the association of phytoplankton blooms and increases in suspended particulate Mn (Morris 1971, Sunda and Huntsman 1988).

The Ba/Ca and Mn/Ca profiles in *V. ambiguus* shell studies from both study sites are suggested to be influenced by seasonal changes in primary productivity in Lake Alexandrina. Geddes (1988) described the seasonality of phytoplankton in Lake Alexandrina from variations in chlorophyll *a* concentration – an indicator of

phytoplankton biomass. Increases in the dominant phytoplankton, *Planctonema lauterbornii*, occur throughout spring and peak in late spring-early summer. Summer algal biomass falls sharply in summer, attributed to freshwater flushing of the lake, limited light availability due to elevated turbidity, and low nutrient supply, particularly NO_3/NO_2-N (Geddes 1988). A variable (small – strong) recovery in algal populations is recorded each year during March-May, before cessation of the growing season is driven by low winter temperatures in ~June-July (Geddes 1988). This yearly cycle is proposed to give rise to the bimodal distribution observed in both micro-increment width, Ba/Ca and Mn/Ca within many of the shell growth increments, whereby the two peaks represent the spring increase and the autumn recovery in phytoplankton, separated by a minimum representing summer declines (Figure 19).

It has been shown through stable isotope data that *V. ambiguus* derives most dietary carbon from algae (Bunn and Boon 1993). Growth rate is strongly correlated with phytoplankton abundance (Walker 1981). It is therefore suggested that increases in primary productivity of the lake effectively increase the food availability of the mussel, which in turn corresponds to an increased growth rate and therefore wider micro-increments.

The second, unimodal distribution is suggested to represent changes in the typical cycle of primary productivity in the lake, whereby parameters that generally cause the summer declines in phytoplankton (flushing, low light availability, low nutrient supply) may not be as severe in these growing seasons, allowing continual growth into autumn. The data from this study therefore suggest that changes in micro-increment width, Ba/Ca and Mn/Ca within the shells of V. ambiguus are potentially a source of seasonal

palaeo-productivity information. Such data could have a number of valuable applications, including studying the dynamics of seasonal carbon burial and release under differing climate/environmental states; better understanding ecological responses to climate and anthropogenic impacts through time; and as a source of indirect palaeo-hydrology and palaeo-climate information, owing to the inherent connection between aquatic productivity and river discharge.

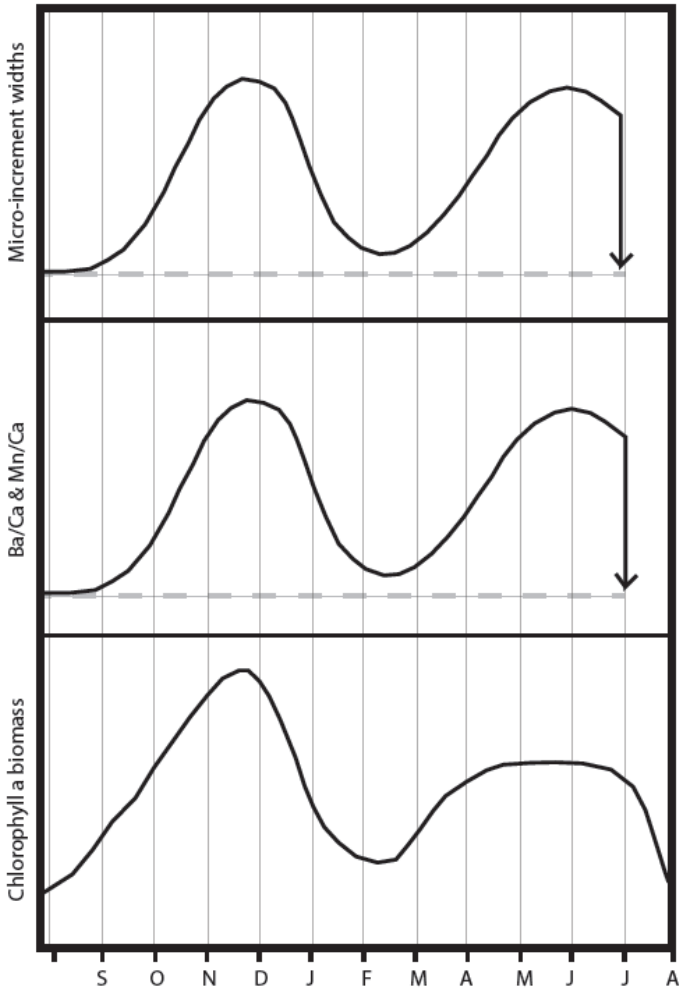

Figure 19: Schematic diagram of proposed trends in micro-structure and Ba/Ca and Mn/Ca geochemistry, as a response to chlorophyll *a* biomass (phytoplankton). Initial peak in late spring, with a sharp decline in summer, and a broad recovery from March – May/June. Downward arrow for July indicates dormancy due to low winter temperatures.

Limitations

The primary issue with interpretations made from geochemical records in the shells of bivalves is the influence of physiological effects, such as ontogenetic age, growth rate and metabolic activity (Schöne 2008). This has been reported in many studies to affect the trace element ratios recorded in shells (Stecher et al. 1996, Gillikin et al. 2005). Metabolic processes (vital effects) can govern the composition of the carbonate-secreting extrapallial fluid, which in turn reflects in the shell chemistry (Urey et al. 1951, Schöne 2008). Metabolism changes with ontogenetic age, which therefore influences the incorporation of metals into shell carbonate across the life of the organism. Physiology also controls shell growth rate. Rate of shell growth is greatest when environmental conditions approach the organism's physiological optimum, and reduces as optimal environmental conditions deteriorate (Schöne 2008). Physiological effects therefore significantly influence the geochemistry of the shell, and have implications for subsequent interpretation. A thorough understanding of the physiology of the species should be established and due considerations made when interpreting geochemical data for a study of this nature.

Direction

Due to the preliminary nature of this study, limitations were encountered throughout the methodology that has led to suggested directions for future investigations.

MACRO- AND MICRO-STRUCTURE

An extended study to establish the true periodicity of shell macro- and micro-growth patterns in individual populations of *V. ambiguus* is suggested though a mark-and-recapture method, whereby the organism is collected from a site, marked on the ventral

margin and released for an extended period (> 1 year). The organism is then re-captured again to determine if the temporal frame is discretely reflected in additional growth – both the number of years (macro growth increments) and the number of days (micro-increments). This method has been successfully utilised in a number of studies (Peterson et al. 1985, Sejr et al. 2002, Villella et al. 2004) to establish the periodicities of shell growth patterns.

Alternatively, oxygen isotope ratio ($\delta^{18}O$) analysis on micro-milled growth increments using isotope ratio mass spectrometry (IRMS) could be used to confirm the annual periodicity of growth increments. The inverse relationship between temperature and the oxygen isotopic composition of molluscan carbonate has been documented in a number of studies (Anderson and Arthur 1983, Grossman and Ku 1986, Versteegh et al. 2009). A clear oscillation should be evident in the $\delta^{18}O$ across growth increments, reflecting seasonal temperature throughout the year. This is a more time-effective method of determining annual growth periodicity, but daily increment growth cannot be validated through this technique. Furthermore, the competing effects of temperature and the isotopic composition of host water (McCrea 1950), which is linked to freshwater input and evaporation (Simpson and Herczeg 1991a, Simpson and Herczeg 1991b), may complicate this approach in Lake Alexandrina.

Studies should also be conducted for both riverine and lacustrine environments to compare the influence of lotic and lentic environments on shell morphology.

GEOCHEMISTRY

It is suggested that geochemical studies of *V. ambiguus* be extended to more populations from a variety of aquatic environments to confidently determine the cause of particular geochemical signals. Specifically, a collection of samples from a

freshwater population, such as Overway Corner, River Murray, should be studied to provide a natural pattern of trace element cyclicity (Tynan et al. 2006). For both micro-structural and geochemical analyses, a major limitation of this study has been the uncertainty as to the age of death of the specimens studied. Bomb-peak radiocarbon dating can achieve precise age determinations within a year in some circumstances (Hua and Barbetti 2004), and could be applied to these specimens to address this problem. If absolute and relative ages of mussels can be established, and associated chlorophyll *a* biomass data can be acquired or collected, direct comparisons and correlations between Ba/Ca and Mn/Ca and primary productivity for the same year can be made.

CONCLUSIONS

This study set out with the intent to test the suitability of the floodplain mussel, *Velesunio ambiguus*, as a palaeo-climatic and -environmental indicator. Although a direct proxy for physico-chemical parameters was not strictly determined, Ba/Ca and Mn/Ca ratios across shell laser transects have been tentatively inferred to represent an environmental parameter of a biological nature, that of primary productivity, which is an indirect function of the entire ecosystem. This inference is supported by the microstructure of *V. ambiguus*, which shows correlating trends to the Ba/Ca and Mn/Ca geochemical profiles.

This study highlights the significant potential of *Velesunio ambiguus* as a productivity and hydrological recorder, which could ideally be utilised in more remote regions of Australia, beyond the means of regular and consistent instrumental water monitoring, in addition to fossil shells in a variety of locations. However, further investigations on an increased sample size are necessary to improve understanding of this system. Future

studies should target a variety of populations from different environments with a greater handle on growth conditions. Once the influence of the environment and the causative mechanism behind barium and manganese uptake into shells has been solidly established, extension of these proxies into the fossil record may allow for reconstruction of ancient productivity and hydrological trends.

ACKNOWLEDGMENTS

Foremost, I'd like to thank my supervisor Dr. Jonathan Tyler for all his support, direction and patience throughout the year. Thanks to my co-supervisors, Dr. Chris Izzo and Prof. Bronwyn Gillanders for their guidance and feedback; to Prof. Keith Walker and Dr. Mike Geddes, for their assistance in fieldwork and their knowledge and expertise of the subject species and study site; to Honours coordinators, Dr. Katie Howard and Dr. Rosalind King; and to the staff at Adelaide Microscopy and particularly Aoife McFadden, for her help in training for SEM and LA-ICP-MS. The Mark Mitchell Foundation is thanked for provision of funds for travel and analytical costs.

REFERENCES

ANDERSON T. F. & ARTHUR M. 1983. Stable isotopes of oxygen and carbon and their application to sedimentologic and paleoenvironmental problems. *In* ARTHUR M.*, et al.* eds. *Stable Isotopes in Sedimentary Geology,* pp. 1-151. The Society of Economic Paleontologists and Mineralogists,

AYLIFFE L., MARIANELLI P., MORIARTY K., WELLS R., MCCULLOCH M., MORTIMER G. & HELLSTROM J. 1998. 500 ka precipitation record from southeastern Australia: Evidence for interglacial relative aridity. *Geology* **26**, 147-150.

BEENTJES M. P. & WILLIAMS B. G. 1986. Endogenous circatidal rhythmicity in the New Zealand cockle *Chione stutchburyi* (Bivalvia, Veneridae). *Marine & Freshwater Behaviour & Phy* **12**, 171-180.

BISHOP J. 1988. The barite-opal-organic carbon association in oceanic particulate matter. *Nature* **332**, p.24.

BOM 2014 Australia - Climate of Our Continent. Australian Government.

BUDDEMEIER R. W., MARAGOS J. E. & KNUTSON D. W. 1974. Radiographic studies of reef coral exoskeletons: Rates and patterns of coral growth. *Journal of Experimental Marine Biology and Ecology* **14**, 179-199.

BUNN S. & BOON P. 1993. What sources of organic carbon drive food webs in billabongs? A study based on stable isotope analysis. *Oecologia* **96**, 85-94.

BUTLER P. G., WANAMAKER A. D., SCOURSE J. D., RICHARDSON C. A. & REYNOLDS D. J. 2013. Variability of marine climate on the North Icelandic Shelf in a 1357-year proxy archive based on growth increments in the bivalve *Arctica islandica*. *Palaeogeography, Palaeoclimatology, Palaeoecology* **373**, 141-151.

CARRÉ M., SACHS J. P., SCHAUER A. J., RODRGUEZ W. E. & RAMOS F. C. 2013. Reconstructing El Niño-Southern Oscillation activity and ocean temperature seasonality from short-lived marine mollusk shells from Peru. *Palaeogeography, Palaeoclimatology, Palaeoecology* **371**, 45-53.

CARROLL M. & ROMANEK C. 2008. Shell layer variation in trace element concentration for the freshwater bivalve *Elliptio complanata*. *Geo-Marine Letters* **28**, 369-381.

CHAUVAUD L., THOUZEAU G. & PAULET Y.-M. 1998. Effects of environmental factors on the daily growth rate of *Pecten maximus* juveniles in the Bay of Brest (France). *Journal of Experimental Marine Biology and Ecology* **227**, 83-111.

CHECA A. 2000. A new model for periostracum and shell formation in Unionidae (Bivalvia, Mollusca). *Tissue and Cell* **32**, 405-416.

CLARK G. R. 1968. Mollusk shell: daily growth lines. *Science* **161**, 800-802.

COMFORT A. 1957. The duration of life in molluscs. *Journal of Molluscan Studies* **32**, 219-241.

DAVIS H. & CALABRESE A. 1964. Combined effects of temperature and salinity on development of eggs and growth of larvae of *M. mercenaria* and *C. virginica*. *Fishery Bulletin* **63**, 643-655.

DAY M. E. 1984. The shell as a recording device: growth record and shell ultrastructure of *Lampsilis radiata radiata* (Pelecypoda: Unionidae). *Canadian journal of zoology* **62**, 2495-2504.

DEHAIRS F., GOEYENS L., STROOBANTS N., BERNARD P., GOYET C., POISSON A. & CHESSELET R. 1990. On suspended barite and the oxygen minimum in the Southern Ocean. *Global Biogeochemical Cycles* **4**, 85-102.

DESMARCHELIER J., GOEDE A., AYLIFFE L., MCCULLOCH M. & MORIARTY K. 2000. Stable isotope record and its palaeoenvironmental interpretation for a late Middel Pleistocene speleothem from Victoria Fossil Cave, Naracoorte, South Australia. *Quaternary Science Reviews* **19**, 763-774.

DIECK R. H. 2007 Measurement Uncertainty: Methods and Applications. (4th Edition edition). ISA - The Instrumentation, Systems, and Automation Society, Research Triangle Park, NC, USA.

DURAND K. 1992 Preliminary investigations into the use of freshwater molluscs (*Alathyria pertexta* and *Velesunio wilsonii*) from the Barkly karst, north west Queensland, as palaeoenvironmental indicators. Discipline of Geography, School of Life Sciences. University of Newcastle, NSW.

EPA 2014 Water quality monitoring data. In AGENCY E. P. ed. http://www.epa.sa.gov.au/environmental_info/water_quality/water_quality_monitoring_data: Environmental Protection Agency.

FENBY C. & GERGIS J. 2013. Rainfall variations in south-eastern Australia part 1: consolidating evidence from pre-instrumental documentary sources, 1788–1860. *International Journal of Climatology* **33**, 2956-2972.

FERGUSON J., JOHNSON K., SANTOS G., MEYER L. & TRIPATI A. 2013. Investigating δ13C and Δ14C within *Mytilus californianus* shells as proxies of upwelling intensity. *Geochemistry, Geophysics, Geosystems* **14**, 1856-1865.

FRANTSEVICH L., KORNIUSHIN A., PANKOV I., ERMAKOV A. & ZAKHARCHUK T. 1996. Application of molluscs for radioecological monitoring of the Chernobyl outburst. *Environmental Pollution* **94**, 91-100.

FREITAS P., CLARKE L. J., KENNEDY H., RICHARDSON C. & ABRANTES F. 2005. Mg/Ca, Sr/Ca, and stable-isotope (δ18O and δ13C) ratio profiles from the fan mussel *Pinna nobilis*: Seasonal records and temperature relationships. *Geochemistry, Geophysics, Geosystems* **6**.

GALLANT A. J. & GERGIS J. 2011. An experimental streamflow reconstruction for the River Murray, Australia, 1783–1988. *Water Resources Research* **47**.

GALLANT A. J. E., KIEM A. S., VERDON-KIDD D. C., STONE R. C. & KAROLY D. J. 2012. Understanding hydroclimate processes in the Murray-Darling Basin for natural resources management. *Hydrology and Earth System Sciences* **16**, 2049-2068.

GEDDES M. C. 1988. The Role of Turbidity in the Limnology of Lake Alexandrina, River Murray, South Australia; Comparisons between Clear and Turbid Phases. *Australian Journal of Marine and Freshwater Research* **39**, 201-209.

GELL P. A., BULPIN S., WALLBRINK P., HANCOCK G. & BICKFORD S. 2005. Tareena Billabong – a palaeolimnological history of an ever-changing wetland, Chowilla Floodplain, lower Murray–Darling Basin, Australia. *Marine and Freshwater Research* **56**, 441-456.

GILLIKIN D. P., LORRAIN A., NAVEZ J., TAYLOR J. W., ANDRÉ L., KEPPENS E., BAEYENS W. & DEHAIRS F. 2005. Strong biological controls on Sr/Ca ratios in aragonitic marine bivalve shells. *Geochemistry, Geophysics, Geosystems* **6**, 1-16.

GROSSMAN E. L. & KU T.-L. 1986. Oxygen and carbon isotope fractionation in biogenic aragonite: Temperature effects. *Chemical Geology: Isotope Geoscience section* **59**, 59-74.

HASKIN H. H. 1954. Age determination in molluscs. *Transactions of the New York Academy of Sciences* **16**, 300-304.

HOUSE M. R. & FARROW G. 1968. Daily growth banding in the shell of the cockle, *Cardium edule*.

HUA Q. & BARBETTI M. 2004. Review of tropospheric bomb 14C data for carbon cycle modeling and age calibration purposes. *Radiocarbon* **46**, 1273-1298.

HUMPHREY C. 1984 Biology and ecology of the freshwater mussel *Velesunio angasi* (Bivalvia: Hyriidae) in the Magela Creek, Alligator Rivers region, Northern Territory. Ph. D. Thesis, University of New England, Armidale.

IPCC 2013 Summary for Policymakers. In STOCKER T. F.*, et al.* eds. Climate Change 2013: the Physical Science Basis. Contribution of Working Group I to the Fifth Assessment report of the Intergovernmental Panel on Climate Change. Cambridge, United Kingdom and New York, NY, USA: Cambridge University Press.

JONES D. S. 1983. Sclerochronology: Reading the Record of the Molluscan Shell: Annual growth increments in the shells of bivalve molluscs record marine climatic changes and reveal surprising longevity. *American Scientist* **71**, 384-391.

KENNEDY H., RICHARDSON C., DUARTE C. & KENNEDY D. 2001. Oxygen and carbon stable isotopic profiles of the fan mussel, *Pinna nobilis*, and reconstruction of sea surface temperatures in the Mediterranean. *Marine Biology* **139**, 1115-1124.

KENNISH M. & OLSSON R. 1975. Effects of thermal discharges on the microstructural growth of *Mercenaria mercenaria*. *Environmental Geology* **1**, 41-64.

KIM W. S., HUH H. T., LEE J. H., RUMOHR H. & KOH C. H. 1999. Endogenous circatidal rhythm in the Manila clam *Ruditapes philippinarum* (Bivalvia: Veneridae). *Marine Biology* **134**, 107-112.

KIM W. S., HUH H. T., JE J. G. & HAN K. N. 2003. Evidence of two-clock control of endogenous rhythm in the Washington clam, *Saxidomus purpuratus*. *Marine Biology* **142**, 305-309.

KINSMAN D. J. J. & HOLLAND H. D. 1969. The co-precipitation of cations with $CaCO^3$—IV. The co-precipitation of Sr^{2+} with aragonite between 16° and 96°C. *Geochimica et Cosmochimica Acta* **33**, 1-17.

KLÜNDER M. H., HIPPLER D., WITBAARD R. & FREI D. 2008. Laser ablation analysis of bivalve shells–archives of environmental information. *Geological Survey of Denmark and Greenland Bulletin* **15**, 89-92.

LAZARETH C., PUTTEN E. V., ANDRÉ L. & DEHAIRS F. 2003. High-resolution trace element profiles in shells of the mangrove bivalve *Isognomon ephippium*: a record of environmental spatio-temporal variations? *Estuarine, Coastal and Shelf Science* **57**, 1103-1114.

LUTZ R. A. & RHOADS D. C. 1980. Growth patterns within the molluscan shell: an overview. *In* RHOADS D. C. & LUTZ R. A. eds. *Skeletal growth of aquatic organisms,* pp. 203-254. Plenum Press,

MANN R. 1982. The seasonal cycle of gonadal development in *Arctica islandica* from the southern New England shelf. *Fish. Bull* **80**, 315-326.

MCCREA J. M. 1950. On the isotopic chemistry of carbonates and a paleotemperature scale. *The Journal of Chemical Physics* **18**, 849-857.

MCDONALD J. 2000 Late Quaternary palaeoclimate reconstruction of central NSW as inferred from the stable isotope and trace element geochemistry of speleothems. BSc Hons thesis. University of Newcastle, Australia.

MCMICHAEL D. & HISCOCK I. 1958. A monograph of the freshwater mussels (Mollusca: Pelecypoda) of the Australian Region. *Marine and Freshwater Research* **9**, 372-508.

MEEHL G., ZWIERS F., EVANS J., KNUTSON T., MEARNS L. & WHETTON P. 2000. Trends in extreme weather and climate events: issues related to modeling extremes in projections of future climate change. *Bulletin of the American Meteorological Society* **81**, 427-436.

MILLS K., GELL P., GERGIS J., BAKER P. J., FINLAYSON C. M., HESSE P. P., JONES R., KERSHAW P., PEARSON S., TREBLE P. C., BARR C., BROOKHOUSE M., DRYSDALE R., MCDONALD J., HABERLE S., REID M., THOMS M. & TIBBY J. 2013a. Paleoclimate studies and natural-resource management in the Murray-Darling Basin II: unravelling human impacts and climate variability. *Australian Journal of Earth Sciences* **60**, 561-571.

MILLS K., GELL P., HESSE P. P., JONES R., KERSHAW P., DRYSDALE R. & MCDONALD J. 2013b. Paleoclimate studies and natural-resource management in the Murray-Darling Basin I: past, present and future climates. *Australian Journal of Earth Sciences* **60**, 547-560.

MOONEY S. 1997. A fine-resolution palaeoclimatic reconstruction of the last 2000 years, from Lake Keilambete, southeastern Australia. *The Holocene* **7**, 139-149.

MORRIS A. W. 1971. Trace metal variations in sea water of the Menai Straits caused by a bloom of *phaeocystis*. *Nature* **233**, 427-428.

NEGUS C. L. 1966. A quantitative study of growth and production of unionid mussels in the River Thames at Reading. *The Journal of Animal Ecology*, 513-532.

NEUKOM R. & GERGIS J. 2012 Southern Hemisphere high-resolution palaeoclimate records of the last 2000 years. The Holocene. pp. 501-524.

NICHOLLS N. 2004. The changing nature of Australian droughts. *Climatic Change* **63**, 323-336.

PANNELLA G. & MACCLINTOCK C. 1968. Biological and environmental rhythms reflected in molluscan shell growth. *Memoir (The Paleontological Society)*, 64-80.

PETERSON C. H., DUNCAN P., SUMMERSON H. & SAFRIT JR G. 1985 A mark-recapture test of annual periodicity of internal growth band deposition in shells of hard clams, *Mercenaria mercenaria*, from a population along the southeastern United States. UNC Sea Grant College Program.

RADKE L. C. 2000 Solute divides and chemical facies in south-eastern Australian salt lakes and the response of ostracods in time and space. PhD thesis: Australian National University, Canberra, Australia.

RICHARDSON C. 1988. Tidally produced growth bands in the subtidal bivalve *Spisula subtruncata*. *Journal of Molluscan Studies* **54**, 71-82.

RICHARDSON C. A. 1987. Tidal bands in the shell of the clam *Tapes philippinarum*. *Proceedings of the Royal Society of London. Series B, Biological Sciences* **230**, 367-387.

RYPEL A. L., HAAG W. R. & FINDLAY R. H. 2008. Validation of annual growth rings in freshwater mussel shells using cross dating. *Canadian Journal of Fisheries and Aquatic Sciences* **65**, 2224-2232.

SCHÖNE B. 2008. The curse of physiology—challenges and opportunities in the interpretation of geochemical data from mollusk shells. *Geo-Marine Letters* **28**, 269-285.

SCHÖNE B. & SURGE D. M. 2012 Treatise Online no. 46: Part N, Revised, Volume 1, Chapter 14: Bivalve sclerochronology and geochemistry. Treatise Online.

SCHÖNE B. R., DUNCA E., MUTVEI H. & NORLUND U. 2004a. A 217-year record of summer air temperature reconstructed from freshwater pearl mussels, *M. margarifitera*, Sweden. *Quaternary Science Reviews* **23**, 1803-1816.

SCHÖNE B. R., FREYRE CASTRO A. D., FIEBIG J., HOUK S. D., OSCHMANN W. & KRÖNCKE I. 2004b. Sea surface water temperatures over the period 1884–1983 reconstructed from oxygen isotope ratios of a bivalve mollusk shell (*Arctica islandica*, southern North Sea). *Palaeogeography, Palaeoclimatology, Palaeoecology* **212**, 215-232.

SCHÖNE B. R., ZHANG Z., RADERMACHER P., THÉBAULT J., JACOB D. E., NUNN E. V. & MAURER A. F. 2011. Sr/Ca and Mg/Ca ratios of ontogenetically old, long-lived bivalve shells (*Arctica islandica)* and their function as paleotemperature proxies. *Palaeogeography, Palaeoclimatology, Palaeoecology* **302**, 52-64.

SCHÖNE B. R. & SURGE D. M. 2014 Bivalve shells: ultra high-resolution palaeoclimate archives. PAGES Magazine. pp. 20-21. Bern, Switzerland: Läderach AG.

SCHWARTZMANN C., DURRIEU G., SOW M., CIRET P., LAZARETH C. & MASSABUAU J. C. 2001. In-situ giant clam growth rate behaviour in relation to temperature: A one-year coupled study of high-frequency noninvasive valvometry and sclerochronology. *Limnology and Oceanography* **56**, 1940-1951.

SEJR M., JENSEN T. & RYSGAARD S. 2002. Annual growth bands in the bivalve *Hiatella arctica* validated by a mark-recapture study in NE Greenland. *Polar Biology* **25**, 794-796.

SIMPSON H. J. & HERCZEG A. L. 1991a. Stable isotopes as an indicator of evaporation in the River Murray, Australia. *Water Resources Research* **27**, 1925-1935.

--- 1991b. Salinity and evaporation in the River Murray Basin, Australia. *Journal of Hydrology* **124**, 1-27.

STECHER H. A., KRANTZ D., LORD III C., LUTHER III G. & BOCK K. 1996. Profiles of strontium and barium in *Mercenaria mercenaria* and *Spisula solidissima* shells. *Geochimica et Cosmochimica Acta* **60**, 3445-3456.

STROOBANTS N., DEHAIRS F., GOEYENS L., VANDERHEIJDEN N. & VAN GRIEKEN R. 1991. Barite formation in the Southern Ocean water column. *Marine Chemistry* **35**, 411-421.

SUNDA W. G. & HUNTSMAN S. A. 1988. Effect of sunlight on redox cycles of manganese in the southwestern Sargasso Sea. *Deep Sea Research Part A. Oceanographic Research Papers* **35**, 1297-1317.

SURGE D. & WALKER K. J. 2006. Geochemical variation in microstructural shell layers of the southern quahog (*Mercenaria campechiensis*): Implications for

reconstructing seasonality. *Palaeogeography, Palaeoclimatology, Palaeoecology* **237**, 182-190.

THOMPSON I., JONES D. S. & DREIBELBIS D. 1980. Annual internal growth banding and life history of the ocean quahog *Arctica islandica* (Mollusca: Bivalvia). *Marine Biology* **57**, 25-34.

TYNAN S., EGGINS S., KINSLEY L., WELCH S. & KIRSTE D. 2005 Mussel shells as environmental tracers: an example from the Loveday Basin. In ROACH I. C. ed. Regolith 2005 - Ten Years of CRC LEME. pp. 314-317. CRC LEME.

TYNAN S., OPDYKE B., ELLIS D., BEAVIS S., WELCH S., KIRSTE D. & WALLACE L. 2006 Interpreting the trace element ratios of freshwater bivalve shells and their application to understand environmental variability. Regolith 2006 - Consolidation and Dispersion of Ideas. pp. 350-354.

UMMENHOFER C. C., ENGLAND M. H., MCINTOSH P. C., MEYERS G. A., POOK M. J., RISBEY J. S., GUPTA A. S. & TASCHETTO A. S. 2009. What causes southeast Australia's worst droughts? *Geophysical Research Letters* **36**, 1-5.

UREY H. C., LOWENSTAM H. A., EPSTEIN S. & MCKINNEY C. R. 1951. Measurement of paleotemperatures and temperatures of the Upper Cretaceous of England, Denmark, and the southeastern United States. *Geological Society of America Bulletin* **62**, 399-416.

VAKILY J. M. 1992 Determination and comparison of bivalve growth, with emphasis on Thailand and other tropical areas. WorldFish.

VANDER PUTTEN E., DEHAIRS F., KEPPENS E. & BAEYENS W. 2000. High resolution distribution of trace elements in the calcite shell layer of modern *Mytilus edulis*: environmental and biological controls. *Geochimica et Cosmochimica Acta* **64**, 997-1011.

VERSTEEGH E. A., TROELSTRA S. R., VONHOF H. B. & KROON D. 2009. Oxygen isotope composition of bivalve seasonal growth increments and ambient water in the rivers Rhine and Meuse. *Palaios* **24**, 497-504.

VILLELLA R., SMITH D. & LEMARIE D. 2004. Estimating survival and recruitment in a freshwater mussel population using mark-recapture techniques. *The American midland naturalist* **151**, 114-133.

VISCHER N. & NASTASE S. 2014 ObjectJ. Amsterdam, Netherlands: University of Amsterdam.

VONHOF H. B., JOORDENS J. C., NOBACK M. L., VAN DER LUBBE J. H., FEIBEL C. S. & KROON D. 2013. Environmental and climatic control on seasonal stable isotope variation of freshwater molluscan bivalves in the Turkana Basin (Kenya). *Palaeogeography, Palaeoclimatology, Palaeoecology* **383**, 16-26.

WALKER K. F. 1981 Ecology of Freshwater Mussels in the River Murray. Australian Government Pub. Service.

WALKER K. F., BYRNE M., HICKEY C. W. & ROPER D. S. 2001. Freshwater mussels (Hyriidae) of Australasia. *Ecology and evolution of the freshwater mussels Unionoida,* pp. 5-31. Springer,

WEFER G. & BERGER W. H. 1991. Isotope paleontology: growth and composition of extant calcareous species. *Marine Geology* **100**, 207-248.

WIDARTO T. H. 2007. Shell Form Variation of a Freshwater Mussel *Velesunio ambiguus* Philippi from the Ross River, Australia. *HAYATI Journal of Biosciences* **14**, 98-104.

WILSON C., FALLON S. & TREVORROW T. O. M. 2012. New radiocarbon ages for the Lower Murray River, South Australia. *Archaeology in Oceania* **47**, 157-160.

APPENDIX A: EXTENDED METHODOLOGY

1. Material and methods

Mussel shells submersed in water depths of ~1m were collected from two locations in Lake Alexandrina in April 2014. Under recommendation from Prof. Keith Walker (pers comms), a previously extensive shoal affected by the 2009 drought was targeted at Point Sturt, with 39 dead articulated samples and 47 single valves collected using hands and feet to locate. 11 dead samples and one live specimen were collected from Tolderol Game Reserve, submersed in ~1m water depths using hands and feet to locate. Water samples were taken in vials from both locations for water chemistry data. Mollusc samples were placed in frozen storage at 2-3ºC prior to shell preparation and water samples were refrigerated at 16ºC.

1.1 Preparation of shell cross-sections for analyses of crystal fabrics and geochemistry – using Schone et al. 2013 as a guide for shell and sample preparation

Shells were cleaned using reverse osmosis de-ionised water and a firm bristle brush to remove sediment and organic material accumulated on the periostracum and eroded surfaces. Samples were then rinsed with reverse osmosis de-ionised water and air-dried. Samples were given a coded label based upon an abbreviation of the species (Va – *Velesunio ambiguus*), sample site (e.g. PS – Point Sturt, TGR – Tolderol Game Reserve), numerical ordering and valve (L – left, R – right) (e.g. Va_TGR_1L). Sample height and length were then measured after McMichael and Hiscock (1958), as

illustrated in Figure 1. Articulated shells were then separated and all valves photographed using a LEICA DFC 320 D-SLR camera fixed to a tripod.

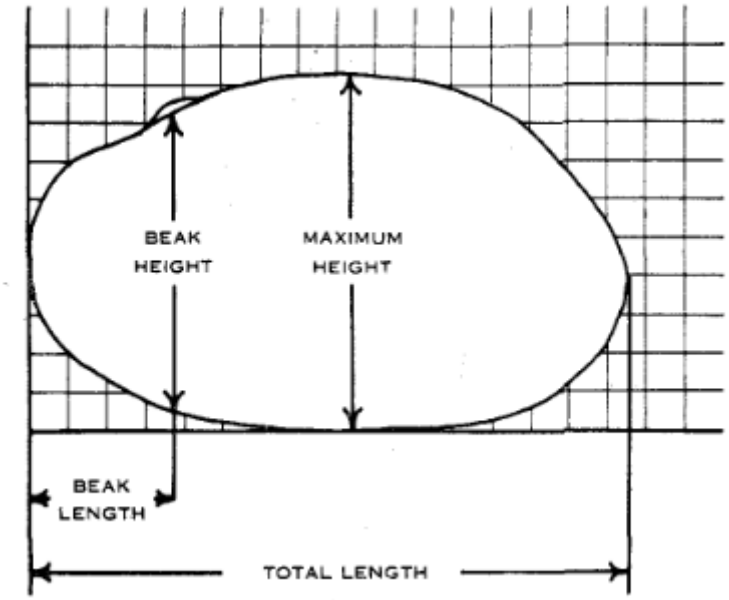

Figure 20: Scheme for measuring dimensions of mollusc shells. Modified from McMichael and Hiscock (1958)

Using a diamond saw, a subsample of left valves were cut into 2 cm sections that incorporated the entire growth axis, from umbo to shell margin. Sections were rinsed again with reverse osmosis de-ionised water to remove milled carbonate and air-dried. Sections were placed in 2.5 cm x 8.0 cm moulds and impregnated in a 15:2 mix of indium-spiked EpoFix resin and EpoFix hardener, and set overnight in a drying oven. Indium within the slides is used to signal when the background slide (rather than the sample) is being ablated during LA-ICP-MS, so that the data from the sample can be bracketed by indium peaks. Further sections of 2.5 mm thickness were cut along the growth axis using a low-speed Buehler IsoMet 1000 precision sectioning saw at a speed of 150 rpm, then ground to ~1.5 mm slides using 600 grit sandpaper (very fine) on a Buelher Metaserv 250 grinder/polisher at 250 rpm. Slides were then polished using three varying grades of lapping film (30 µm, 9 µm and 3 µm) on the same polishing

table at 250 rpm, and a further two hand polishes with a 3 µm diamond paste and a 0.04 µm colloidal silica solution. After each hand polish, slides were placed in a beaker of reverse osmosis de-ionised water which was placed in a sonicator for five minutes to remove polishing debris. After samples were dried with tissue paper, a carbon coat was applied to the surface of the slide in preparation for SEM analysis.

1.2 Examination of shell structure and microstructure – scanning electron microscopy (SEM) – using Schone et al. 2013 as a guide for SEM analysis

Growth increments and aragonite crystal structure were analysed under SEM using three polished sections from Tolderol Game Reserve, which were the best preserved of eight samples impregnated in resin. Slides were inserted into the QUANTA 500 Scanning Electron Microscope chamber. At a magnification of 43,000x (10kV) and using back-scatter electron imaging (BSE), transect imaging was undertaken across the sections in three different, evenly spaced locations, including the umbo, to scope within-shell variability in the number of micro-increments across growth increments. Transects were orientated perpendicular to growth increments in order to view the nature of the aragonite crystal fabric from the outer periostracum layer to inner surface.

Images from transects were combined together using the image composite editor program, Mircosoft ICE. Four images were combined at a time in order to maintain original resolution by uploading to the software package through the ‘New Structured Panorama’ option. Composite images were than combined together again to create continual images encompassing the entirety of each transect.

1.3 Geochemical analyses by LA-ICP-MS – using Schone et al. 2013 as a guide for LA-ICP-MS analysis

All major and trace geochemical data from cross-sectional transects were obtained using a New Wave UP-213 Nd:YAG laser-ablation system coupled to an Agilent HP-7500 inductively coupled plasma mass spectrometer (Adelaide Microscopy, University of Adelaide). The laser was used in accordance with the Up Series Nd:YAG Laser Ablation Systems Operators Manual February 2, 2001 provided by the manufacturer and the Agilent 7500 series ICPMS Hardware manual (Adelaide Microscopy, University of Adelaide).

Prior to inserting sample slides the laser-ablation system chamber, the carbon coat applied for SEM was removed using tissue paper and 70% ethanol. Sample slides and standards (standard silicate glass [NIST612 - elemental abundance of ~50 ppm] and carbonate [MACS-01]) were then mounted into the block mount. Beam spot size was set at 16 μm, with a laser repetition rate of 5 Hz and energy set to produce a fluence of 3.5-4.0 Jcm^{-2}, with argon as the ablation gas. Data were collected using time-resolved data acquisition from linear transects, and graphical interpretation of data was carried out using GLITTER data reduction software. Laser ablation times for each analysis was determined by dividing the length of each transect line (in microns) by the laser speed, 3 μm/s. 40 s was then added to this time to account for a preceding background measurement, equating to total acquisition time. Calibration was performed against the NIST 612 glass and MACS carbonate reference materials. Due to distinct morphological differences between the umbo and hinge region observed in *V. ambiguus* and the subject species used in other studies, namely the lack of hinge plate (which is often used to age specimens and the target of LA-ICP-MS, (Schöne et al. 2011)),

transects were conducted through the equivalent umbo region of the shell, where a condensed archive of growth increments forms within the inner shell layer (Widarto 2007). Batches of five transects were bracketed by three repeat analyses of NIST612 and two repeat analyses of MACS, allowing for measurement of the ablation yield, and monitoring of, and correction for, instrumental drift, degree of fractionation and plasma variances. A linear drift correction based on the analysis sequence and on the bracketing analyses of NIST612 and MACS, was applied to the count rate for each sample. 56.03 % CaO was used as the internal standard for aragonite. Samples were systematically analysed for a customised suite of major and trace elements, and trialled dwell times were modified to the most ideal parameters based upon varying concentrations of elements and the number of counts per second sensed by the detector (Table 1). As trace element concentrations throughout the sample were high enough to allow for a reduction in dwell time, which would still provide a sufficient signal to be recorded, the spatial resolution across the transect was increased. Data acquired was imported into GLITTER data reduction software and graphical interpretations generated.

Table 3: Trace elements analysed and associated dwell times

Element	7Li	23Na	24Mg	39K	43Ca	44Ca	55Mn	57Fe	63Cu	88Sr	115In	138Ba	208Pb
Dwell Time	0.2	0.01	0.05	0.05	0.01	0.01	0.05	0.05	0.1	0.1	0.1	0.05	0.1

1.4 Statistical analysis

1.51 SEM transect imaging

The nature of the aragonite crystal fabric within shell cross-sections were analysed from transect images acquired from the QUANTA 500 Scanning Electron Microscope. Shell

growth increments were defined by dark organic growth hiatuses within the samples. Growth increments (both light crystal fabric and dark layer) represent annual growth. Individual aragonite crystal layers bracketed by dark organic growth bands were counted to determine number of crystal layers deposited per annum, which in turn was used to correlate growth to environmental variables. Yet to be completed/confirmed.

1.52 Statistical analysis

Some statistical analysis will be performed on the data. Yet to be completed/confirmed. Instrumental water chemistry data for Lake Alexandrina were downloaded from the EPA (Environmental Protection Agency) South Australia website (EPA, 2014) and instrumental weather data (daily rainfall) were sourced from the Australian Government Bureau of Meteorology website (BOM, 2014). Instrumental data was used to correlate trends between isotope geochemistry preserved in growth increments of mussel shells and variances in weather and water chemistry data.

Method and materials summary

Sample collection

Mussel shells were collected from two locations in Lake Alexandrina in April 2014. Dead single and articulated shells were acquired from ~1 m water depths using hands and feet to locate. 39 dead articulated samples and 47 single valves were collected from Point Sturt, and 11 dead articulated sample and one live sample were collected from Tolderol Game Reserve. Water samples for each location were taken. Both shell and water samples were placed in cold storage (see Appendix A for detailed methodology).

Sample preparation

Samples were cleaned to remove organic material. Articulated samples were separated and all samples were catalogued based on their species, location of origin, numerical

ordering and valve side (left or right). Samples were measured according to McMichael and Hiscock (1958) and photographed (see Appendix A for detailed methodology).

Using a diamond saw, samples were cut into 2.5 cm wide sections to incorporate the entire growth axis from umbo to shell margin. Samples were impregnated in indium-spiked resin and set overnight. 2.5 mm sections were cut from the resin blocks along the growth axis of the shell. Slides were then polished and carbon coated, in preparation for scanning electron microscopy (see Appendix A for detailed methodology).

Scanning Electron Microscopy

Slides were inserted into the QUANTA 500 Scanning Electron Microscope chamber, and detailed analysis and transect imaging of shell structure and microstructure was conducted at 43,000x (10kV) magnification (see Appendix A for detailed methodology).

LA-ICP-MS

After removal of the carbon coating, slides were inserted into the New Wave UP-213 Nd:YAG laser-ablation system chamber for geochemical analysis. Transects perpendicular to growth increments were ablated using a beam spot size of 16 μm, with a laser repetition rate of 5 Hz and energy set to produce a fluence of 3.5-4.0 Jcm^{-2}. Data acquired were imported into GLITTER data reduction software and graphical interpretations generated (see Appendix A for detailed methodology).

Statistical Analysis

Using SEM images, approximate age of the molluscs were determined based on annual growth bands. Individual aragonite crystal layers bracketed by dark organic growth bands were counted to determine number of crystal layers deposited per annum, which in turn was used to correlate growth to environmental variables. Instrumental lake water

chemistry and weather data were sourced from the EPA SA website and Bureau of Meteorology website, respectively, which was then used to correlate trends in geochemical data to environmental variables.

APPENDIX B: EXTENDED RESULTS

TGR 1L	Transect 1	Transect 2	Transect 3
Incr. 1	102	286	156
Incr. 2	209	210	83
Incr. 3	164	190	168
Incr. 4	306	181	182
Incr. 5	227	173	86
Incr. 6	226	171	
Incr. 7	291		
Incr. 8	174		

TGR 4L	Transect 1	Transect 2	Transect 3
Incr. 1	157	167	82
Incr. 2	343	251	203
Incr. 3	298	315	198
Incr. 4	279	257	237
Incr. 5	170	130	
Incr. 6	260	263	121
Incr. 7	284	67	
Incr. 8	374		

TGR 87L	Transect 1	Transect 2	Transect 3
Incr. 1	358	334	169
Incr. 1a		116	174
Incr. 2	414	214	373
Incr. 3	502	361	
Incr. 4	405	355	325
Incr. 5	263		
Incr. 6	307	123	247
Incr. 7	230		
Incr. 8	183		

Tables 2-4 demonstrate the inconsistency along growth increments in the number of micro-increments. Dark grey cells (as in Table 4, Transect1) indicate where a growth

increment observed in an adjacent transect of the same shell was not observed. Red values indicate where correlation of growth increments and associated micro-increment counts was difficult to establish between adjacent transects. Purple values indicate abnormally high counts (outliers), which may be associated with red values. There is not a consistent increase or decrease micro-increment numbers evident across the transects.

Barium

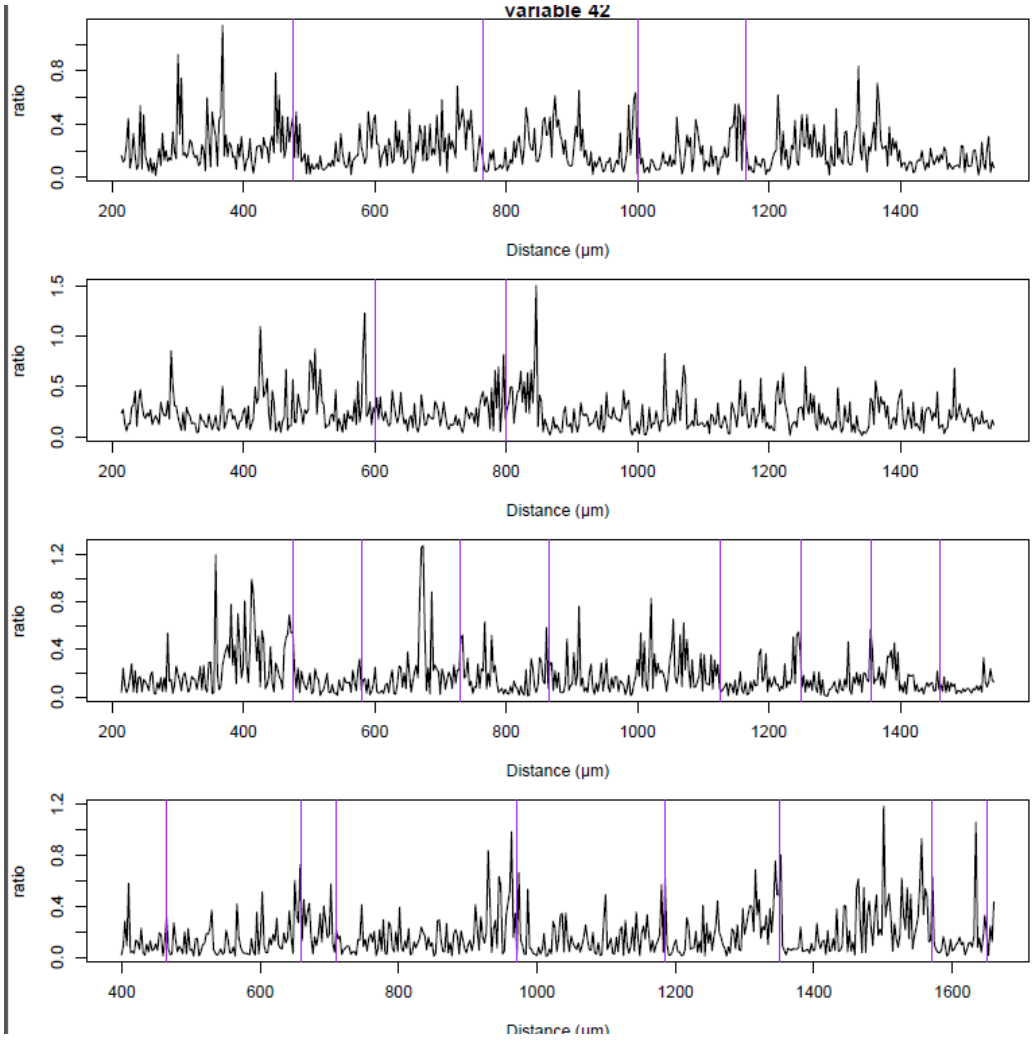

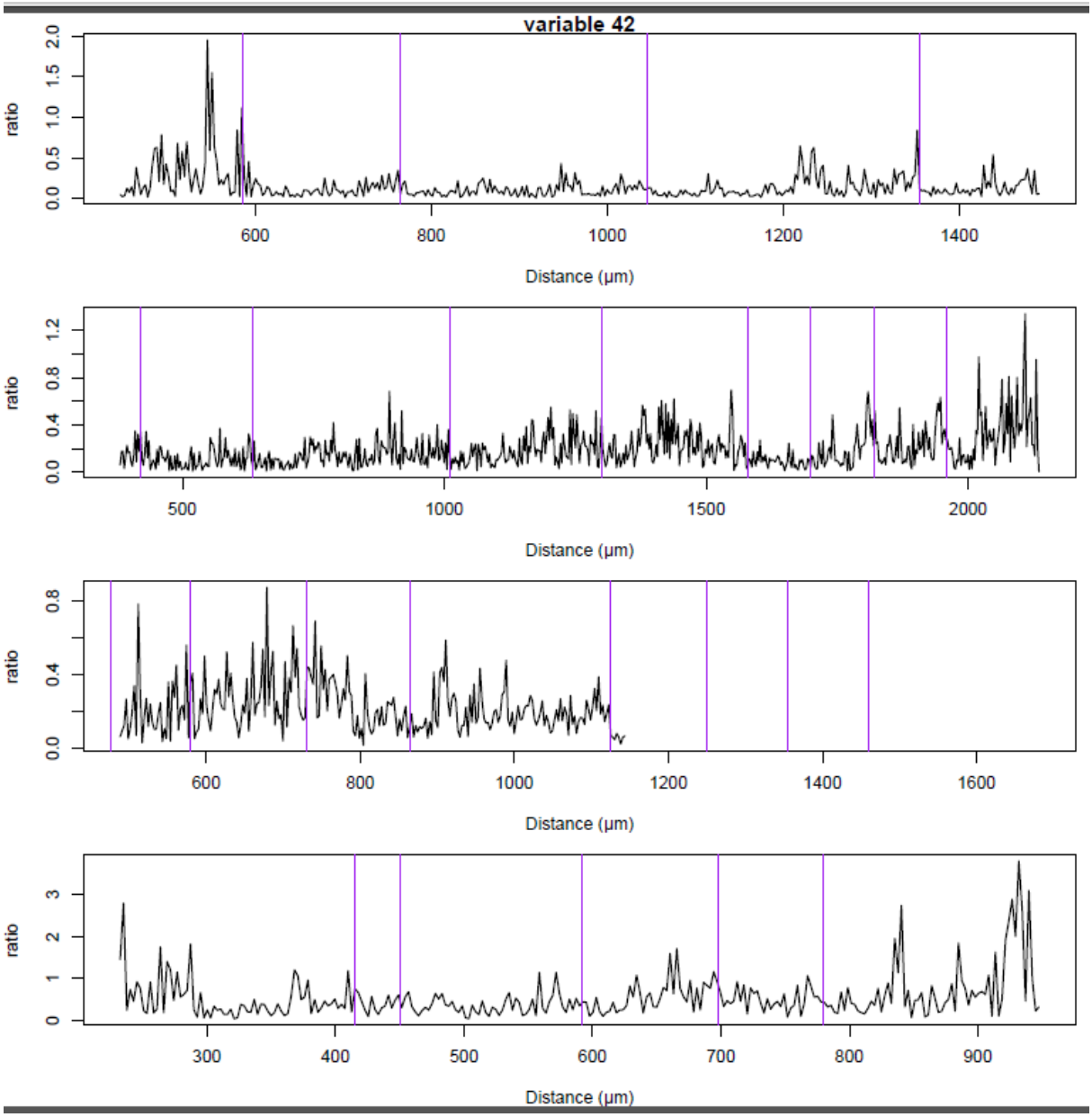
variable 42
ratio
0.0 0.5 1.0 1.5 2.0
600 800 1000 1200 1400
Distance (µm)
ratio
0.0 0.4 0.8 1.2
500 1000 1500 2000
Distance (µm)
ratio
0.0 0.4 0.8
600 800 1000 1200 1400 1600
Distance (µm)
ratio
0 1 2 3
300 400 500 600 700 800 900
Distance (µm)

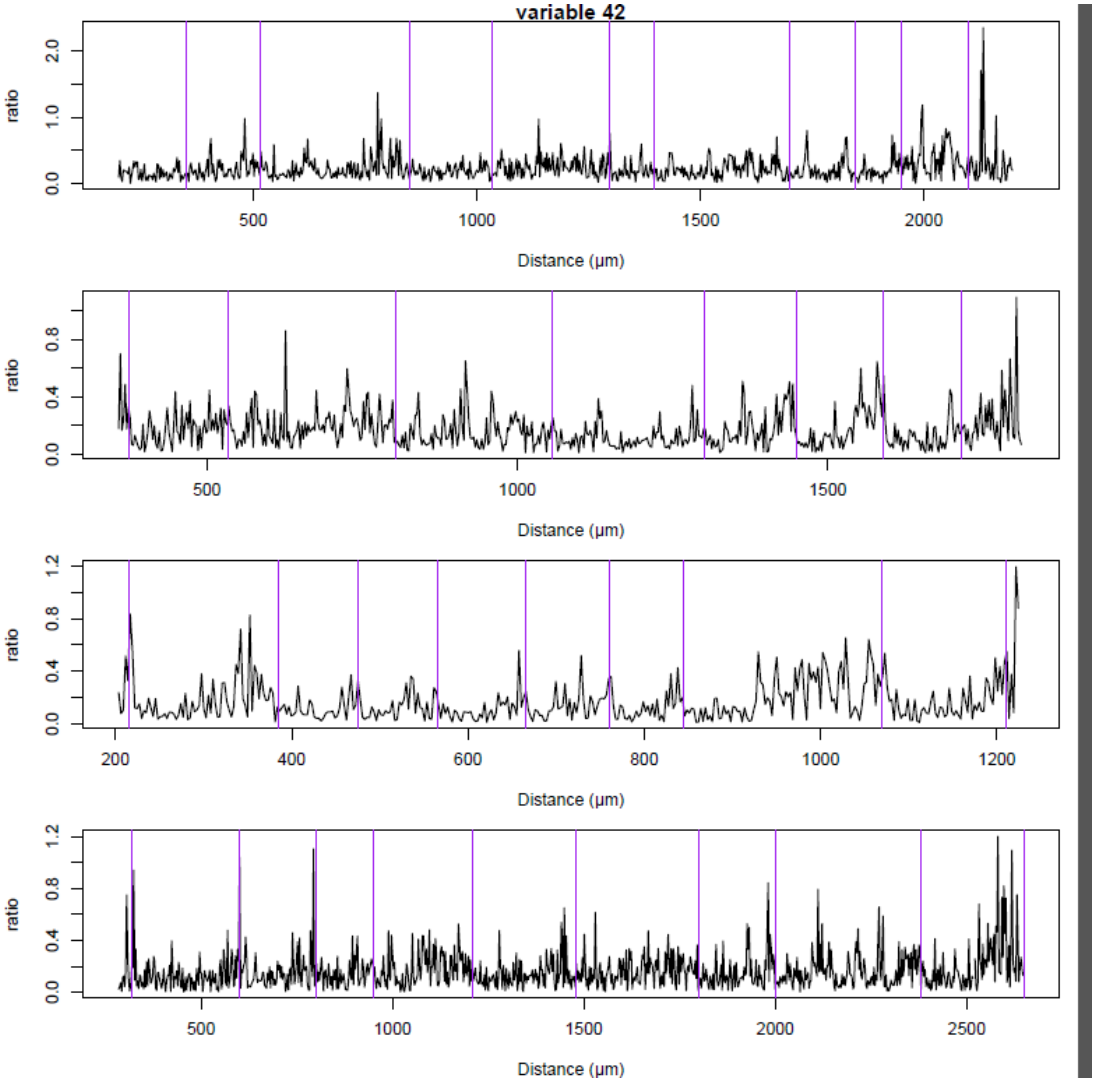
variable 42
ratio
0.0
1.0
2.0
500
1000
1500
2000
Distance (µm)
ratio
0.0
0.4
0.8
500
1000
1500
Distance (µm)
ratio
0.0
0.4
0.8
1.2
200
400
600
800
1000
1200
Distance (µm)
ratio
0.0
0.4
0.8
1.2
500
1000
1500
2000
2500
Distance (µm)

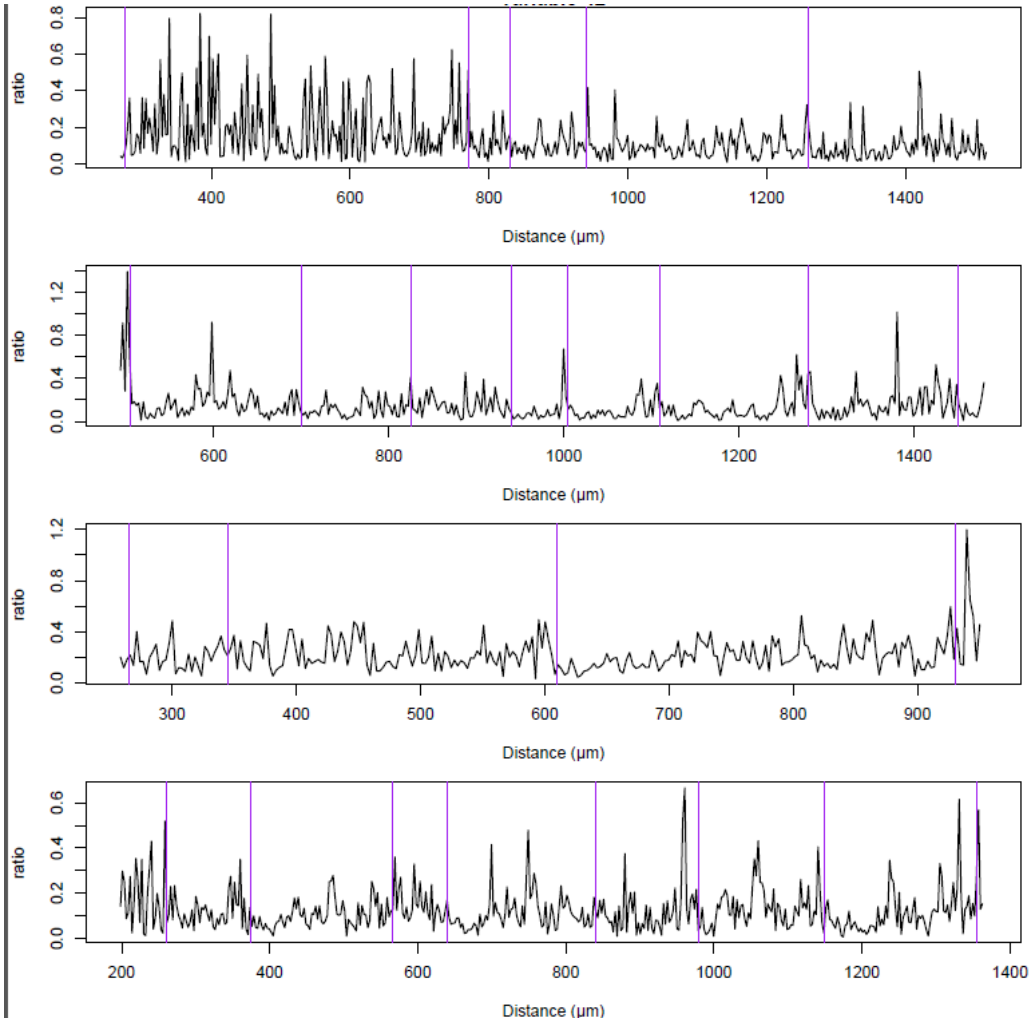
ratio
0.0 0.2 0.4 0.6 0.8
400 600 800 1000 1200 1400
Distance (µm)
ratio
0.0 0.4 0.8 1.2
600 800 1000 1200 1400
Distance (µm)
ratio
0.0 0.4 0.8 1.2
300 400 500 600 700 800 900
Distance (µm)
ratio
0.0 0.2 0.4 0.6
200 400 600 800 1000 1200 1400
Distance (µm)

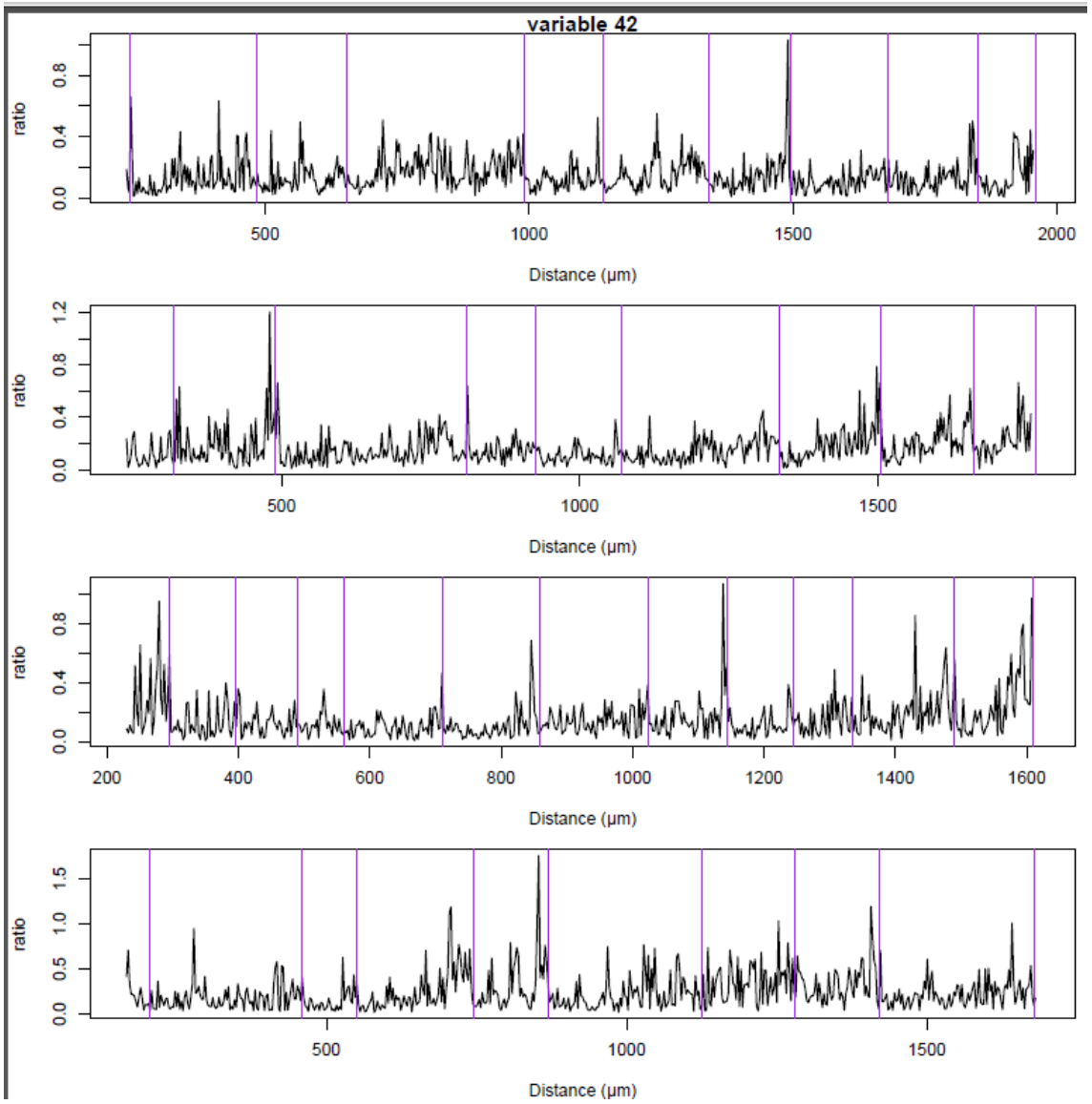
variable 42
ratio
0.0
0.4
0.8
500
1000
1500
2000
Distance (µm)
ratio
0.0
0.4
0.8
1.2
500
1000
1500
Distance (µm)
ratio
0.0
0.4
0.8
200
400
600
800
1000
1200
1400
1600
Distance (µm)
ratio
0.0
0.5
1.0
1.5
500
1000
1500
Distance (µm)

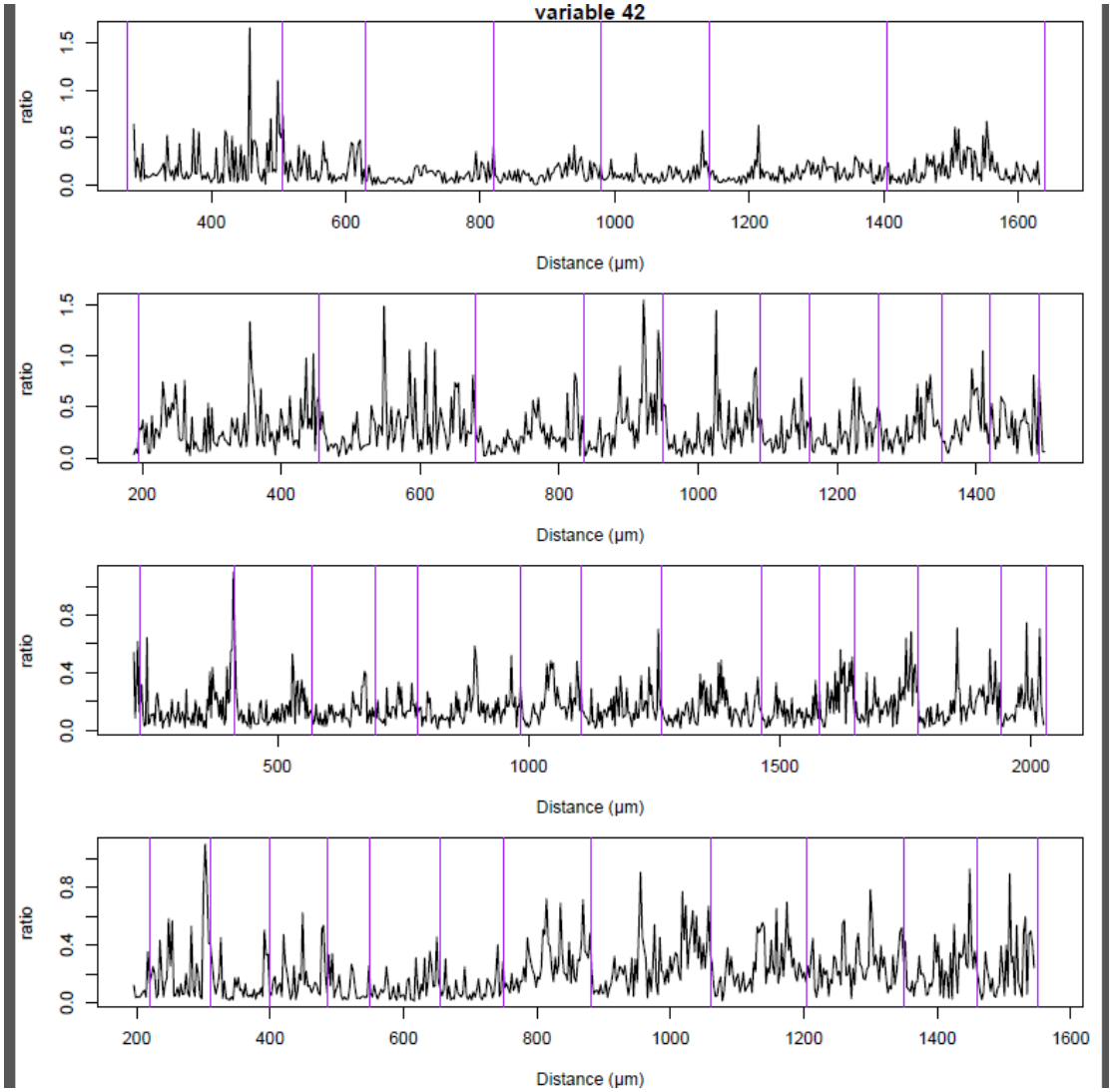
variable 42
ratio
0.0
0.5
1.0
1.5
400
600
800
1000
1200
1400
1600
Distance (µm)
ratio
0.0
0.5
1.0
1.5
200
400
600
800
1000
1200
1400
Distance (µm)
ratio
0.0
0.4
0.8
500
1000
1500
2000
Distance (µm)
ratio
0.0
0.4
0.8
200
400
600
800
1000
1200
1400
1600
Distance (µm)

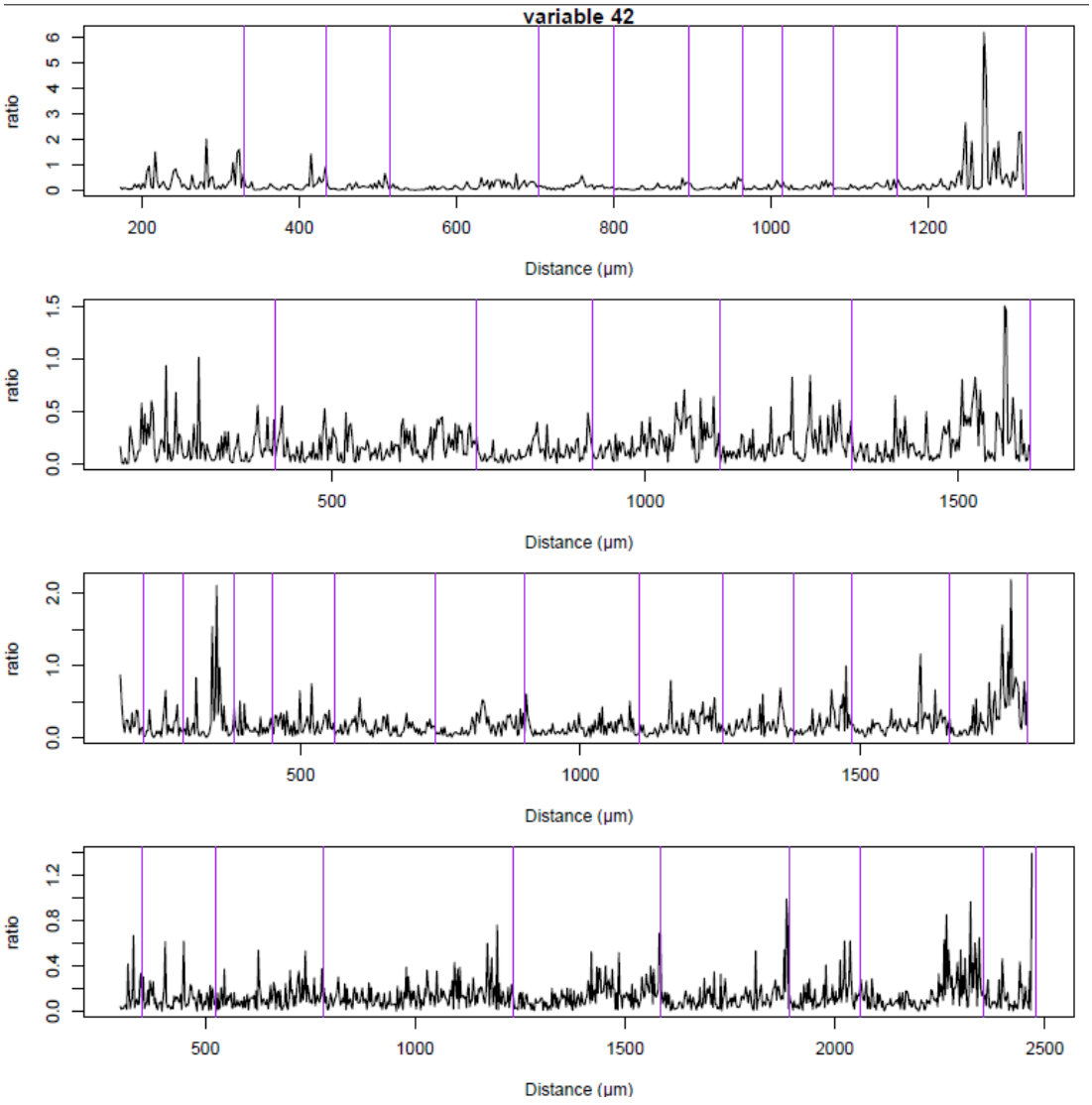
variable 42
ratio
0 1 2 3 4 5 6
200 400 600 800 1000 1200
Distance (µm)
ratio
0.0 0.5 1.0 1.5
500 1000 1500
Distance (µm)
ratio
0.0 1.0 2.0
500 1000 1500
Distance (µm)
ratio
0.0 0.4 0.8 1.2
500 1000 1500 2000 2500
Distance (µm)

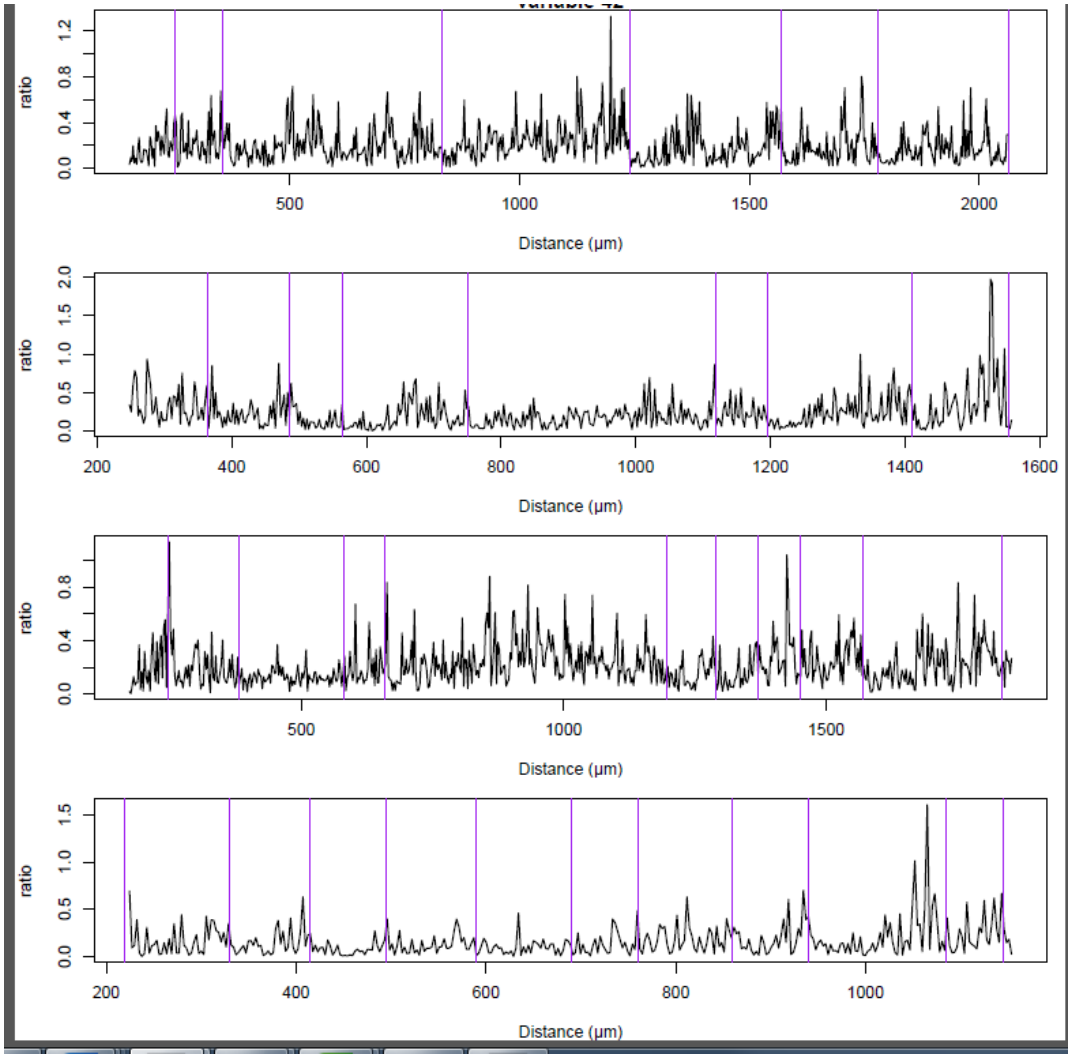
ratio
0.0
0.4
0.8
1.2
500
1000
1500
2000
Distance (µm)
ratio
0.0
0.5
1.0
1.5
2.0
200
400
600
800
1000
1200
1400
1600
Distance (µm)
ratio
0.0
0.4
0.8
500
1000
1500
Distance (µm)
ratio
0.0
0.5
1.0
1.5
200
400
600
800
1000
Distance (µm)

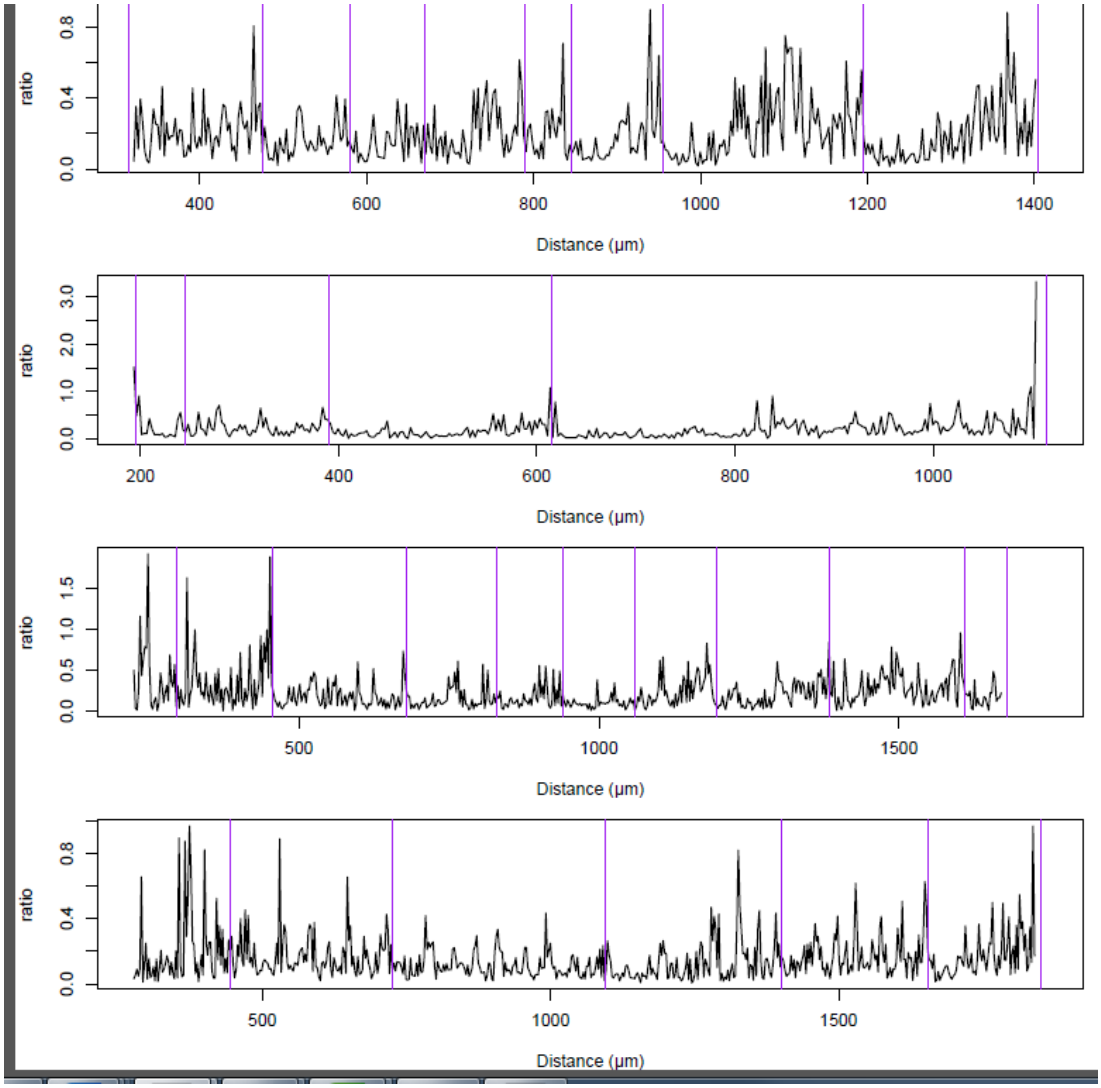
ratio
0.0
0.4
0.8
400
600
800
1000
1200
1400
Distance (µm)
ratio
0.0
1.0
2.0
3.0
200
400
600
800
1000
Distance (µm)
ratio
0.0
0.5
1.0
1.5
500
1000
1500
Distance (µm)
ratio
0.0
0.4
0.8
500
1000
1500
Distance (µm)

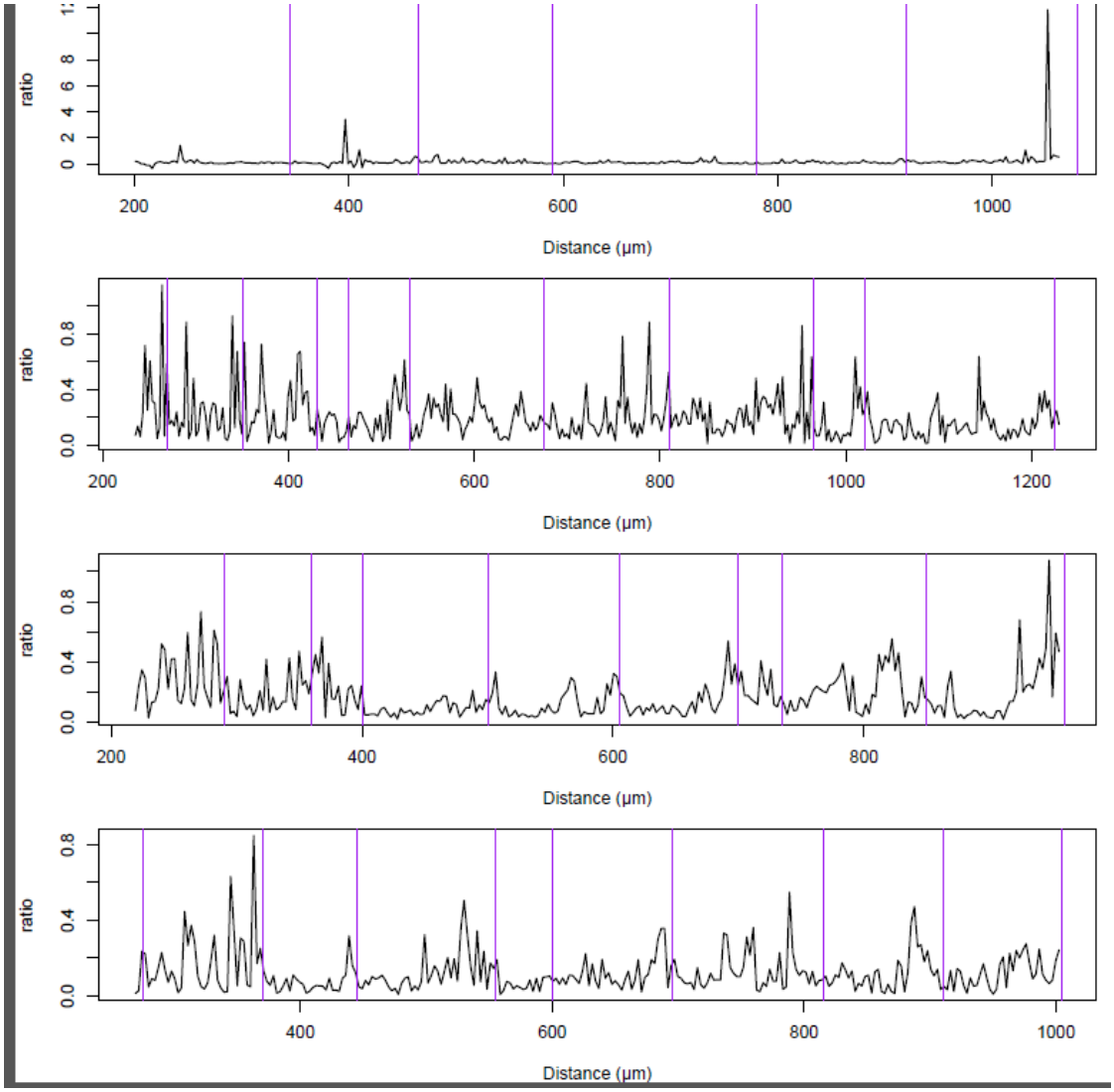
ratio
0 2 4 6 8
200 400 600 800 1000
Distance (µm)
ratio
0.0 0.4 0.8
200 400 600 800 1000 1200
Distance (µm)
ratio
0.0 0.4 0.8
200 400 600 800
Distance (µm)
ratio
0.0 0.4 0.8
400 600 800 1000
Distance (µm)

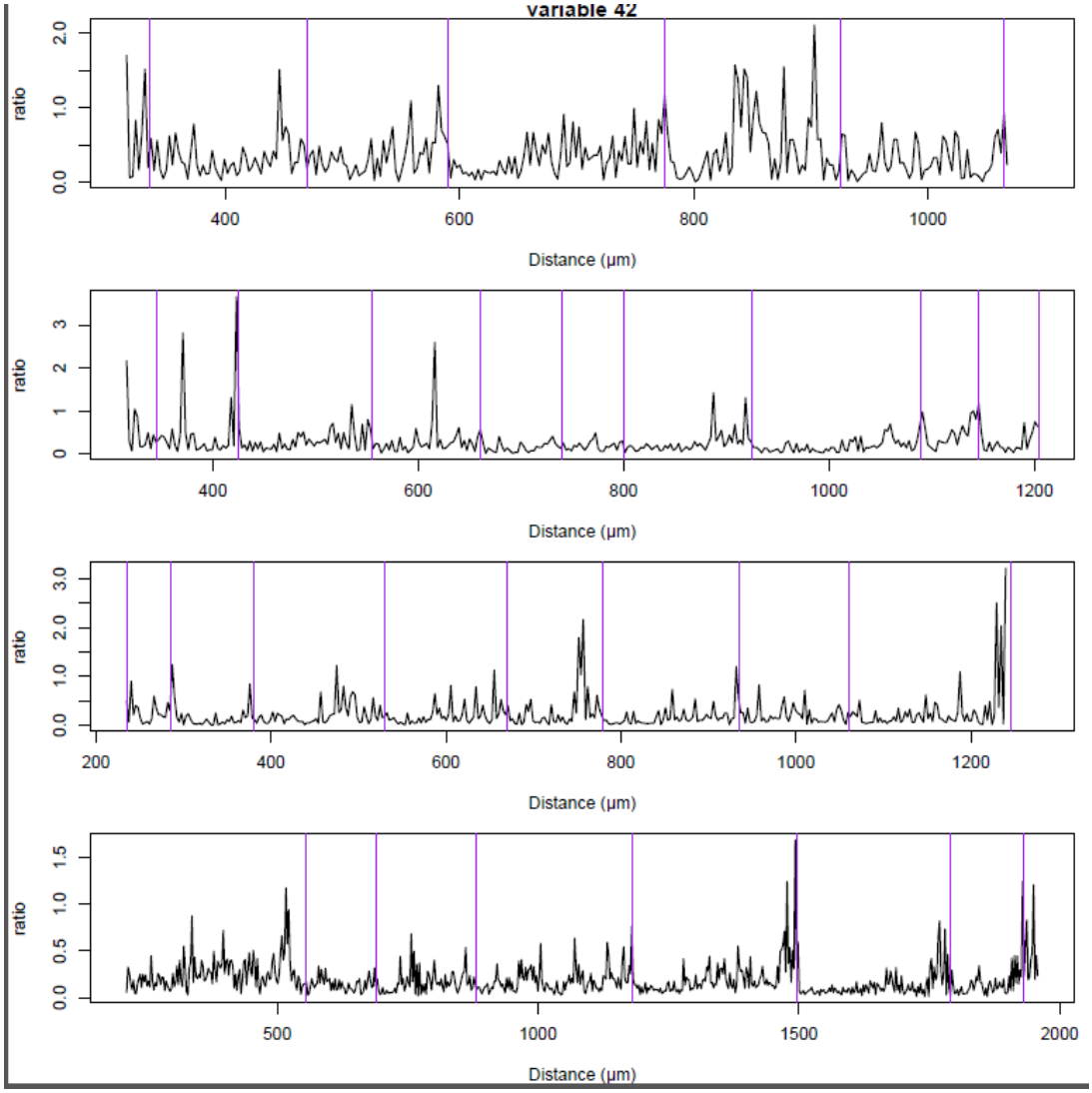
variable 42
ratio
0.0
1.0
2.0
400
600
800
1000
Distance (µm)
ratio
0
1
2
3
400
600
800
1000
1200
Distance (µm)
ratio
0.0
1.0
2.0
3.0
200
400
600
800
1000
1200
Distance (µm)
ratio
0.0
0.5
1.0
1.5
500
1000
1500
2000
Distance (µm)

Copper

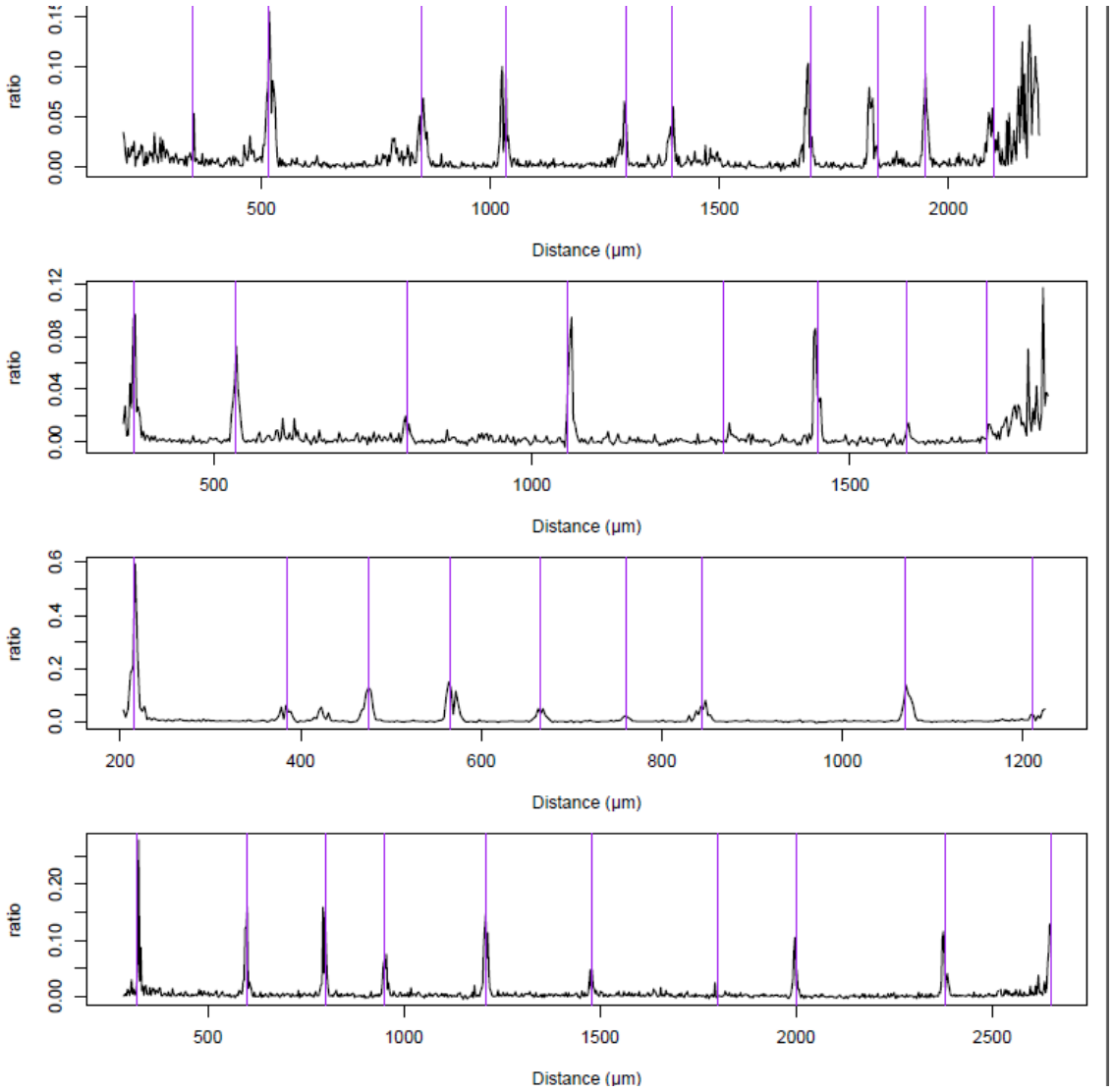
ratio
0.00
0.05
0.10
500
1000
1500
2000
Distance (µm)
ratio
0.00
0.04
0.08
0.12
500
1000
1500
Distance (µm)
ratio
0.0
0.2
0.4
0.6
200
400
600
800
1000
1200
Distance (µm)
ratio
0.00
0.10
0.20
500
1000
1500
2000
2500
Distance (µm)

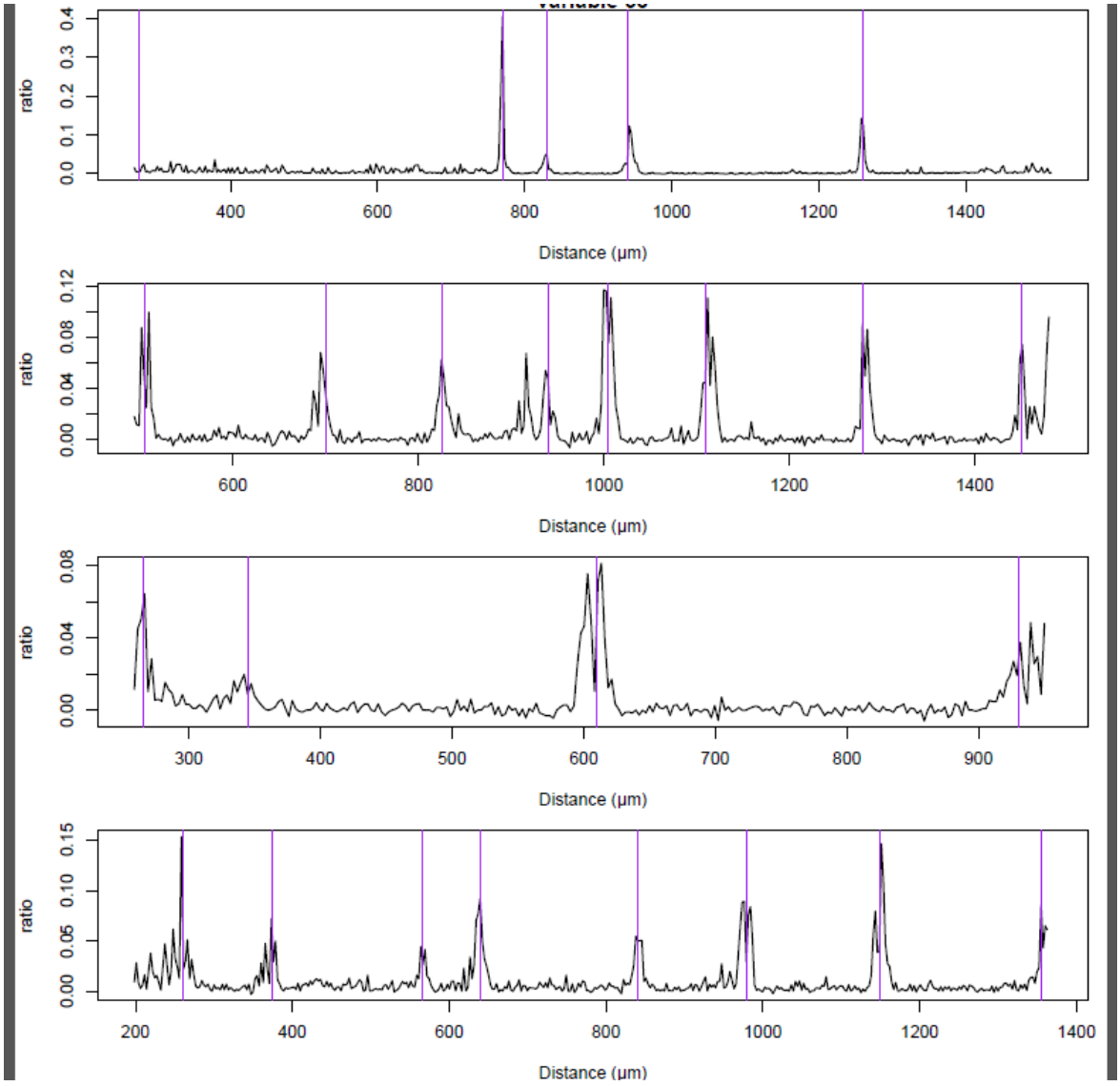
ratio
0.0 0.1 0.2 0.3 0.4
400 600 800 1000 1200 1400
Distance (µm)
ratio
0.00 0.04 0.08 0.12
600 800 1000 1200 1400
Distance (µm)
ratio
0.00 0.04 0.08
300 400 500 600 700 800 900
Distance (µm)
ratio
0.00 0.05 0.10 0.15
200 400 600 800 1000 1200 1400
Distance (µm)

Magnesium

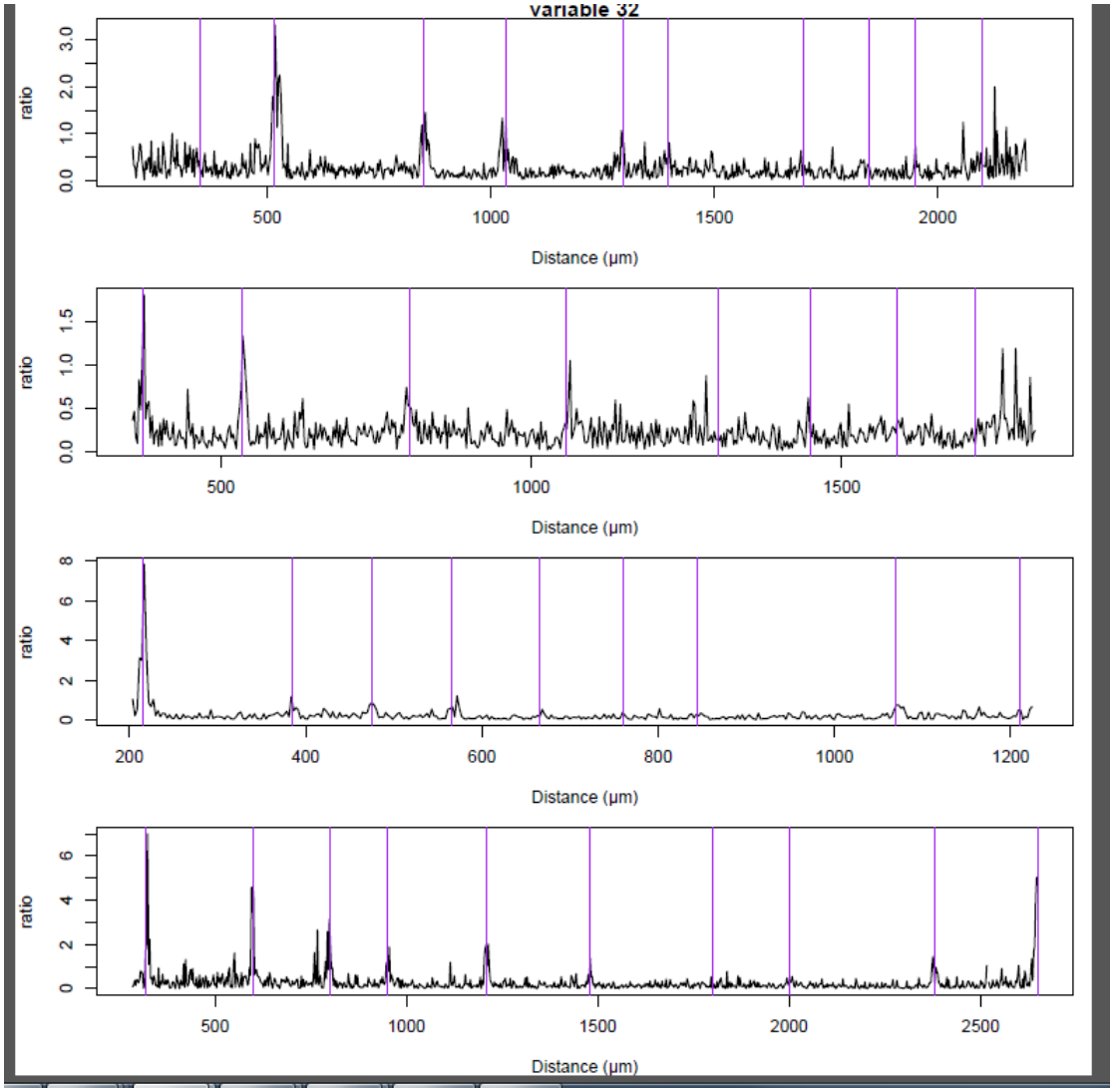
variable 32
ratio
0.0
1.0
2.0
3.0
500
1000
1500
2000
Distance (µm)
ratio
0.0
0.5
1.0
1.5
500
1000
1500
Distance (µm)
ratio
0
2
4
6
8
200
400
600
800
1000
1200
Distance (µm)
ratio
0
2
4
6
500
1000
1500
2000
2500
Distance (µm)

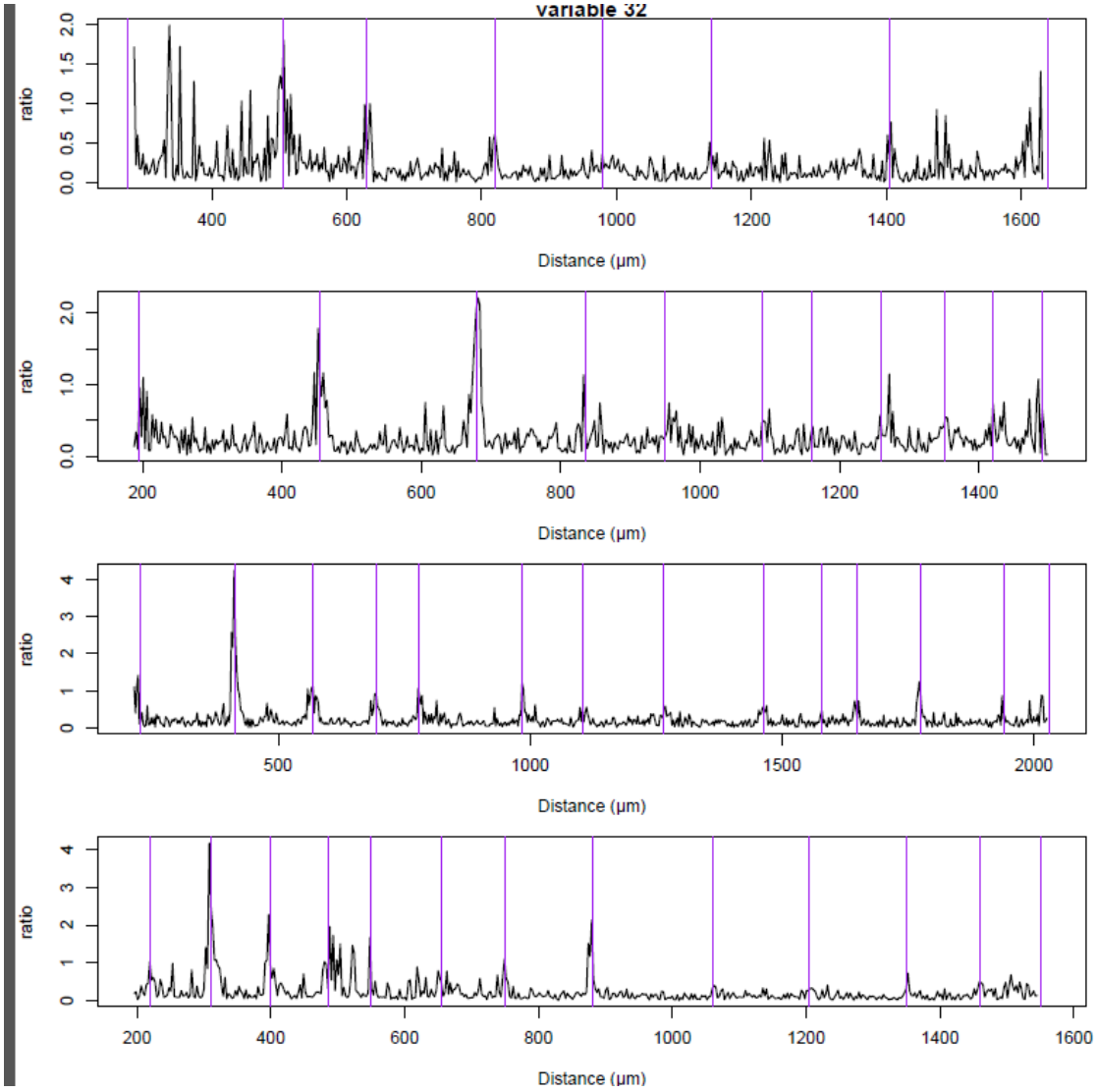
variable 32
ratio
Distance (µm)
ratio
Distance (µm)
ratio
Distance (µm)
ratio
Distance (µm)

Strontium

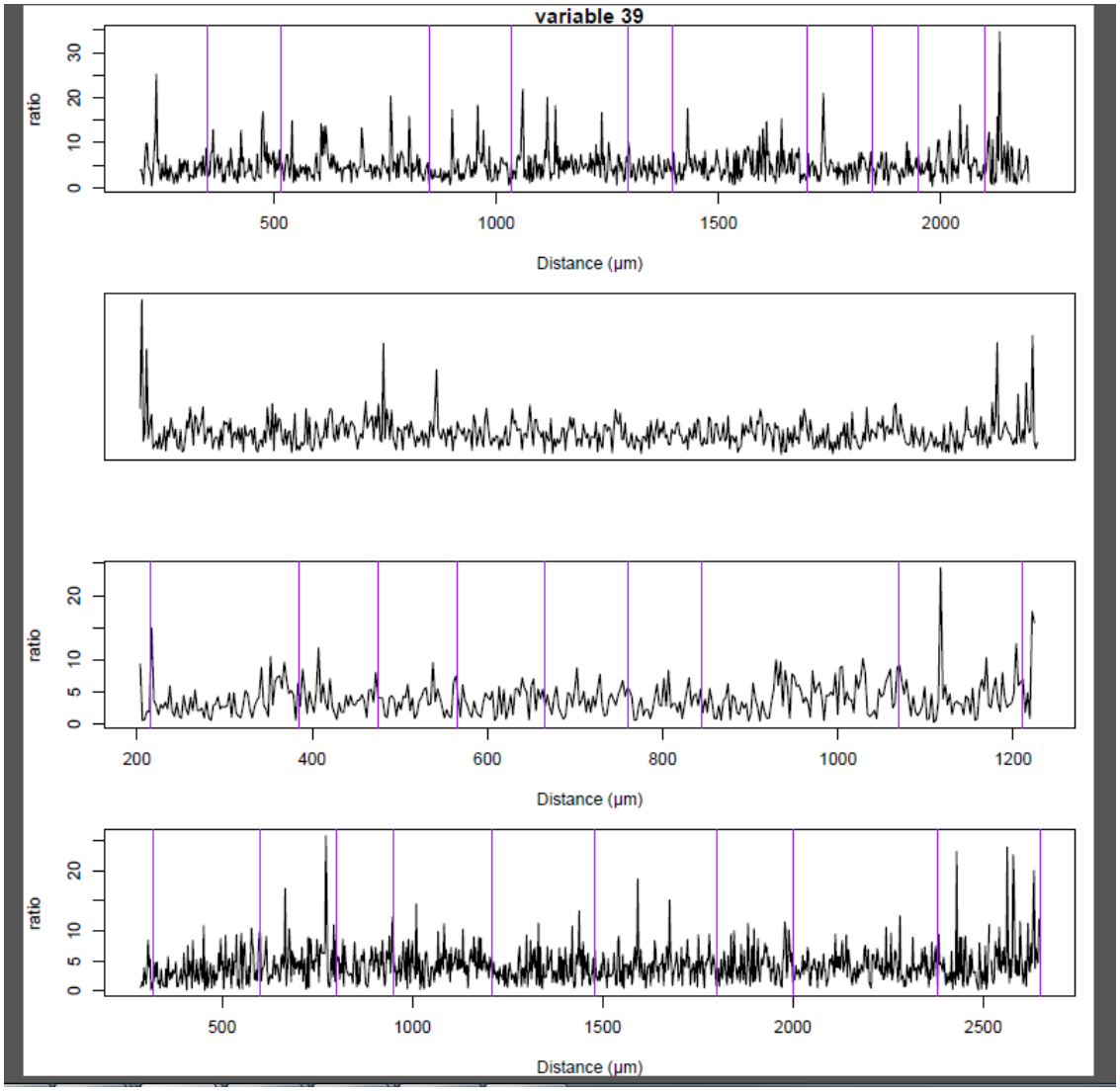
variable 39
ratio
0
10
20
30
500
1000
1500
2000
Distance (µm)
ratio
0
5
10
20
200
400
600
800
1000
1200
Distance (µm)
ratio
0
5
10
20
500
1000
1500
2000
2500
Distance (µm)

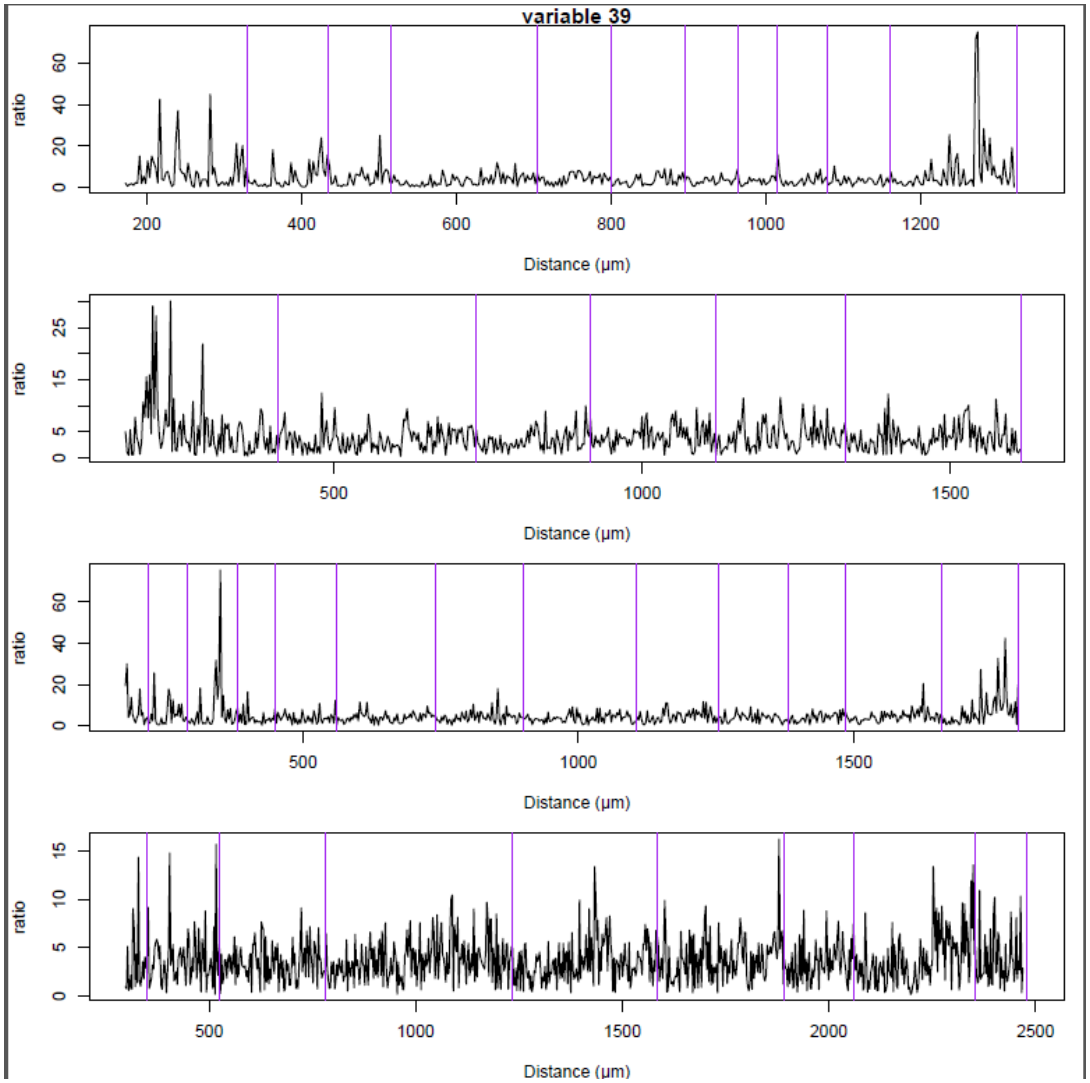
variable 39
ratio
0
20
40
60
200
400
600
800
1000
1200
Distance (µm)
ratio
0
5
15
25
500
1000
1500
Distance (µm)
ratio
0
20
40
60
500
1000
1500
Distance (µm)
ratio
0
5
10
15
500
1000
1500
2000
2500
Distance (µm)

Manganese

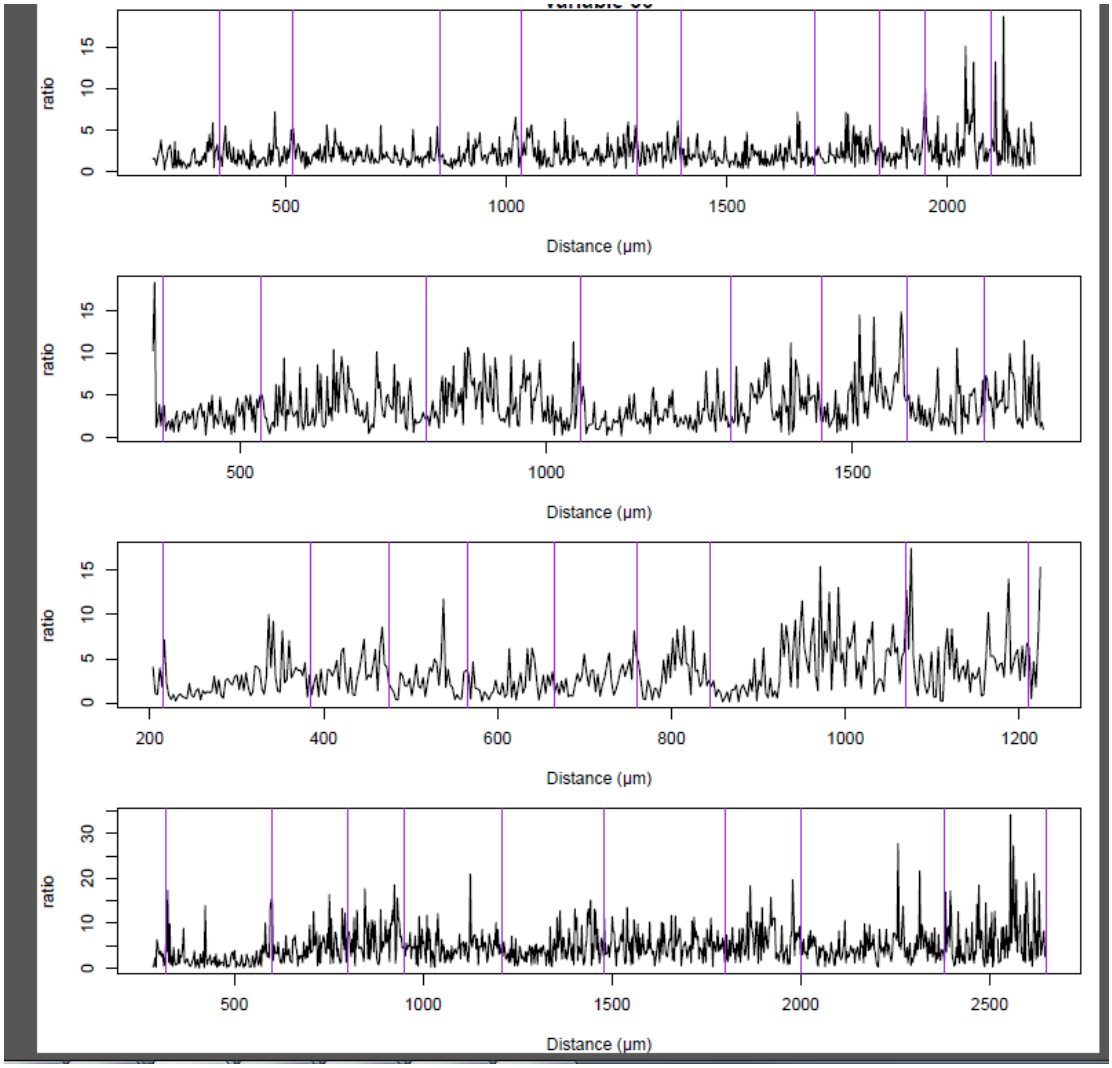
ratio
0
5
10
15
500
1000
1500
2000
Distance (µm)
ratio
0
5
10
15
500
1000
1500
Distance (µm)
ratio
0
5
10
15
200
400
600
800
1000
1200
Distance (µm)
ratio
0
10
20
30
500
1000
1500
2000
2500
Distance (µm)

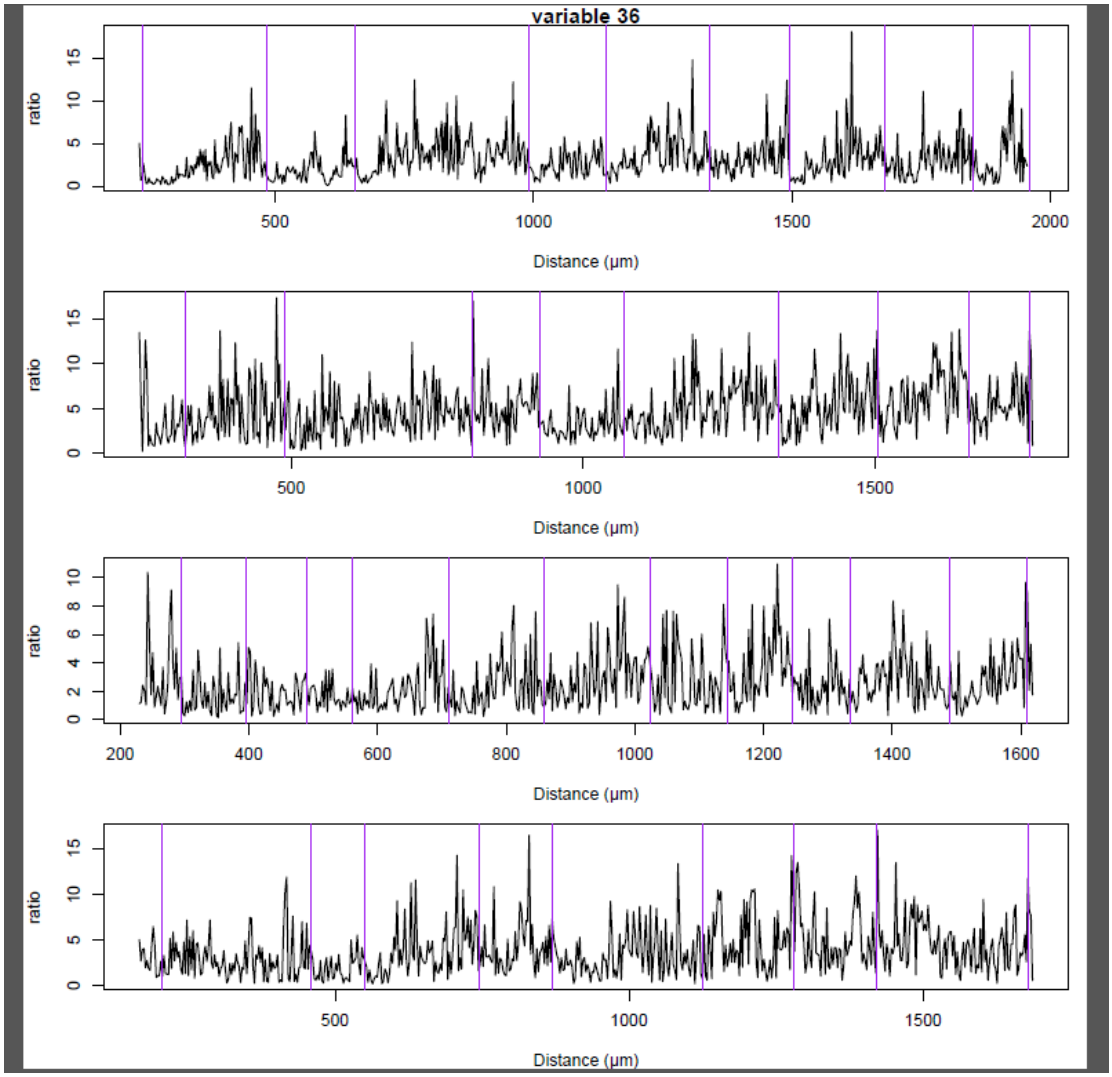
variable 36
ratio
Distance (µm)
ratio
Distance (µm)
ratio
Distance (µm)
ratio
Distance (µm)

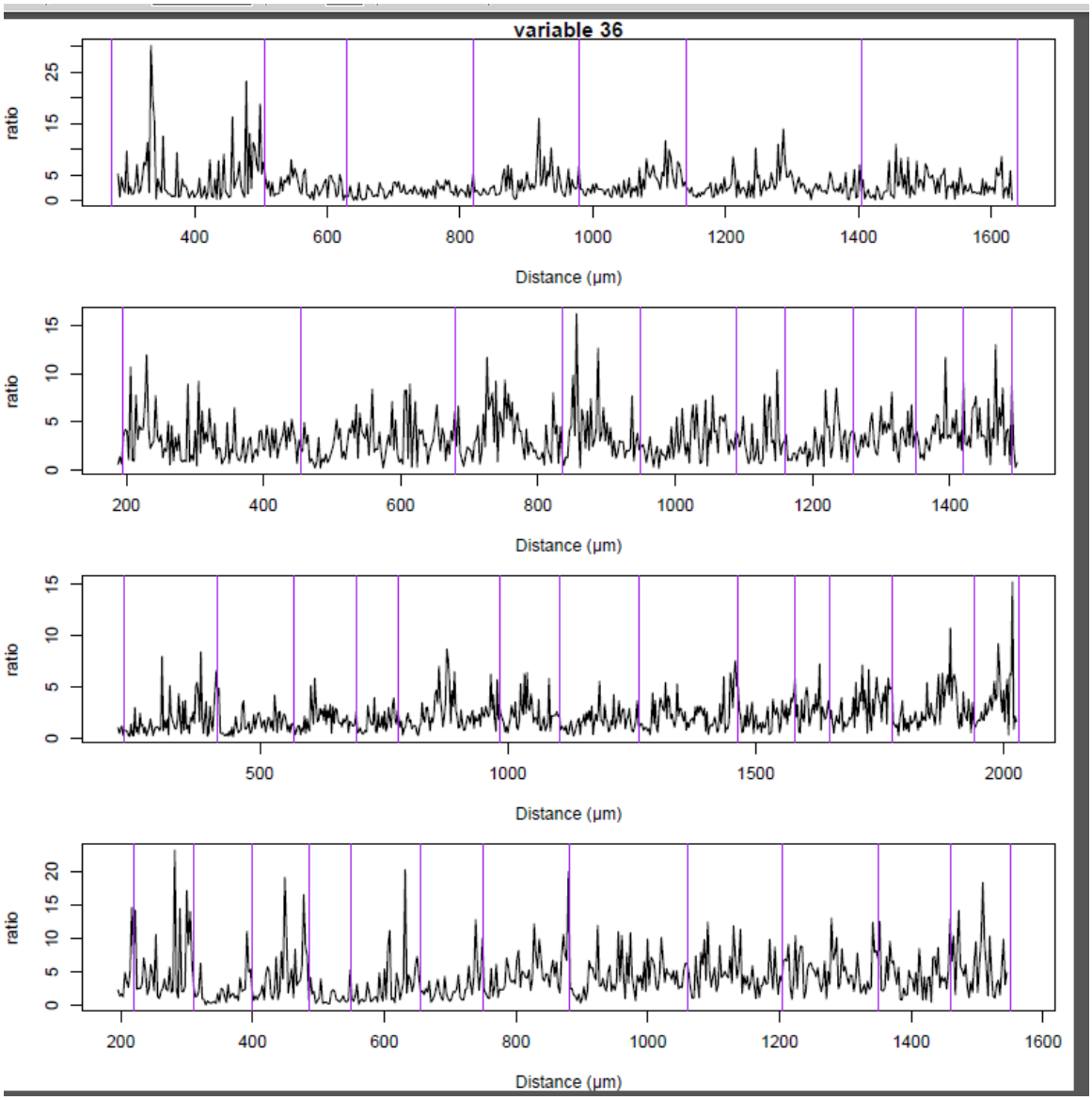
variable 36
ratio
Distance (µm)
ratio
Distance (µm)
ratio
Distance (µm)
ratio
Distance (µm)

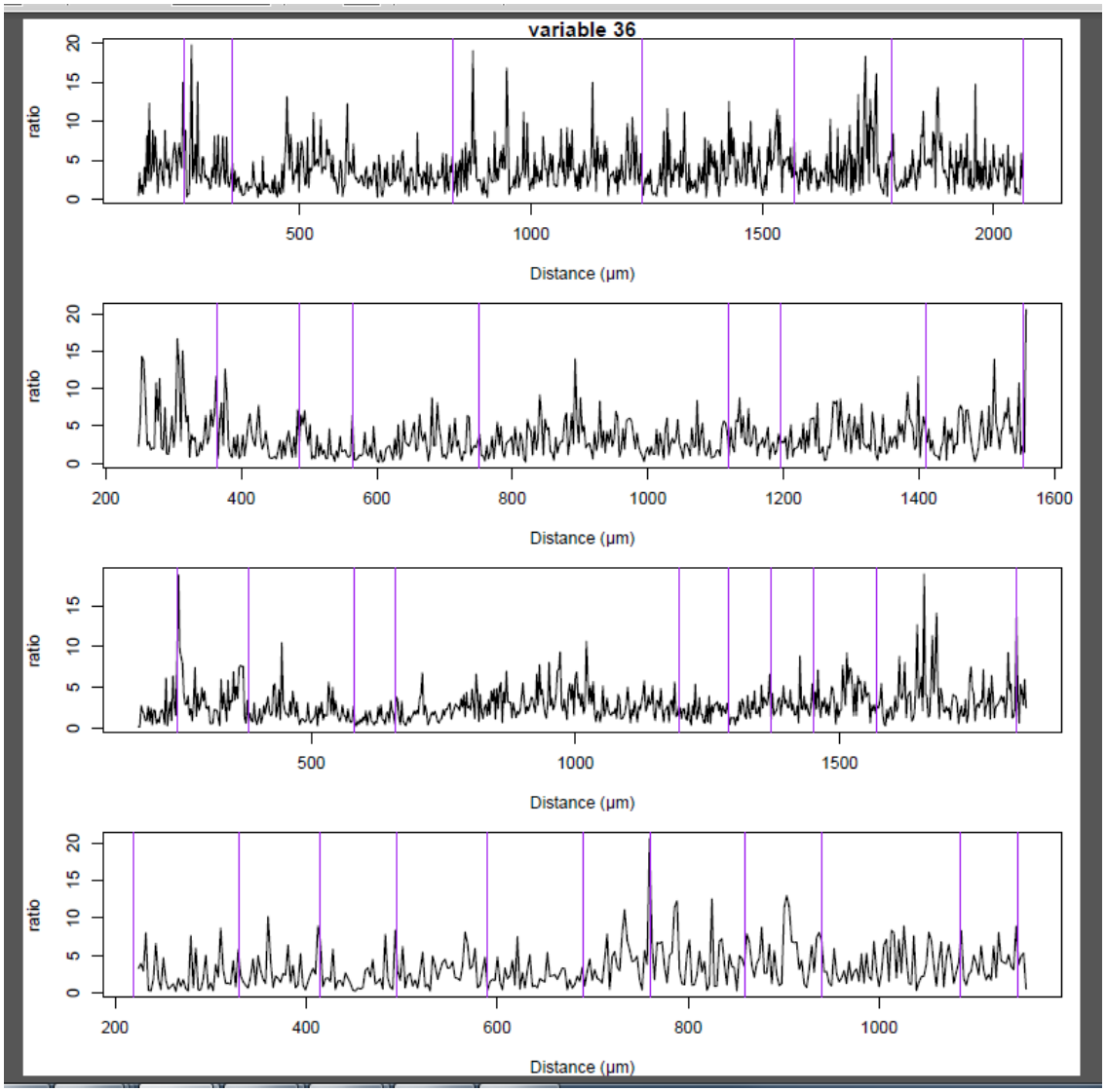
variable 36
ratio
Distance (µm)
ratio
Distance (µm)
ratio
Distance (µm)
ratio
Distance (µm)